Dissolved Gas Analysis of Transformer Liquid-Paper Insulations under Laboratory Simulated Thermal Faults by Using Tube-heating Method

A thesis submitted to The University of Manchester for the degree of Doctor of Philosophy
in the Faculty of Science and Engineering

2020

Xiaohan Li

School of Engineering
Department of Electrical and Electronic Engineering

Contents

Word count: 48,618

List of Figures

List of Tables

Abstract

Dissolved gas analysis (DGA) has been widely used for detecting incipient faults in transformers. Previously published DGA experiments were mainly conducted in liquid insulation with less consideration of the presence of solid insulation like Kraft paper. The relationships between fault gas generation characteristics and paper ageing indicators like degree of polymerization (DP) and 2-FAL in oil are rarely studied. Meanwhile, the CO_2/CO ratio used to identify paper related thermal faults in mineral oil defined in IEC/IEEE standards has evolved through revisions. In addition, technical challenges are faced by asset managers of ester liquid filled transformers since the condition monitoring features of ester liquid filled transformers might not be the same as those of mineral oil filled transformers due to the different chemical structures of the liquids. Therefore, this PhD study focuses on the experimental investigation on fault gas generation characteristics in different transformer oil-paper insulations under laboratory simulated thermal faults using the tube-heating method.

A tube-heating experimental setup previously used for liquid only experiments was further developed to conduct DGA experiments in liquid-paper insulation systems. Temperature profile tests were conducted in mineral oil and synthetic ester liquid to help understanding temperature distribution inside the heating tube. During the experiments, a small amount of liquid or liquid-Kraft paper insulation inside the heating tube was heated using a furnace, with the generated fault gases detected using an online DGA monitor. The liquid only experiments were performed at various thermal fault temperatures ranging from 350 ºC to 750 ºC, and the liquid-Kraft paper experiments were performed at 250 ºC under various heating durations.

The results in synthetic ester liquid only experiments reveal that CO_2 and CO are generated in large amounts and hence are the dominant fault gases created during 350 ºC to 650 ºC thermal faults. Except for carbon oxide gases, C_2H_6 is the typical hydrocarbon gas from 450 ºC to 650 ºC. Under a 750 ºC thermal fault, C_2H_4 becomes the dominant fault gas. For mineral oil, less CO_2 and CO are generated. CH_4 is the typical gas of the occurrence of a thermal fault. C_2H_6 is the typical gas generated by 450 ºC and 550 ºC thermal faults. C_2H_4 is the typical gas generated by 650 ºC and 750 ºC thermal faults. For both insulating liquids, H_2 starts to be generated during a 550 ºC thermal fault and C_2H_2 starts to appear during 650 ºC and 750 ºC thermal faults.

The results of both liquid-Kraft paper insulations reveal that the generated CO_2 and CO increase exponentially with the reduction of the DP and increases linearly with the increasing CSN. A linear relationship has been observed between the generation of carbon oxide gases and 2-FAL in oil. Compared with accelerated ageing studies at lower temperatures, more CO is generated at the same level of DP, indicating that different CO generation mechanisms exist under different thermal fault temperatures. Meanwhile, a static CO_2/CO ratio in mineral oil immersed insulation is not an optimal indicator of paper degradation, whereas a dynamic ratio change under a thermal fault could be explored in the future as being an indicator of the occurrence of a thermal fault involving paper insulation.

Declaration

No portion of the work referred to in this thesis has been submitted in support of an application for another degree of qualification of this or any other university, or other institution of learning.

Copyright Statement

i. The author of this thesis (including any appendices and/or schedules to this thesis) owns certain copyright or related rights in it (the "Copyright") and s/he has given The University of Manchester certain rights to use such Copyright, including for administrative purposes.

ii. Copies of this thesis, either in full or in extracts and whether in hard or electronic copy, may be made only in accordance with the Copyright, Designs and Patents Act1988 (as amended) and regulations issued under it or, where appropriate, in accordance with licensing agreements which the University has from time to time. This page must form part of any such copies made.

iii. The ownership of certain Copyright, patents, designs, trademarks and other intellectual property (the "Intellectual Property") and any reproductions of copyright works in the thesis, for example graphs and tables ("Reproductions"), which may be described in this thesis, may not be owned by the author and may be owned by third parties. Such Intellectual Property and Reproductions cannot and must not be made available for use without the prior written permission of the owner(s) of the relevant Intellectual Property and/or Reproductions.

iv. Further information on the conditions under which disclosure, publication and commercialisation of this thesis, the Copyright and any Intellectual Property and/or Reproductions described in it may take place is available in the University IP Policy (see http://documents.manchester.ac.uk/DocuInfo.aspx?DocID=24420), in any relevant thesis restriction declarations deposited in the University Library, The University Library's regulations (see http://www.library.manchester.ac.uk/about/regulations/) and in The University's policy on Presentation of Theses.

Acknowledgement

First and foremost, I would like to express my sincere gratitude to my supervisor, Dr. Qiang Liu and co-supervisor, Prof. Zhongdong Wang, since any tiny step of my improvements in the last four years was tied closely with their continuous support and kind encouragement. I thank them for their supervision, guidance and understanding throughout my PhD study. It has been a great honour to me to work and grow up in their group.

I would like to convey my great appreciation to Dr. Lin Jiang, Prof. Zengping Wang and Prof. Joseph Yan who recommended me to The University of Manchester to start this adventure. Great thanks are also given to Dr. Tony Chen and Dr. Victor Levi for their kind and helpful suggestions during transfer viva. A big thanks to Dr. Richard Gardner, Dr. Yiming Huang, Dr. Shanika Matharage, Dr. Xiongfei Wang and Mr. Haichuan Yu for their tremendous support and help on my work. I would like to extend my thanks to Prof. Peter Crossley, Dr. Jun Jiang, Prof. Zanji Wang and Dr. Xiang Zhang for their inspirational advices. I also want to say thank you to the student I mentored, Mr. Cheng Li for his involvements to my research work.

I want to thank all my colleagues in our group and others working in Ferranti Building. I am also grateful to my dear friends for their kind help, encouragements and standing beside me in the period of study, including Dr. Siyuan Chen, Bozhi Cheng, Yi Cheng, Zihan Gao, Ziye Guo, Qinghua Han, Muye Li, Wenyuan Li, Chengxing Lian，Dr. Gaoyuan Liu, Dr. Xiaozhou Mao, Berihu Mebrahtom, Dr. Zhou Mu, Dr. Yingqiang Shang, Dr. Shuhang Shen, Yue Wang, Dr. Jing Xiang, Zongwen Yan, Yaoxian Yang, Xu Zhang and his wife Rongrong Wang. Many thanks to my roommates Hang Xu and his wife Shuyang Shen and Sicheng Zhao for their warm company.

Last but not least, I wish to express my deepest and heartful thanks to my parents Mr. Hongtao Li, Mrs. Fengjuan Zhu together with my family for their selfless love and support, to my beloved girlfriend Ms. Yifan He for her endless love and care.

Chapter 1 Introduction

1.1 Background

A transformer is an electrical device that takes electrical power of a certain voltage and current levels through its primary terminals and delivers this power to its secondary terminals at changed voltage and currents levels. At the end of the 19th century, the invention of the power transformer made possible the development of the modern high-voltage (HV) power transmission system [1]. High voltage power transformers have made it possible to transfer a large amount of power from the point of generation to the point of consumption over a long distance with reduced power losses. Nowadays, a reliable supply of electricity is important to economic activities and normal life, the efficient transmission of electrical power relies on the reduction of the transmission losses by reducing the transmitted current [2]. Transformers playing an important role in optimising generation, transmission, distribution and utilisation of electrical power [3]. In a future low carbon power network, more dynamic loading with potential excessive overloading increases the likelihood of transformer failures, especially for existing ageing assets. Therefore, reliable diagnostic and condition monitoring technique is recommended to continuously monitor the health of critical transformers to avoid any potential catastrophic failures and allow timely maintenance action.

Most existing power transformers are still the liquid immersed type that mainly consist of an iron core, copper windings insulated with paper insulation, a liquid insulation medium, supporting solid structure and tank that holds everything together [1]. A typical liquid immersed arrangement of a transformer is illustrated in Figure 1-1 [4]. The insulation system in a transformer includes insulating liquid and cellulose-based solid insulation to withstand high electric stresses, both under normal and abnormal operating conditions [5]. The insulating liquid should have excellent dielectric insulating properties to act as electrical insulation, cooling medium and

information carrier [6]. The solid insulation mainly provides sufficient electrical strength to withstand high voltage stresses and sufficient mechanical strength to support the integrity of the transformer winding structure [6]. The design life of a transformer is related to its specifications and manufacturing process. The expected life is related to its operational experience such as loading and maintenance. One of the determining factors of transformer life is the condition of the insulation system [7-11]. The insulation condition then depends on loading, ambient temperature, moisture content and oxygen content in oil, etc [10]. In addition, the condition of other components, such as tap-changers and bushings, can also influence the health of transformers according to statistical surveys [12, 13].

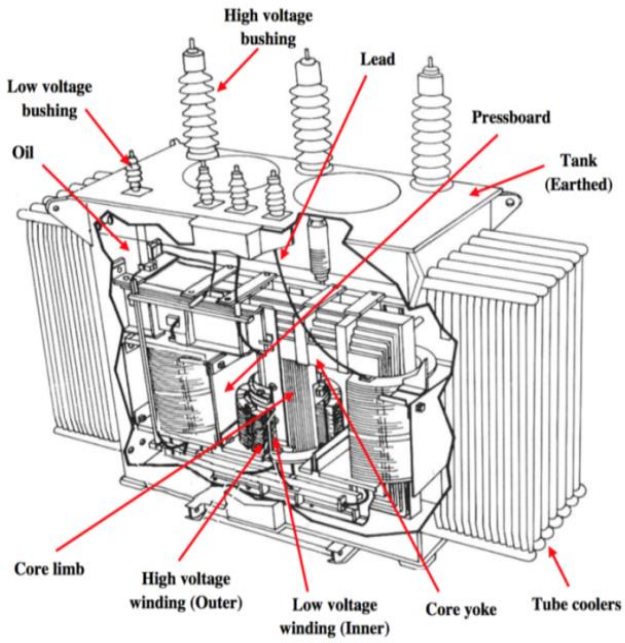

Figure 1-1 Typical liquid-filled transformer arrangement [4]

In the 1960s and early 1970s, large transformer populations were commissioned in the UK and the other developed countries [14, 15]. An international transformer reliability survey conducted by CIGRE Working Group A2.37, found that a large proportion of the 1004 UK transformers were beyond 40 years old and that the majority of failures occurred in the 36 to 40 year age band [16]. The electrical utilities are facing a significant challenge managing this large fleet of ageing transformers. Therefore, transformer asset management activities, especially condition monitoring, are of great

importance to assess the health status of in-service transformers [5, 17-19].

Within the last few decades, several condition monitoring and fault diagnosis techniques, such as dissolved gas analysis (DGA), partial discharge (PD) measurement and frequency response analysis (FRA), have been developed to assess the condition of power transformers and minimise the possibility of catastrophic failure [5, 17, 19]. Among these condition monitoring techniques, DGA has been widely used and is regarded as probably the most powerful diagnostic technique for detecting incipient faults in transformers [13, 20-22]. These incipient faults include electrical faults and thermal faults [22-24].

A thermal fault is defined as an excessive temperature rise in the insulation [22]. Typical causes of thermal faults in transformers can be insufficient cooling, excessive current circulating in adjacent metal parts or through the insulation, overheating of the internal winding or bushing connection lead, and overloading [24]. DGA related thermal faults are specified as being within three temperature ranges including [22]:

- T1 ($T < 300$ ºC)
- T2 (300 ºC $< T < 700$ ºC)
- T3 ($T > 700$ ºC)

The decomposition of the insulation materials under thermal faults causes the breaking of different chemical bonds that consist of carbon (C), hydrogen (H) and oxygen (O) chemical atoms and results in the formation of different active fragments. Different gases are then produced through the recombination or rearrangement processes of these active fragments [22]. The principal gases used to identify faults by the DGA technique are hydrogen (H_2), methane (CH_4), ethane (C_2H_6), ethylene (C_2H_4), acetylene (C_2H_2), carbon monoxide (CO) and carbon dioxide (CO_2). Oxygen (O_2) and nitrogen (N_2) are also measured and used in the interpretation, although they are not fault by-products [22].

1.2 Research Motivation

Many DGA studies have conducted laboratory simulated thermal faults using different heating methods [21, 25-36]. Conventionally, there are three heating methods that are commonly used in laboratory experiments to simulate thermal faults including oven-heating method, immersed-heating method and tube-heating method. Among these methods, the oven-heating method provides a uniform temperature profile best able to simulate thermal faults in the T1 thermal fault range [21, 25]. The immersed-heating method cannot achieve some of the temperatures in the T2 and T3 range due to the pool boiling phenomenon [26-32]. On the other hand, the tube-heating method has the ability to cover the whole temperature range of defined thermal faults in transformers and provide a stable localised hotspot similar to those that occur in real transformers [33-36]. In addition, there have not been DGA studies to investigate fault gas generation characteristics of oil-paper insulation system by using tube-heating method. Therefore, it is of key importance to develop a tube-heating setup to perform DGA experiments under T2 and T3 thermal faults and also in oil-paper insulation system.

Mineral oil has been used in power transformers for over a century due to its reliable features, such as high dielectric strength, high heat dissipation efficiency and low price. However, with increasing awareness about environmental impacts and safety considerations, the disadvantages of mineral oil are exposed more than ever. Synthetic ester liquid has been increasingly used in recent decades as an alternative to mineral oil due to its biodegradability and fire safety properties. At the same time, its challenges are related to condition monitoring because the monitoring features of a synthetic ester liquid filled transformer might not be the same as for those using mineral oil. The chemical structure of the synthetic ester liquid is different from mineral oil which may lead to different generation mechanisms of fault gases. Meanwhile, the criteria to interpret fault types based on relative pattern ratios of fault gases may differ from those used for mineral oil. Therefore, it is worth investigating

and comparing fault gas generation characteristics in both mineral oil filled transformers and synthetic ester liquid filled transformers.

A thermal fault is usually represented in a transformer by a localised hotspot that often occurs at the top part of the windings where not only include insulating liquid but also solid insulation. However, previous DGA thermal studies have rarely focused on insulating liquid-Kraft paper insulation systems [29-31, 35]. In addition, although ageing studies have investigated insulating liquid-Kraft paper insulation systems but rarely conducted DGA measurements [37-42]. A significant volume of knowledge about the condition of a transformer can be inferred by analysing certain properties of the insulating liquids and solid insulations [5, 13, 43]. The DGA technique can analyse the generated fault gases dissolved in oil. The furan analysis can indicate paper degradation [13]. Therefore, it is of key importance to investigate and compare fault gas generation characteristics in both mineral oil-Kraft paper insulation system and synthetic ester liquid-Kraft paper insulation system, and correlate fault gas generation with other paper degradation indicators.

Moreover, the CO_2/CO ratio is suggested by both the IEEE standard and IEC standard for use as an indicator to identify whether mineral oil immersed transformers are experiencing paper related thermal faults. The CO_2/CO ratio defined in standards has evolved through revision. IEC standard 60599-1978 [44] suggests that 'any case in which CO_2/CO is below about 3 or above about 11 should be regarded as perhaps indicating a fault involving cellulose'. IEC standard 60599-1999 [45] suggests that 'CO_2/CO ratios less than 3 are generally considered as an indication of probable paper involvement in a fault'. Additionally, IEC standard 60599-2016 [24] suggests that the accepted range of the CO_2/CO ratio for a normal transformer is between 3 and 10. However, IEEE standard C57.104-1991 [46] and IEEE standard C57.104-2008 [47] suggest that 'The ratio of CO_2/CO is sometime used as an indicator of the thermal decomposition of cellulose. This ratio is normally more than seven'. However, IEEE standard C57.104-2019 [22] suggests that a low CO_2/CO ratio (< 3) together with the

formation of significant amounts of hydrocarbon gases maybe indicate a fault in paper, and a high CO_2/CO ratio (> 20) and high furan values can indicate slow paper degradation at low temperatures (< 140 ºC). Therefore, it is worth conducting DGA thermal experiments in both mineral oil-Kraft paper insulation system and synthetic ester liquid-Kraft paper insulation system to investigate CO_2/CO ratio characteristics.

1.3 Research Objectives

The aim of this research is to investigate the fault gas generation characteristics in different transformer insulations under the laboratory simulated thermal faults using the tube-heating method. A mineral oil (MO), a synthetic ester liquid (SE) and non-thermally upgraded Kraft paper are used in the investigations. The generated fault gases dissolved in the insulating liquids are measured and analysed using an online DGA monitor. Meanwhile, paper ageing indicators, such as DP and 2-FAL, will be measured. To achieve the aim, the following objectives have been identified:

i. Develop a tube-heating experimental setup suitable for both insulating liquid only and insulating liquid-solid insulation system experiments.

ii. Investigate the fault gas generation characteristics of mineral oil and synthetic ester liquid under T2 and T3 thermal faults.

iii. Investigate the fault gas generation characteristics of mineral oil-Kraft paper insulation system and synthetic ester liquid-Kraft paper insulation system under T1 thermal faults.

iv. Correlate the fault gas generation characteristics with paper degradation indicators of mineral oil-Kraft paper insulation system and synthetic ester liquid-Kraft paper insulation system.

1.4 Main Contributions

The main contributions of this PhD study can be summarized as follows:

- A tube-heating experimental setup previously used to simulate a localised thermal fault in transformers was further developed to conduct experiments in liquid-paper insulation systems. Temperature profiles of a mineral oil and a synthetic ester liquid inside the heating tube were measured at different controlled temperatures. Understanding the temperature profile inside the heating tube made a significant contribution to interpreting the DGA results of liquid-paper insulations.

- There have been many studies investigating liquid-paper insulation systems by using oven-heating method or immersed-heating method. The gas generation characteristics of liquid-paper insulation system under thermal faults were, for the first time, investigated by using the tube-heating method. Carbon oxide gases generation characteristics were obtained in mineral oil-Kraft paper and synthetic ester-Kraft paper insulation systems under T1 thermal fault.

- The indicators of the degradation of cellulose such as DP of Kraft paper samples and 2-FAL in oil were measured to help understanding the generation characteristics of fault gases under various durations of the thermal faults. The relationships between the generation of fault gases and paper degradation indicators are correlated.

- As the CO_2/CO ratio has been suggested in IEC/IEEE standards to help indicating paper related thermal faults, the CO_2/CO ratio was also discussed with considerations of material ratio and fault size in a transformer. It was found that the dynamic ratio change under a thermal fault could potentially be an indicator of the occurrence of a thermal fault involving paper insulation.

1.5 Thesis Outline

The thesis is divided into seven chapters, with a brief introduction of each chapter presented in the following.

Chapter 1 Introduction

This chapter briefly introduces the background, motivation and objectives of this study. An outline of the thesis is also presented in this chapter.

Chapter 2 Literature Review

This chapter introduces the development history of the DGA technique. Basic knowledge related to the DGA technique is reviewed, including DGA related fault types, formation of fault gases from the decomposition of insulation materials and the interpretation methods of DGA results. In addition, published research on DGA experimental setups and previous results for the fault gas generation characteristics of different insulation systems are both reviewed.

Chapter 3 Experimental Descriptions

This chapter initially introduces the insulation materials under investigation. Secondly, the experimental setup employed in this study is introduced, including the design, construction and liquid filling procedure. Two design related tests are also described in this chapter, including the temperature profile measurement and sealing performance test. The sample preparation process is then presented. Finally, the calculation method for the DGA measurement results is introduced.

Chapter 4 Generation of Fault Gases in Mineral Oil and Synthetic Ester Liquid under Simulated Thermal Faults

This chapter reports the experimental results of gas-in-oil fault gas generations in

mineral oil and synthetic ester liquid under T2 and T3 thermal faults at various temperatures (350 ºC, 450 ºC, 550 ºC, 650 ºC and 750 ºC). A comparison of the gas-in-oil fault gas generation characteristics between the two insulating liquids is also discussed.

Chapter 5 Generation of Carbon Oxide Gases in Mineral Oil and Kraft Paper Insulation System under Simulated Thermal Faults

This chapter presents the experimental results of the gas-in-oil carbon oxide gases generated in a mineral oil-Kraft paper insulation system under a 250 ºC thermal fault with different heating durations. The temperature gradient across the paper layers is estimated. The correlation between carbon oxide gas generation and paper degradation is also investigated. The comparison between carbon oxide gases generation and the concentration of 2-FAL in oil is presented. Meanwhile, a comparison of carbon oxide gases generation with accelerated ageing studies is discussed. Finally, a case study with scaled up carbon oxide gases generation is discussed.

Chapter 6 Generation of Carbon Oxide Gases in Synthetic Ester Liquid and Kraft Paper Insulation System under Simulated Thermal Faults

This chapter reports the experimental results of gas-in-oil carbon oxide gases generation in a synthetic ester liquid-Kraft paper insulation system under a 250 ºC thermal fault with different heating durations. The same analysis in Chapter 5 is conducted in order to make a comparison with the mineral oil-Kraft paper insulation system, including the temperature gradient across paper layers, the correlation of carbon oxide gases generation with paper degradation and the comparison of carbon oxide gases generation with the concentration of 2-FAL in oil. In addition, a comparison of carbon oxide gases generation with accelerated ageing studies is also discussed. The CO_2/CO ratio is discussed at the end of the chapter.

Chapter 7 Conclusions and Future Research

This chapter summarises the research topics covered in this PhD thesis and concludes the main findings. Finally, ideas for future research are suggested.

Chapter 2 Literature Review

2.1 Introduction

The development history of the DGA technique will be firstly reviewed in this chapter, followed by the introduction of DGA fault types and related fault gases. The commonly used DGA interpretation methods will then be explained in detail, before comparing the different experimental setups designed to investigate the gas generation characteristics of transformer insulation under thermal faults. Finally, the experimental results of DGA studies under thermal faults will be reviewed.

2.2 DGA Technique

2.2.1 Development history of DGA

The history of power transformers dates back to the 1880s. The first patented open core transformer was built by Gaulard and Gibbs in 1882 [48]. Almost at the same time, the first closed wound core transformer was constructed in 1885 by three Hungarian engineers at the Ganz factory in Budapest [49]. A power transformer mainly consists of an iron core, copper windings insulated with paper insulation, a liquid insulation medium, supporting solid structure and a tank that holds everything together [1]. Generally, in-service transformers suffer from two types of stress, classified as electrical stress and thermal stress [50]. As a result of these stresses, the insulation material used in transformers can decompose into gaseous by-products. The presence of these gases was recognised from World War I [51]. Researchers then started to investigate the characteristics and behaviours of dissolved gases and aimed to diagnose the type of faults occurring in transformer insulating oil.

The problem with such an investigation concerned extracting the dissolved gases from insulating liquid. Several attempts were performed to collect and analyse these gases.

The first attempt at detecting gases started with a device named the Buchholz relay introduced in Germany in 1928 [52]. The device could detect gas bubbles generated in transformers. The attempt had a development in 1956 that gases were collected from Buchholz relay for a detailed fault assessment [53]. Once the gases were detected, the gases were sampled and sent to a laboratory for further analysis. In the 1960's, gas chromatography (GC) techniques were employed to identify gases dissolved in transformers [50]. The earliest chromatography attempts dated back to the turn of the century by a Russian botanist named M. S. Tsvet [54].

As early as in 1968, an extensive research work on transformer fault gas analysis and interpretation was pioneered at the Central Electricity Generating Board of Great Britain (CEGB) [55]. The production of fault gases was probably, for the first time, studied and evaluated from both experimental and thermodynamic approaches in 1973 by Halstead [56]. Halstead first predicted that with the increase of fault temperature, low molecular weight fault gases would be formed following the sequence: methane, ethane, ethylene and finally acetylene. The empirical studies in CEGB had verified this prediction later. In 1974 in Switzerland, Dornenburg and Strittmatter introduced the differentiation between electrical and thermal fault types by using different gas ratios [57]. Then, in 1975 in the UK, Rogers developed a comprehensive interpretation scheme of the modern DGA diagnostics [53].

The promotion and implementation of DGA started with the publication of several international standards. In 1977, IEC 60567-1977 standard was published, and was a guide for the sampling of gases and oil from oil-filled electrical equipment, and for the analysis of free and dissolved gases [58]. In this standard, the main information concerned the sampling methods, with less focus on analysing gases. One year later, the standard IEC 60599-1978 was published for the interpretation of the analysis of gases in transformers and other oil-filled electrical equipment in service [44]. Also in 1978, IEEE C57.104-1978 standard was published to provide a guide for the detection and determination of generated gases in oil-immersed transformers and their relation

to the serviceability of the equipment [59]. With the development of technology, these standards have been revised and updated several times, with three revisions of IEC 60567 [23, 60, 61], two revisions of IEC 60599 [24, 45] and three revisions of IEEE C57.104 [22, 47, 62]. The latest versions are IEC 60567-2011 [23], IEC 60599-2016 [24] and IEEE C57.104-2019 [22].

The traditional method for precise DGA investigation is collecting oil samples from in service transformers and transporting those oil samples to the laboratory to extract gases out of the oil and make a diagnosis based on GC techniques [20]. The common extraction methods used to separate dissolved gases from insulating liquids in the laboratory are the headspace extraction method, vacuum extraction method and stripping extraction method [23]. Meanwhile, ASTM standard D3612 also introduced three methods to analyse dissolved gases using GC including the vacuum extraction method, the stripper column extraction method and the headspace sampling method [63]. This standard was initially published in 1977 and the latest version was updated in 2017 [63].

Once the dissolved gases have been detected, the interpretation of the results and the identification of the incipient faults are another challenge. Overtime, many interpretation methods have been developed. The current commonly used interpretation methods include the Key Gas Method, Dornenburg Ratio Method, Rogers Ratio Method, IEC Ratio Method, Duval Triangle Method and CIGRE method [64].

Since the traditional DGA requires sampling oil from transformers and transporting it to the laboratory for future diagnosis, some online DGA monitors have been produced to monitor transformers on site. There are two aspects that are really important in the design of online monitors. Firstly, the monitor is required to have the ability to separate dissolved gases from the insulating liquids. Secondly, the monitor should be able to conduct a quantitative analysis [65]. Up to present, several detection techniques have been used in online DGA monitors, including gas chromatography

(GC), photo-acoustic spectroscopy (PAS), thermal conductivity detector (TCD), non-dispersive infrared (NDIR), infrared (IR), near infrared (NIR), Fourier transform infrared (FTIR), fuel cell (FC), micro-electronic sensor and electrochemical cell [66]. Several commercial pieces of DGA equipment for the online monitoring of transformer oil were summarised in [66], as well as the differences between the main existing DGA monitors to aid the selection of the most suitable DGA monitor.

It is worth noting that the standards mentioned above are mostly focusing on the traditional mineral oil which has been used in oil-immersed transformers for over a century. However, with the increasing awareness of environmental impacts and safety considerations, the use of mineral oils is not deemed environmentally friendly today. Hence, alternative insulating liquids have been selected to replace the mineral oil in power transformers. These new insulating liquids include synthetic ester liquid, natural ester liquid and gas-to-liquid (GTL). Considering the different characteristics between mineral oil and ester liquids, IEEE published related standards for the application of new insulating liquids in power transformers [67-69]. IEEE C57.147-2008 standard was initially published in 2008 and concerned the acceptance and maintenance of natural ester fluids in transformers [67], and was revised in 2018 [69]. Meanwhile, IEEE C57.155-2014 standard concerned the interpretation of gases generated in natural ester and synthetic ester immersed transformers and was published in 2014 [68].

As the above highlights, the DGA technique has advanced significantly within the last 50 years and is widely used and regarded as one of the most effective diagnostic techniques for detecting incipient faults in transformers. The application of DGA can not only be conducted offline but can also be applied in real time today after the creation of online monitors. The condition of a transformer can be measured more frequently via online monitoring than via an offsite laboratory analysis. Several interpretation methods are specified in IEC and IEEE standards to help analyse DGA results [22, 24]. Meanwhile, with the increasing application of environmental friendly

insulating liquids, the DGA investigation is still important in laboratory research to understand fault gases behaviours in different transformer insulations under different transformer stresses.

2.2.2 DGA related fault types

In early investigations of the DGA technique, the causes of faults in transformers mainly concerned corona (partial discharge), thermal heating and arcing problems [54]. DGA related transformer incipient faults were then specified by categorising them as either electrical faults or thermal faults in both IEC and IEEE standards [22, 24].

IEEE 60599-2016 [24] defines electrical faults as a partial or disruptive discharge through the insulation. A partial discharge fault is an electric discharge that only partially bridges the insulation between conductors. A partial discharge can occur inside the insulation or adjacent to a conductor. Disruptive discharges are defined as the passage of an arc following a breakdown and normally include arcing, breakdown or short circuits. Using the DGA technique, the electrical faults are split into three types including Partial Discharge (PD), Discharge of Low Energy (D1) and Discharge of High Energy (D2) [22, 24]. Partial Discharge mainly focuses on a corona type partial discharge. Discharge of Low Energy includes sparking, tracking and small arcing. Discharge of Higher Energy includes arcing with power follow-through [70].

Thermal faults are generally caused by an excessive temperature rise in the insulation or any internal component. The cause of the temperature rise can be insufficient cooling, excessive currents circulating in adjacent metal parts or through the insulation, overheating of bushing connection lead or internal winding and overloading [24]. With DGA techniques, thermal faults can be classified into three temperature ranges, which are T1, a temperature lower than 300 ºC, T2, a temperature higher than 300 ºC but lower than 700 ºC, and T3, a temperature higher than 700 ºC. It is generally acknowledged that the thermal faults can cause the carbonisation of paper

or oil and even metal coloration and fusion [24]. Table 2-1 summarises DGA fault types and related visually detectable evidence through the internal inspection of hundreds of faulty transformers [22].

Table 2-1 DGA fault types and related visually detectable evidence [22]

		Visually detectable evidence
Electrical faults		
PD	**Partial Discharge**	Corona type: possible X-wax deposition on paper insulation Sparking type: pinhole and carbonised perforations in paper
D1	**Discharge of Low Energy**	Larger carbonised perforations through paper Carbonisation of the paper surface or carbon particles in the oil
D2	**Discharge of High Energy**	Extensive destruction and carbonisation of paper Metal fusion at the discharge extremities Extensive carbonisation of the oil Tripping of the equipment
Thermal faults		
T1	**T < 300 ºC**	Paper turns brownish
T2	**300 ºC < T < 700 ºC**	Carbonised paper
T3	**T > 700 ºC**	Carbonisation of the oil Metal coloration and fusion

In the latest IEEE C57.104-2019 [22], five additional sub-types of faults have been added. These five sub-types of faults are listed in Table 2-2 [22]. It needs to be noted that these fault sub-types should only be considered and identified after confirming one of the fault types listed in Table 2-1.

Table 2-2 DGA fault sub-types [22]

S	Stray gassing at temperatures lower than 200 ºC
O	Overheating without carbonisation of paper, lower than 250 ºC

C	Possible paper carbonisation
T3-H	T3 thermal faults in mineral oil only
R	Catalytic reaction

2.2.3 DGA related fault gases

The DGA identifies fault gases generated from the decomposition of the insulation under electrical or thermal faults, or both. Normally, DGA related fault gases are hydrogen, methane, ethane, ethylene, acetylene, carbon monoxide and carbon dioxide. Meanwhile, non-fault gases, oxygen and nitrogen, are also measured [22, 24]. The gases are also divided into combustion gases and non-combustible gases. The combustion gases mainly include hydrogen, hydrocarbon gases and carbon monoxide, and non-combustible gases, include carbon dioxide, oxygen and nitrogen. The unit for the expression of the concentration of dissolved gases is microliters per litre (ul/l) or as parts per million by volume (ppm) [22].

The generation and formation of fault gases refer to two types of mechanisms including the decomposition of oil and the decomposition of cellulose insulation [22, 24].

2.2.3.1 Decomposition of oil

The breakdown of oil molecules can be caused by energy dissipating from overheating and electrical discharges. Different levels of energy are required to break or form different types of chemical bonds. Moreover, the decomposition mechanism can differ for the various types of insulating liquid [5].

In mineral oils, the decomposition is highly linked to different hydrocarbon molecules. C-C molecular bonds link hydrocarbon molecule CH_3, CH_2 and CH groups together. Due to electrical and thermal faults, the scission of some of the C-C bonds and C-H bonds can result in the formation of small unstable fragments in different forms [24]. These small unstable fragments can recombine rapidly into different gas molecules

like hydrogen, methane, ethane, ethylene and acetylene via complex reactions. The structures of these products are shown in Figure 2-1 [5]. These fault by-products dissolve in oil as dissolved gases or are released to the headspace as free gases if the generation is in a large quantity [5, 24]. Meanwhile, there are some other by-products, including C_3 and C_4 hydrocarbon gases, carbon solid particles and hydrocarbon polymers [24].

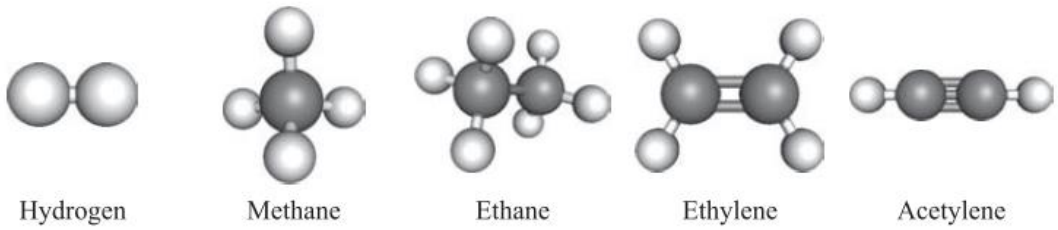

Figure 2-1 Main hydrocarbon gases produced by decomposing oil [5]

The scission of the weakest C-H bonds require 338 kJ/mol and is mainly caused by low energy faults [24]. The scission of the C-C bonds and the recombination into different bonds requires more energy from high energy discharges or high temperatures. The formation of a C-C single bond requires 607 kJ/mol, 720 kJ/mol for a C=C double bond and 960 kJ/mol a C≡C triple bond [24].

Methane and ethane are produced by a lower energy discharge and low temperature thermal faults [22]. Ethylene is mainly produced by thermal faults when the temperature is over 500 ºC but can still be generated in lower temperature thermal faults in a small quantity [24]. Higher temperatures and higher energy discharges can result in the production of acetylene [22, 24]. Hydrogen is the predominant gas produced by a partial discharge. In addition, carbon particles are formed between 500 ºC and 800 ºC, and are observed after arcing in oil or around very hotspots [24].

For ester liquids, the fundamental steps of the decomposition of esters under electrical faults or thermal faults are the same as mineral oil that include the scission of C-C bonds and C-H bonds. The same fault gases can be produced under the recombination of hydrogen and hydrocarbon fragments. However, there are differences in the

production, proportions and solubility of generated gases due to the abundance of the ester groups and carbon chains when compared with mineral oils [68]. Carbon monoxide and carbon dioxide can be produced abundantly from ester liquids under thermal faults. With the increasing temperature, the amount of carbon oxide gases generated also increases. What's more, due to the particular chemistry of esters, more carbon monoxide is generated than carbon dioxide [68]. Methane, ethane and ethylene can be produced in larger amounts at lower temperature overheating, resulting in different proportions compared to mineral oil. At the highest temperatures, the production of methane and ethane are similar to those produced in mineral oils. Meanwhile, ethane can be produced without a fault if the ester liquid contains linolenic acid [68].

2.2.3.2 Decomposition of cellulose insulation

Another important component of the insulation system is solid insulation. The solid insulation mainly includes Kraft paper, pressboard and other solid supporting structure [1]. The energy that causes the breakdown of insulating liquid can also cause the breakdown of solid insulation material [5]. The large number of anhydroglucose rings, weak C-O molecular bonds and glycosidic bonds are thermally less stable than hydrocarbon molecular bonds in insulating liquids and result in the decomposition of cellulosic insulation that can happen at lower temperatures. When the temperature is above 105 ºC, significant polymer chain scissions can occur. When the temperature is further increased to higher than 300 ºC, complete decomposition and carbonisation can occur. The by-products not only include carbon monoxide, carbon dioxide and water but also include minor amounts of hydrocarbons, furans and other compounds [24]. The structures of these by-products are shown in Figure 2-2 [5]. Among those by-products, furans are another important indicator confirming whether cellulosic insulation experiences aging or faults [71].

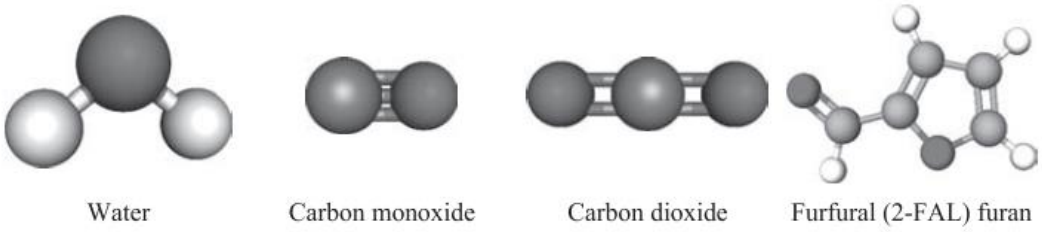

Figure 2-2 Products produced by cellulose decomposition [5]

2.2.4 DGA related non-fault gases

2.2.4.1 Stray gassing

Besides the generation of fault gases caused by the decomposition of oil and cellulosic insulation, the formation of gases can also be caused by another gas production mechanism called stray gassing. Stray gassing was defined in CIGRE TF 15/12.01.11 in 2006 as the formation of gases from insulating mineral oils heated at relatively low temperatures (90 ºC to 200 ºC) [70]. Two test procedures for stray gassing at 120 ºC and 200 ºC of pure oil system were introduced in CIGRE TF 15/12.01.11 [70]. It is shown that the main gas produced was hydrogen and then methane under 120 ºC test procedures, whilst the main gases produced under 200 ºC test procedures were methane and ethane [70]. ASTM D7150-05 also introduced the method to test stray gassing [72]. The difference is that hydrogen can be produced from oils sparged with air and that more hydrocarbons, in relation to hydrogen, are produced from oils sparged with nitrogen [73]. In addition, IEC 60296-2012 standard [74] presented that inhibited oils produce less stray gassing than uninhibited oils.

What's more, numerous researchers had investigated stray gassing. Some unusual cases of gassing in in-service transformers were reported in 2006 [75], which indicated that the production of gases due to stray gassing could be affected by oxidation, transformer materials, type of insulating oil, type of transformers and manufacture. The formation of gases can reach a plateau status and then stop due to the reduction of the oxygen content in oil. The same experiment result was also obtained in [70, 76]. Both studies in [73, 77] revealed that ethylene can be generated at

low temperatures as stray gas. In addition, a reliable way to contain samples for stray gassing measurements was presented in [78] and concerns using syringes sealed with vacuum grease. Some methods preventing the generation of stray gas were introduced in [79], such as the use of high grade inhibited oils, removal of oxygen, cooling optimisation and reclamation. On the other hand, stray gassing in ester liquids has also been investigated in [35, 68]. Stray gassing occurred in natural esters containing linolenic acid. Ethane can be easily generated due to oxidation and higher amounts of linolenic acid.

The products of stray gassing under low temperature heating are not related to electrical or thermal faults [80]. After the observation of stray gassing at lower temperatures, stray gassing might interfere with the DGA evaluation [70, 75]. Stray gassing might be mistaken as a corona partial discharge, T1/T2 thermal faults or catalytic reactions on the metal surface. Regular checks on transformers and gas increase rates can help identify stray gassing or faults [75]. In addition, establishing a trending baseline is considered a good way to monitor the stray gassing phenomenon [68].

2.2.4.2 Other sources of gases

In some cases, gases can be generated through rusting or other chemical reactions involving steel, uncoated surfaces or protective paints [24]. The same as stray gassing of oil, the generation of these gases is not caused by faults. Hydrogen and hydrocarbons may be formed in new steel and then absorbed during the manufacturing process, or produced by welding and slowly released into the oil. Meanwhile, gases can also be formed by exposing oil to sunlight or formed in internal transformer paints, such as alkyd resins and modified polyurethanes containing fatty acids [24].

2.2.5 Identification of DGA results

2.2.5.1 General identification

Hydrogen is primarily generated from a corona partial discharge, sparking discharges and arcs. Meanwhile, hydrogen can also be generated from stray gassing and a chemical reaction with galvanised steel [22]. For hydrocarbons, methane, ethane and ethylene are generated from the heating of oil and paper. The generation of acetylene is a special indicator and can be generated from oil and paper under high energy faults, such as arcing and high temperatures [22]. For carbon oxide gases, the generation of carbon monoxide and carbon dioxide are mainly from the thermal heating of cellulosic insulation material and insulation liquids, particularly ester liquids [22].

Figure 2-3 is an example showing the relative percentage of dissolved gas concentrations in mineral oil as a function of temperature and fault type [22]. It shows that hydrogen accounts for a high proportion in electrical faults. Methane accounts for a higher proportion in the T2 fault range. Ethane accounts for its highest proportion in the T1 fault range and ethylene in the T3 fault range. Although acetylene accounts for a small proportion in the T3 fault range, the occurrence of acetylene provides evidence that the fault energy has already reached a high level.

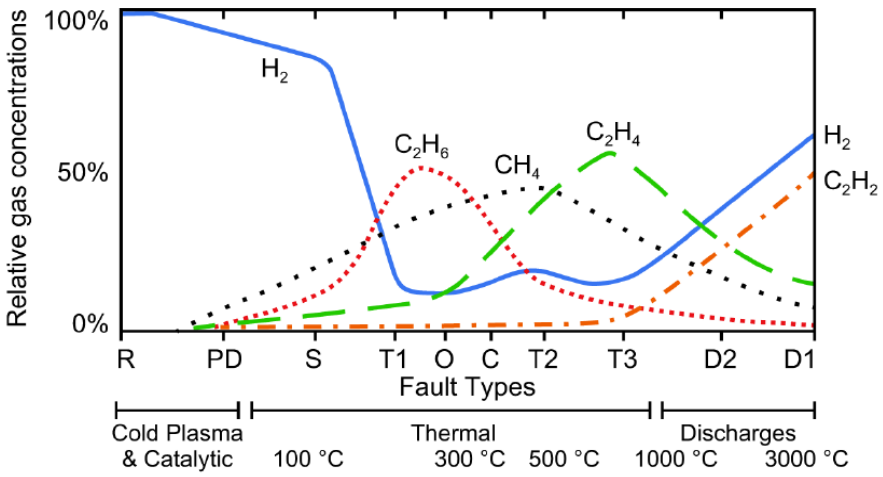

Figure 2-3 Relative percentage of dissolved gas concentrations in mineral oil as a function of temperature and fault type [22]

2.2.5.2 Gas ratios

Three common basic gas ratios based on hydrogen and hydrocarbons are used to interpret DGA results and identify fault types. These three basic ratios are reported in IEC 60599-2016 [24] as C_2H_2/C_2H_4, CH_4/H_2 and C_2H_4/C_2H_6. Normally, the combination of these three basic ratios with their gas ratio limits can indicate each of the six broad fault classes (shown in Table 2-3 [24]).

Table 2-3 DGA interpretation table based on three basic ratios [24]

Case	C_2H_2/C_2H_4	CH_4/H_2	C_2H_4/C_2H_6
PD	NS[a]	< 0.1	< 0.2
D1	> 1	0.1-0.5	> 1
D2	0.6-2.5	0.1-1	> 2
T1	NS[a]	> 1 but NS[a]	< 1
T2	< 0.1	> 1	1-4
T3	< 0.2[b]	> 1	> 4

a NS = Non-significant whatever the value.

b An increasing value of the amount of C_2H_2 may indicate that the hot spot temperature is above 1000 ºC

Besides these three ratios, there are three more ratios used to identify specific fault types. These ratios include C_2H_2/H_2, O_2/N_2, and CO_2/CO [24].

The ratio C_2H_2/H_2 in a power transformer's main tank can indicate contamination of its on load tap changer (OLTC). Gases produced from the operation of the OLTC through a low energy discharge may diffuse between the OLTC compartment and the main tank, or between the respective conservators, then contaminate the oil in the main tank. If contamination occurs, the ratio is higher than 2 to 3. It should be noted that the gas decomposition pattern in the OLTC caused by a low energy discharge is different from that in the main tank. This identification can be confirmed by comparing DGA results in the main tank, in the OLTC and in the conservators. [24].

In the conservator of air-breathing equipment or sealed equipment that have a leakage, dissolved oxygen and nitrogen can be detected due to it coming into contact with atmospheric air. The concentration of oxygen and nitrogen are around 32000 ppm and 64000 ppm when at equilibrium status [81], leading to a O_2/N_2 ratio of around 0.5. However, if oxygen is consumed more rapidly than replaced by diffusion, such as oil oxidation or paper ageing, the O_2/N_2 ratio will decrease. A ratio lower than 0.3 can indicate excessive oxygen consumption. Also, the latest IEEE C57.104-2019 suggests that a ratio decrease can indicate overheating and oxidation of mineral oil, and also can confirm thermal faults [22].

The ratio CO_2/CO is more complex and has evolved through revision in the standards. There is common consensus that carbon monoxide and carbon dioxide are good paper related fault indicators. Degrading cellulose insulation can result in an increase in the carbon monoxide concentration, leading to the decreasing of CO_2/CO ratio. The interpretation in IEEE C57.104-2019 is the latest interpretation [22] and suggests that a low CO_2/CO ratio (< 3) together with the formation of hydrocarbon gases may be an indicator of a paper related fault, while a high CO_2/CO ratio (> 20) and high furan values can reveal slow paper degradation at low temperatures. Moreover, in order to improve accuracy, the carbon monoxide and carbon dioxide concentrations in oil should exceed 1000 ppm and 10000 ppm respectively. The CO_2/CO ratios considered above are all based on the investigation of mineral oils, with there being fewer publications or standards using the CO_2/CO ratio to interpret faults in ester liquids. IEC C57.155-2014 [68] introduces a guide for interpreting gases generated in ester liquid immersed transformers, with interpretation of the CO_2/CO ratio being the same as the one introduced in IEEE C57.104-2009 [47], which suggests a ratio for a normal condition being higher than 7.

2.2.5.3 Fault identification methods

There are five fault identification methods in total presented in latest version of IEEE C57.104-2019 [22] including the Key Gas Method, the Doernenburg Ratio_Method,

the Rogers Ratio Method, the Duval Triangle Method and the Duval Pentagon Method.

The Key Gas Method uses typical or predominant gases to identify four general fault types. The typical gases are divided into main gas and secondary gases to help accurately identify different faults. This method is summarised in Table 2-4 [22]. When the main gas formed in the DGA results is one of the four main gases in column 1, together with the secondary gases in column 2, the relevant fault listed in column 3 can be identified. The disadvantage of the Key Gas Method concerns incorrect fault identification or many inconclusive cases due to it being difficult to classify the main gas because there may be more than one main gas.

Table 2-4 The Key Gas Method [22]

Key gas	Typical proportions of generated combustible gases	Fault type
CO	Predominantly CO with much smaller quantities of Hydrocarbon Gases	Thermal mineral oil and cellulose
C_2H_4	Predominantly C_2H_4 with smaller proportions of C_2H_6, CH_4 and H_2	Thermal mineral oil
H_2	Predominantly H_2 with small quantities of CH_4, and traces of C_2H_4 and C_2H_6	Electrical low energy partial discharge (PD)
H_2 and C_2H_2	Predominantly H_2 and C_2H_2 with minor traces of CH_4, C_2H_4 and C_2H_6. Also, CO if cellulose is involved.	Electrical high energy (arcing)

The Doernenburg Ratio Method, initially developed by Dornenburg in 1974 [64] and specified in IEEE C57.104-1978 [59], uses gas concentration ratios to indicate three fault types. It uses six gases as four gas ratios to help identify faults. The method is summarised in Table 2-5, based on IEEE C57.104-2019 [22]. The ratios differ when the fault gases are extracted from either the oil phase or gas phase. In order to use this

method and make a final decision, some validation tests are needed in advance. Validation test L1 creates a critical level for each gas (listed in Table 2-6 [47]). These concentrations are defined as special gas concentration values used to ascertain whether there really is a problem with the unit and then whether there is sufficient generation of each gas for the ratio analysis to be applicable [47]. When applying this identification method, at least one gas from each ratio needs to be higher than the concentration listed in L1. The disadvantages of Doernenburg Ratio Method include the fault identifications being limited to three types that do not cover the full spectrum of fault types, and the limitation of L1 concentrations needing to be overcome [82]. This method is a little out dated and not widely used now [22].

Table 2-5 The Doernenburg Ratio Method [22]

Suggested fault diagnosis	**Ratio 1 (R1) CH_4/H_2**		**Ratio 2 (R2) C_2H_2/C_2H_4**		**Ratio 3 (R3) C_2H_2/CH_4**		**Ratio 4 (R4) C_2H_6/C_2H_2**	
	Oil	Gas	Oil	Gas	Oil	Gas	Oil	Gas
Thermal decomposition	> 1.0	> 0.1	< 0.75	< 1.0	< 0.3	< 0.1	> 0.4	> 0.2
Corona (low intensity PD)	< 0.1	< 0.01	Not significant		< 0.3	< 0.1	> 0.4	> 0.2
Arcing (high intensity PD)	> 0.1 < 1.0	> 0.01 < 0.1	> 0.75	> 1.0	> 0.3	> 0.1	< 0.4	< 0.2

Table 2-6 L1 critical level for each gas [47]

Gas	**H_2**	**CH_4**	**CO**	**C_2H_2**	**C_2H_4**	**C_2H_6**
Limit	100 ppm	120 ppm	350 ppm	1 ppm	50 ppm	65 ppm

The Rogers Ratio Method was initially developed by R. R. Rogers in 1978 [53] and was also specified in IEEE C57.104-1978 [59]. Five gases as three gas ratios are calculated to help identify faults. The Rogers Ratio Method is summarised in Table 2-7, based on IEEE C57.104-2019 [22]. Initially, the Rogers Ratio Method included

four gas ratios and twelve suggested fault identification results, but in the improved version, the ratio C_2H_6/CH_4 was deleted and the fault identification results simplified to six types. One of these six types is the normal operation condition, which is considerably different when compared to other methods [22, 53]. This method can be used to detect more thermal fault types than the Dornenburg Ratio Method. Although this method is effective, data misinterpretation can still occur. Moreover, it cannot classify multiple faults [82].

Table 2-7 The Rogers Ratio Method [22]

Case	C_2H_2/C_2H_4	CH_4/H_2	C_2H_4/C_2H_6	Suggested fault diagnosis
0	< 0.1	0.1 to 1.0	< 1.0	Unit normal
1	< 0.1	< 0.1	< 1.0	Low energy density arcing – PD
2	0.1 to 0.3	0.1 to 1.0	> 3.0	Arcing – high energy discharge
3	< 0.1	0.1 to 1.0	1.0 to 3.0	Low temperature thermal
4	< 0.1	> 1.0	1.0 to 3.0	Thermal < 700 ºC
5	< 0.1	> 1.0	> 3.0	Thermal > 700 ºC

Concerning the Duval Triangle Method, the first Duval Triangle version was introduced in 1974 [83]. The method used three dissolved gases and located in a triangle shape to make a diagnosis. In the latest IEEE C57.104-2019 [22], there are three Duval Triangle types used to identify different faults based on different dissolved gases. Duval Triangle 1 is used to indicate all fault types. Duval Triangle 4 and Duval Triangle 5 are used to identify the sub-type fault after the main fault has been identified using Duval Triangle 1.

Duval Triangle 1 uses three gases including methane, ethylene and acetylene. These three gases represent different faults. Methane represents low energy and low temperature faults, ethylene high temperature faults and acetylene very high energy, high temperature and arcing faults. These gases are presented as a relative percentage on each side of the triangle, as shown in Figure 2-4 [22]. The advantages of Duval Triangle 1 are that all six basic fault types, together with the mixture of electrical and

thermal faults in the DT zone, are covered in the identification. It can always identify a fault and allows to visually and rapidly follow the evolution of a fault in a transformer. However, the results can be unreliable and inaccurate when there are low level gas concentrations [82].

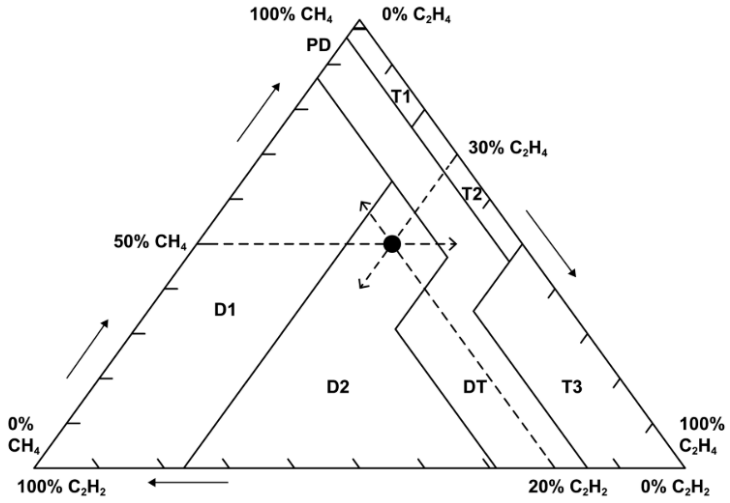

Figure 2-4 Example of the Duval Triangle 1 representation [22]

An example is shown in Figure 2-4 [22], with there being 25 ppm of methane, 15 ppm of ethylene and 10 ppm of acetylene. The relative percentages are 50%, 30% and 20%, respectively. The point is dropped in the D2 zone which zone represents a D2 electrical fault. The methods used to calculate the relative percentages of these three gases are shown below:

$$\%C_2H_2 = \frac{x}{x+y+z} \times 100 \quad \textbf{(2-1)}$$

$$\%C_2H_4 = \frac{y}{x+y+z} \times 100 \quad \textbf{(2-2)}$$

$$\%CH_4 = \frac{z}{x+y+z} \times 100 \quad \textbf{(2-3)}$$

Where: x represents C_2H_2, y represents C_2H_4 and z represents CH_4.

The Duval Pentagon Method was initially published in 2014 [84]. There are two types of Duval Pentagon which are Duval Pentagon 1 and Duval Pentagon 2. Five dissolved gases are used in Duval Pentagon 1 to identify six basic faults and also the stray

gassing of mineral oil (S). The same as Duval Triangles 4 and 5, Duval Pentagon 2 can be used to identify sub-type faults after the main fault has been identified using Duval Pentagon 1 (see Figure 2-5 for Duval Pentagon 1 [22]). The calculation of the relative gas percentages is similar to the calculation method reported in the Duval Triangle Method.

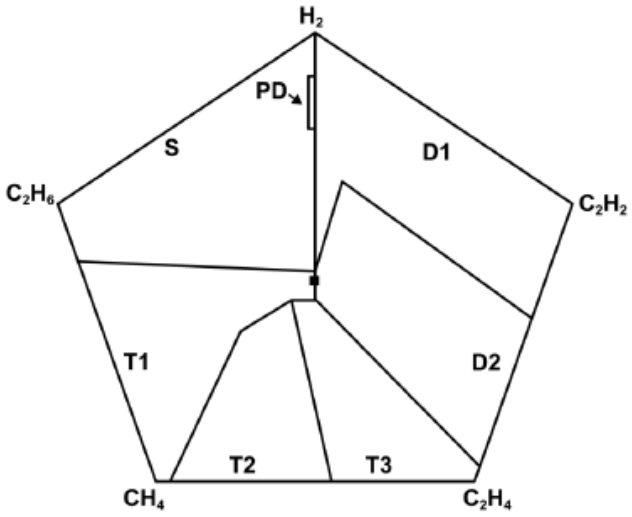

Figure 2-5 The Duval Pentagon 1 Method [22]

Also, the Duval Triangle Method and Duval Pentagon Method also have versions for analysing faults that happen in synthetic ester liquid (see Figure 2-6 [85] and Figure 2-7 [86], respectively).

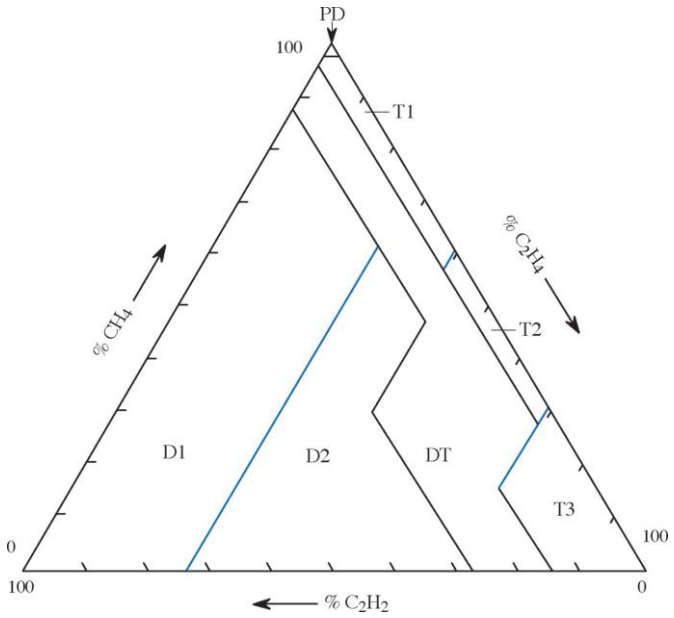

Figure 2-6 Duval Triangle for synthetic ester liquid [85]

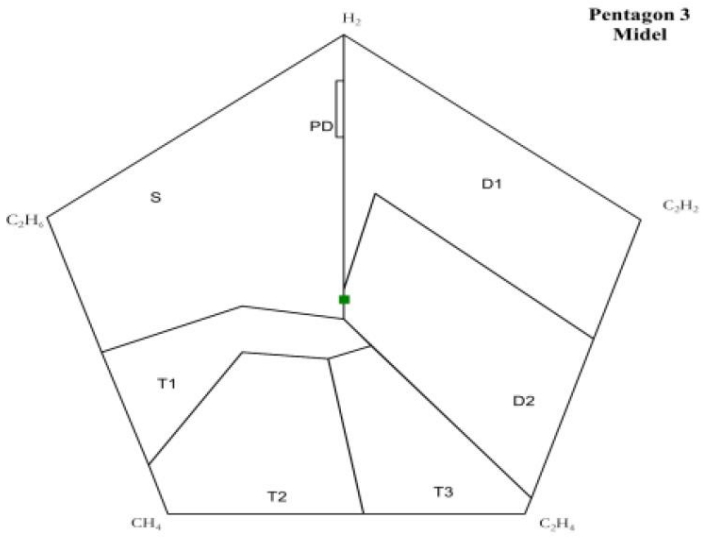

Figure 2-7 Duval Pentagon for synthetic ester liquid [86]

2.3 Review of Existing Experimental Methods to Simulate Thermal Faults

2.3.1 Oven-heating method

An oven-heating method setup was designed in [25] (see Figure 2-8). The maximum temperature can be achieved using the oven-heating method is in T1 thermal fault range. The insulation experienced a uniform temperature provided by the oven. The method was also used in accelerated thermal ageing experiments. Specially designed bottles that could suffer from vacuum and excessive pressure were used to hold oil or oil-paper insulation. A temperature resistant screw-cap was fit with a PTFE-coated silicon seal and matching pouring ring to seal the gas bottles tightly. Meanwhile, the headspace in the bottles was filled with argon. The maximum temperature achieved by this design was 260 ºC based on the oven working temperature and features of the materials. The oven-heating method was also used in [21] to investigate fault gases that evolved after low temperature thermal faults in both oil and oil-paper insulation systems. The samples were sealed in glass bottles and heated using an air circulating oven at temperatures of 90 ºC, 150 ºC and 200 ºC for different periods up to 14 days.

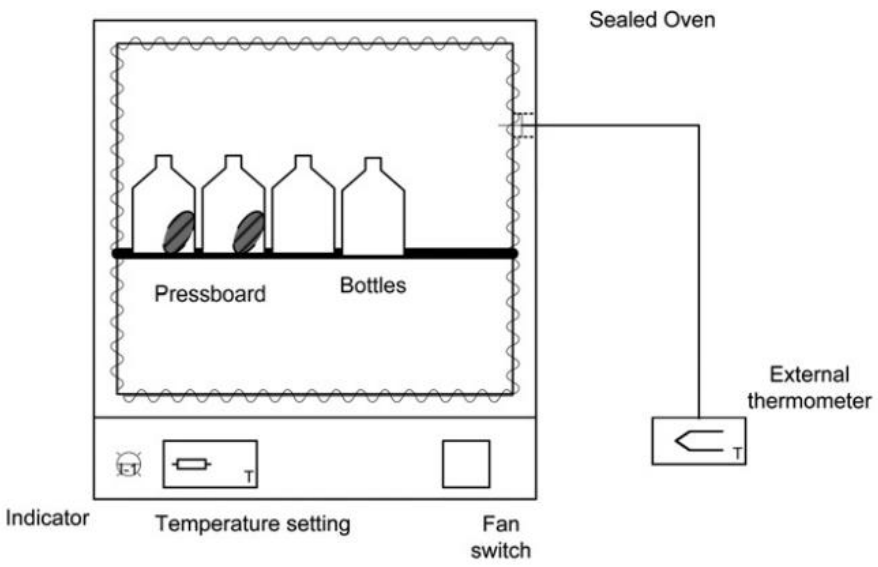

Figure 2-8 Oven-heating setup designed in [25]

2.3.2 Immersed-heating method

In 1999, a DGA thermal test setup was published to analyse the relation between faults and generated gases in transformer liquids [26]. The test setup is shown in Figure 2-9. The method used to maintain thermal faults was the immersed-heating method that used a Konstantan made heating wire. The heat element was fixed by a Borosillicat test vessel and a Teflon-cover using clamps. A NiCrNi-temperature sensor was used to monitor the temperature of the liquid around the heating element. A power current transformer was employed to deliver current to the heating element to create the thermal faults. The temperature was regulated by an amperemeter connected to the primary and secondary circuits. The generated gases entered the funnel-shaped Teflon device over the heating element and then passed through the burette to be further analysed. Meanwhile, an equalising vessel was installed for safety reasons. The reported temperature achieved by this setup was 1000 ºC.

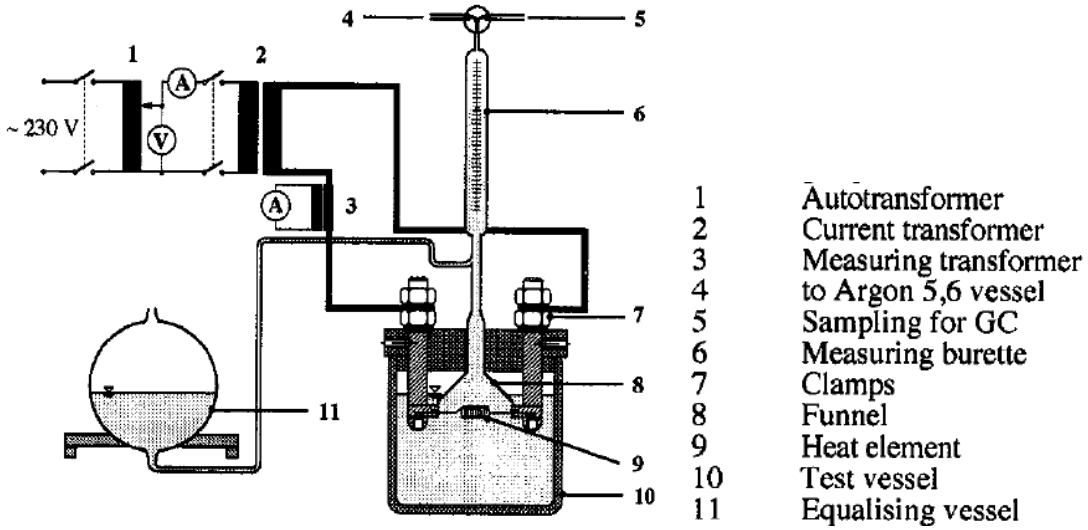

Figure 2-9 Immersed heating setup designed in [26]

Other three similar immersed-heating method setups were designed to investigate the gassing behaviour of various alternative dielectric fluids under thermal stress in 2011 and 2012 [28-30]. In [28, 29], the heating wire material was a special metal called Resistherm NiFe 30 with a diameter of 0.6 mm. To achieve different temperatures, heating wire with different lengths were used. By measuring the voltage and current, the average temperature could be calculated as the heating element had the property of being able to change its resistivity linearly across a wide temperature range up to 550 ºC. In [30], the heating element was made from copper and it was blended into the shape shown in Figure 2-10. The dimension of the heating element was 150 mm in length and 1.5 or 1.9 mm in diameter. Two holes were drilled on the heating element so that the thermocouples could be inserted into the holes to achieve a better contact between the sensor tip and the heating element. During the experiments, the maximum temperature measured by the thermocouples in natural ester insulating liquid FR3 was 600 ºC. The maximum temperature measured by the thermocouples in mineral oil Gemini X was 400 ºC but the actual temperature was apparently much higher than 400 ºC since the heating element would melt down, indicating a local temperature of 1100 ºC (the melting point of copper) being reached. For both of the immersed-heating experimental setups in [28-30], the same funnel-shaped device was used to collect generated gases. In addition, two syringes were used for different functions. One syringe was placed on the top of the funnel to collect the free gases generated during

the experiment. The other one syringe was installed bypass aside for thermal expansion.

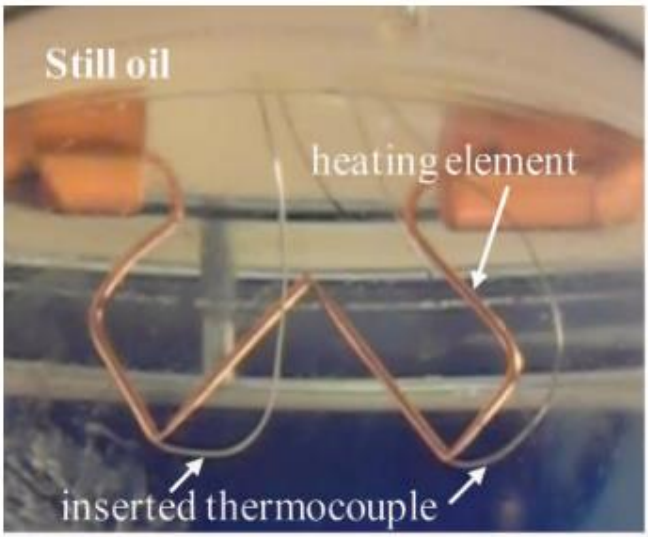

Figure 2-10 The shape of the heating element in [30]

In 2018, researchers found that the temperature of the immersed heating element was limited by the pooling phenomenon [31]. The same test setup was used as in [30] but with a different structure of heating element. It was a straight Kanthal A-1 heating element made from iron, aluminum and chromium that had a melting point of 1400 ºC. The method used to measure the temperature of the heating element was a thermocouple embedded in a ceramic thermocouple insulator inside the coil. Other thermocouples were also used to measure temperature distribution in oil around the heating element. Based on a series of experiments, the temperature of the immersed heating element was limited by the pool boiling theory and there was a temperature range that the heating element could not provide stable heating temperature. Therefore, some thermal fault levels could not be achieved using the immersed-heating method.

Concerning the heating process in insulating liquid, there were three regions include the natural convection region, nucleate boiling region and film boiling region. During the heating process in the natural convection region, the temperature of the heating element could increase with an input power increase. However, in the nucleate boiling region, the temperature of the heating element would remain stable even if the input

power was increasing. This was due to the energy being dissipated by vaporisation and strong oil convection. Once the input energy exceeded the critical heat flux (CHF, indicates the upper limit of the nucleate boiling region) point, the temperature of the heating element would reach from the stable temperature in the nucleate boiling region directly to the heating element's melting point temperature. Thus, the immersed-heating method could not reach temperatures between the Nukiyama temperature (temperature at the CHF point) and the burnout temperature. The Nukiyama temperature depended on the boiling point of the liquid, with a higher boiling temperature leading to a higher Nukiyama temperature.

In 2019, an immersed-heating setup was published in [32] (see Figure 2-11). The pool boiling phenomenon was considered in this study and the tested temperatures were below 450 ºC. The main vessel was a gas tight chamber made from glass tube and polyacetal base and lid. The dimension of the glass tube was 107 mm in diameter and 130 mm in height. Different from the funnel-shaped design, a lid was directly installed on the main vessel. Three components could be inserted in the lid, which were current carrying wires, a temperature probe and a copper pipe. The copper pipe was used to monitor the pressure and sample gas samples above the surface of the insulating liquid. The temperature achievement ability of the heating method was confirmed using an IR camera. Steel wire of 40 mm in length and 0.6 mm in diameter was used as the heating element. The temperature was 450 ºC in esters and 400 ºC in mineral oil for two hours. Different from other designs, a magnetic stirrer was placed under the chamber to help reduce the temperature gradient in the tested insulating liquid. Moreover, a water tank was employed in this design to help cool down the system and place the water level higher than the level of the tested insulating liquid.

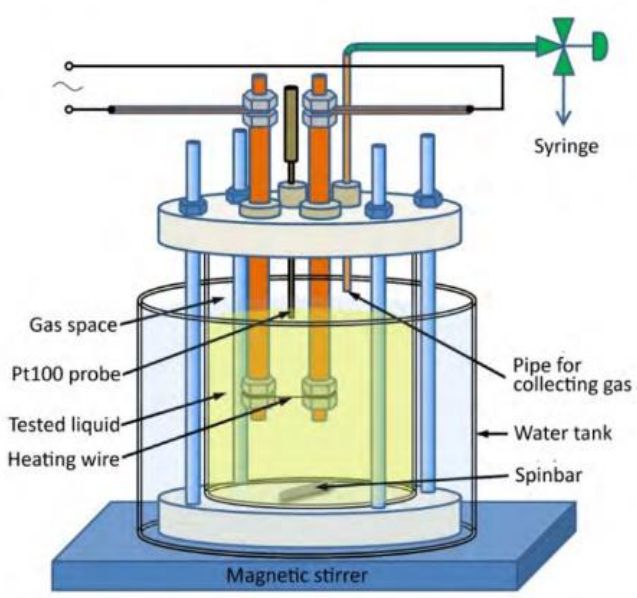

Figure 2-11 Immersed heating setup designed in [32]

There were a few immersed-heating experimental setups designed and conducted to investigate characteristics of the generated gases in an oil-paper insulation system under thermal faults. Normally, the investigation of an oil-paper insulation system has traditionally concerned thermal ageing at temperatures lower than 150 ºC, with the experiment period lasting hundreds of days. An immersed-heating experimental setup was designed in 2013 to study dissolved gases caused by the thermal degradation of insulating paper in transformer oil [87]. A heating unit was designed to create localised low temperature overheating up to 200 ºC (see Figure 2-12). For the heating part, a thermocouple was installed between two ceramic heaters and copper plates. Another thermocouple was used to monitor the oil temperature in the experiment chamber. There was 850 ml of transformer oil in the chamber during the experiment. The gas phase was filled with 400 ml of argon. The same test setup with some improvements was used to model the overheating degradation of oil-paper insulation in 2014 [88] (the complete diagram is shown in Figure 2-13). This design allowed for the removal of moisture and gas in the insulating oil using a vacuum pump. Moreover, the heating temperature and time could be controlled automatically by a heat control device. After the thermal stress, both the combustible gases in the oil phase and gas phase could be extracted and analysed by the GC system. The maximum reported temperature was 225 ºC.

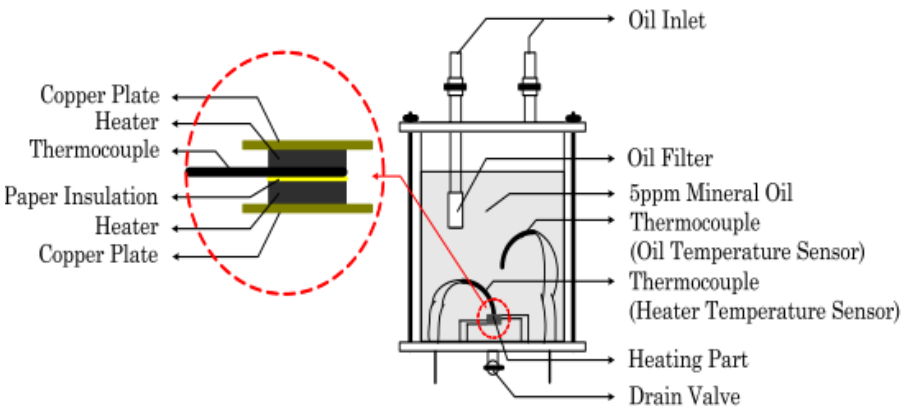

Figure 2-12 Schematic diagram for the chamber and heating unit setup deigned in [87]

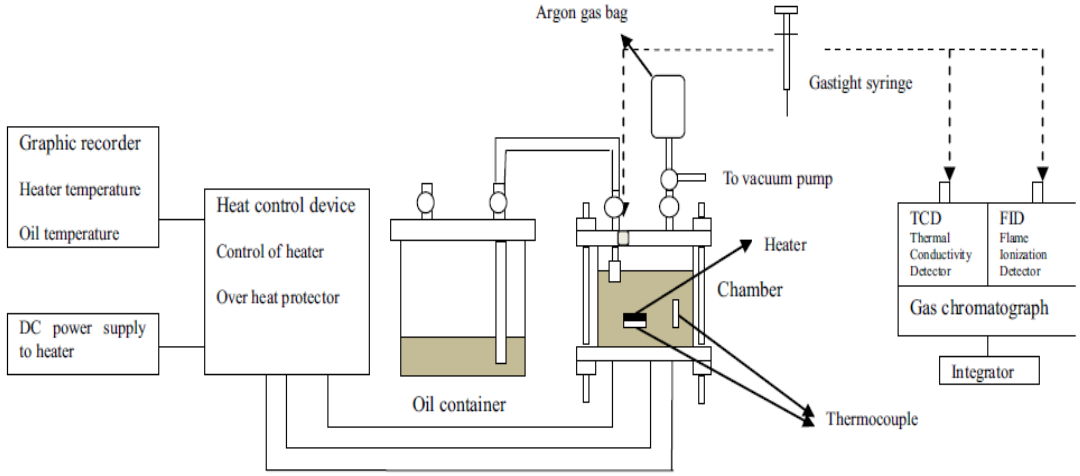

Figure 2-13 Diagnostic system to generate and measure overheating in [88]

2.3.3 Tube-heating method

The tube-heating method is another method used to conduct DGA thermal fault experiments. A tube-heating setup was published in 2012 (see Figure 2-14 [34]) in which the temperature achieved was reported to be from 300 ºC to 800 ºC. This tube-heating setup contained a pipe heater covered by a muffle furnace, an L-shaped stainless steel container. During the heating process, 30 ml of oil was heated in the pipe heater. The fault gases would diffuse to 5 L of oil in the L-shaped stainless steel container. The volume of the L-shaped stainless steel container was changed to a 0.5 L container in the study published in 2016 [36] leading to the measured concentration of fault gases being higher than before under the same fault condition. Meanwhile, a heat insulation thermocouple sensor was used to contact the surface of the heating tube to

reflect the approximate oil temperature.

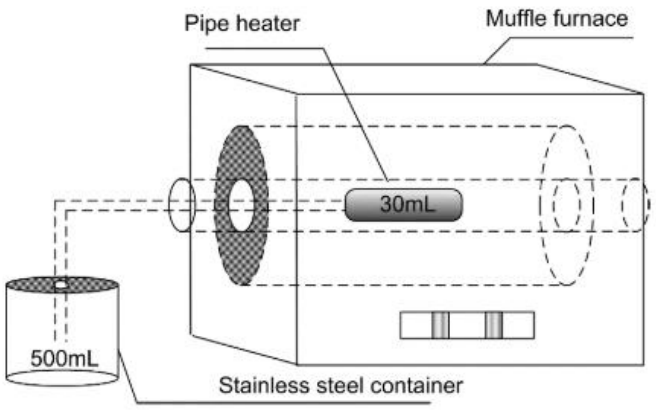

Figure 2-14 Tube heating setup designed in [34]

Another tube heating method test setup was designed by TJH2B [33, 35] (see Figure 2-15). A tank was used and divided into two phases which were a headspace phase and an oil phase. A high temperature oven was used to heat the tube to generate thermal faults. The insulating liquid in the system was circulated using a pump. Although the volume of the insulating liquid used in the test was 1.5 L, 100 L of free gases were generated from ester liquids under a 700 ºC thermal fault. So, a pressure expansion chamber device was installed on the top of the tank and a pressure gauge was used to detect the pressure. This system was reported to provide a fault temperature as high as 700 ºC.

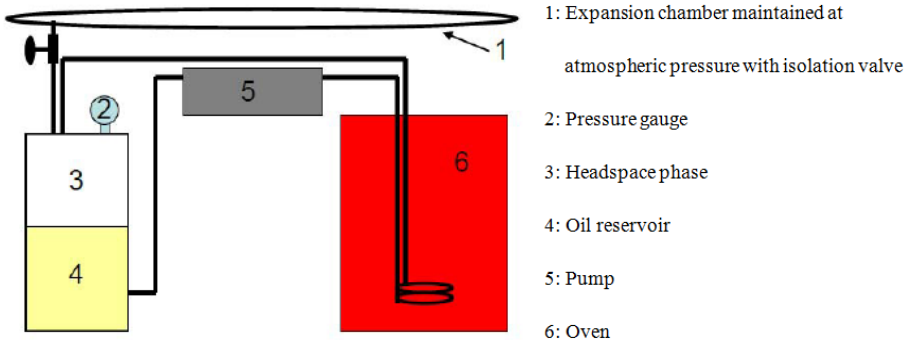

Figure 2-15 Tube heating setup designed by TJH2B [33, 35]

2.3.4 Comparison of the different heating methods

The summary of the reported temperature ranges of different studies is listed in Table

2-8. The tube-heating method achieved higher temperatures than the immersed-heating and oven-heating methods. The oven-heating method only simulated temperatures under the T1 thermal fault range. Due to the pool boiling theory, the immersed-heating method only generated a T1 thermal fault and had a limited temperature range of a T2 thermal fault. Although the maximum temperature achieved by the immersed-heating method can reach to the melting point temperature of the heating element, it is less controlled and depends on the material features of the heating element. The stable temperature simulated using the immersed-heating method is determined by the boiling point of the tested insulting liquid and the Nukiyama temperature. Normally, the maximum temperature achieved by the immersed-heating method is around 400 ºC. Meanwhile, the designs used to simulate thermal faults in an oil-paper insulation system also use the immersed-heating method. The simulated temperatures are lower than that in an oil only insulation system.

On the other hand, the tube-heating method provides a hotspot temperature like in real transformers. Fault gases are generated around the fault area and then diffused into the bulk oil in the oil container, which represents the overall insulating liquid in a transformer. The DGA measurements are based on oil samples from the oil container. It is the same as in transformers that the samples used for DGA measurements are sampled at the oil drain valve but not from fault area. Therefore, the conditions produced by the tube-heating method are closer to a real transformer and it has the ability to cover the whole range of DGA related thermal faults. There are no investigations on fault gas generation characteristics in an oil-paper insulation system under thermal faults using the tube-heating method.

Table 2-8 Summary of the reported temperature ranges of different studies

Heating method	Reported temperature range	Reference
Oven-heating	90 ºC to 200 ºC	[21]
	< 260 ºC	[25]
Immersed-heating	75 ºC to 200 ºC	[87]
	100 ºC to 300 ºC in oil only insulation; 150 ºC to 225 ºC in oil-paper insulation system	[88]
	330 ºC in mineral oil; 390 ºC in synthetic ester	[31]
	400 ºC in mineral oil; 450 ºC in ester liquids	[32]
	400 ºC in mineral oil; 600 ºC in natural ester	[30]
	300 ºC to 600 ºC	[28, 29]
	Up to 1000 ºC	[26]
Tube-heating	< 700 ºC	[33, 35]
	300 ºC to 800 ºC	[34, 36]

2.4 Review of Existing DGA Studies under Laboratory Simulated Faults

2.4.1 DGA studies in oil only insulation

2.4.1.1 Results based on the immersed-heating method

The immersed-heating setup in [26] was used to investigate the generation of different undissolved gases under 1000 ºC thermal fault in both mineral oil, SHELL DIALA D and ester liquid, MIDEL 7131. The results are shown in Figure 2-16 [26]. It is worth noting that the reported results were the dissolved gas concentrations released into the headspace. Both of the insulating liquids generated hydrogen and hydrocarbon gases under a 1000 ºC thermal fault, and the generation characteristics were similar. Hydrogen was the dominant gas, followed by methane and ethylene. However, as the solubility of different gases differ, the concentrations of key gases dissolved in

insulating liquids differed from the undissolved gases.

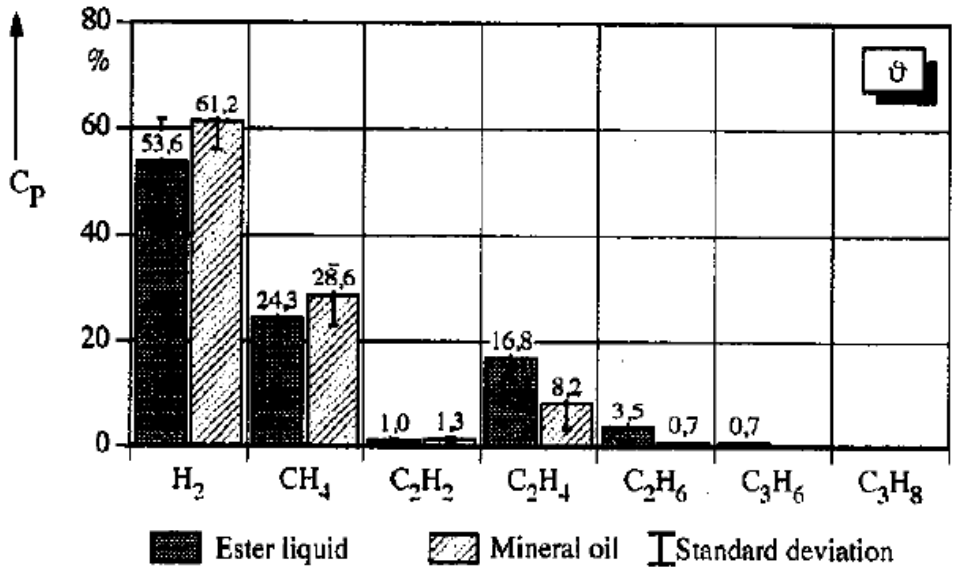

Figure 2-16 Concentration of different undissolved gases under a 1000 ºC thermal stress in [26]

The immersed-heating setup in [28, 29] was used to investigate the fault gas generation characteristics in mineral oil, Lyra X, and natural ester liquid, FR3. The tested temperatures for the mineral oil were 300 ºC and 400 ºC, while for the natural ester liquid were 300 ºC, 400 ºC, 500 ºC and 600 ºC. The maximum temperature achieved in the mineral oil was 400 ºC due to the cooling of the wire being very efficient in mineral oil. Table 2-9 [29] presents the fault gas generation results in mineral oil. Free gases were generated in mineral oil. It should be noted that the results in Table 2-9 were results without consideration of the free gases. The key gases at 300 ºC were carbon oxide gases and the key hydrocarbon gas was methane, while at 400 ºC, they were carbon monoxide and ethylene, with the key hydrocarbon gas being ethylene. Accordingly, more gases were detected in a 400 ºC thermal fault. In addition, acetylene was only clearly detected in the 400 ºC thermal fault.

Table 2-9 Dissolved gases in mineral oil under 300 ºC and 400 ºC thermal faults without consideration of free gases in [29]

	CO_2	C_2H_4	C_2H_2	C_2H_6	CH_4	CO	H_2
300 ºC (1.5 h)	57	8	< 1	2	20	510	11
400 ºC (1 h)	169	198	38	7	149	687	70

The fault gas generation results in natural ester liquid are shown in Table 2-10 [28, 29]. For all thermal fault temperatures, carbon monoxide and carbon dioxide were the key gases, and the dominant hydrocarbon gas was ethane. The other gases were also generated in high amounts. Propane and propylene were detected in the studies which have higher amounts compared with other hydrocarbon gases except ethane. In addition, the fault gas concentrations increased with the increasing thermal fault temperature, except for acetylene. Different from the mineral oil results, there were no free gases generated in natural ester liquid during the experiments.

Table 2-10 Dissolved gases in natural ester liquid under 300 ºC to 600 ºC thermal faults in [28, 29]

	300 ºC (6 h)	**400 ºC (6 h)**	**500 ºC (2 h)**	**600 ºC (1 h)**
CO_2	1353	2973	3698	3923
C_2H_4	27	209	631	1061
C_2H_2	<1	<1	<1	<1
C_2H_6	489	934	1005	1307
CH_4	33	214	351	453
CO	932	4219	3095	5148
C_3H_6	17	354	675	1158
C_3H_8	27	439	866	1520
H_2	92	278	472	382

Studies [28-30] showed that stable thermal fault temperatures higher than 400 ºC could not be achieved using the immersed-heating method. The investigations in [31] firstly pointed out that the temperature of the heating element in oil only experiments was limited by the boiling points of the insulating liquids, leading to the high temperatures not being achieved using the immersed-heating method. The pool boiling curves for mineral oil, Gemini X, and synthetic ester liquid, MIDEL 7131, are shown in Figure 2-17 [31]. There were three different regions including the natural convection region, nucleate boiling region and film boiling region. In the natural convection region, the boiling curves of both insulating liquids overlapped with each

other. In the nucleate boiling region, the heater surface temperature in Gemini X was between 320 ºC and 330 ºC, and between 380 ºC and 390 ºC in MIDEL 7131. In the film boiling region, the heating was inhomogeneous and the heating element likely to burnout. In Gemini X, the temperature jumped to over 1000 ºC and was measured by the thermocouples due to the red-hot zone being near the thermocouple location. However, the highest temperature measured in MIDEL 7131 was about 410 ºC, which might be caused by the hot-zone not being near the thermocouple location. Accordingly, the immersed-heating method can only achieve a stable temperature in the nucleate boiling region, with the maximum temperature for Gemini X being 330 ºC and for MIDEL 7131 390 ºC.

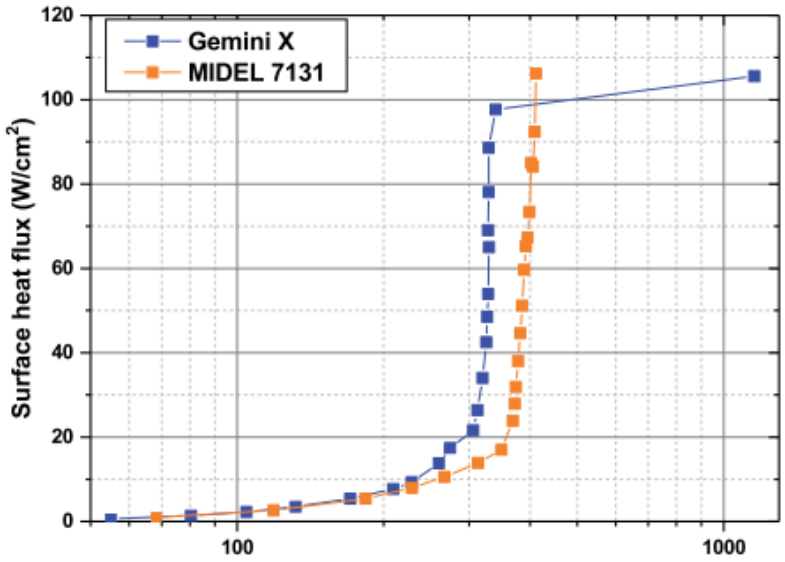

Figure 2-17 Pool boiling curves of the mineral oil and synthetic ester liquid investigated in [31]

The total gas generation rates in different boiling regions are shown in Figure 2-18 [31] to Figure 2-20 [31]. In the natural convection region, methane was the key hydrocarbon gas in Gemini X and ethane the key hydrocarbon gas in MIDEL 7131. In the nucleate boiling region, the total gas generation rates from MIDEL 7131 were higher than Gemini X under the same condition. The same as in the natural convection region, the key hydrocarbon gas in Gemini X was methane and MIDEL 7131 ethane. However, the thermal faults experienced by these two insulating liquids were different due to different boiling temperatures. The thermal fault experienced by Gemini X was a T1 fault and by MIDEL 7131 it was a T2 fault. This could potentially explain the

generation of carbon oxide gases being larger in MIDEL 7131. In the film boiling region, acetylene was clearly generated by both insulating liquids, so could be an indicator of high temperature thermal faults. Meanwhile, the key hydrocarbon gas for both insulating liquids was ethylene, with the generation of hydrocarbon gases in Gemini X higher than in MIDEL 7131. Carbon oxide gases were largely generated in MIDEL 7131 because of the large amounts of oxygen atoms in the synthetic ester liquid.

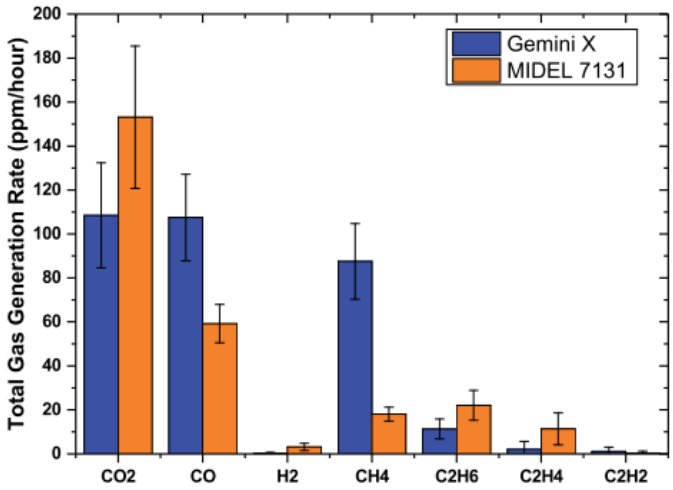

Figure 2-18 Total gas generation rates of mineral oil and synthetic ester liquid in the natural convection region investigated in [31]

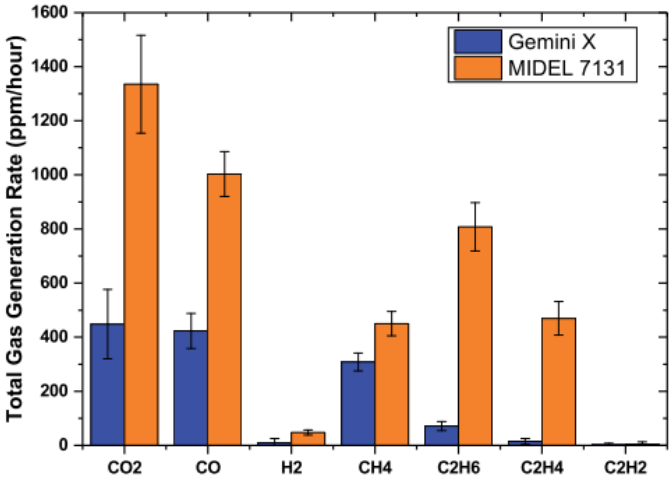

Figure 2-19 Total gas generation rates of mineral oil and synthetic ester liquid in the nucleate boiling region investigated in [31]

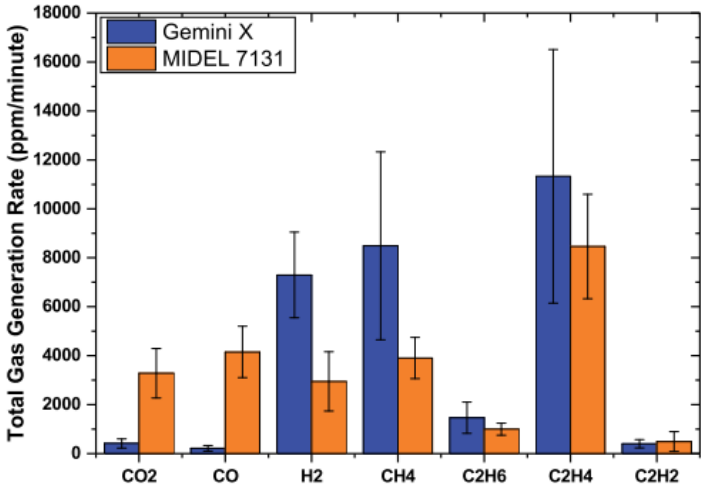

Figure 2-20 Total gas generation rates of mineral oil and synthetic ester liquid in the film boiling region investigated in [31]

The study in [32] also conducted thermal fault experiments under consideration of the pool boiling theory. Natural ester liquid, FR3, was also used in this study. The other insulating liquids used were mineral oil, Nynas Draco and synthetic ester liquid, MIDEL 7131. The tested temperatures were 250 ºC, 350 ºC and 450 ºC (400 ºC for mineral oil). The pool boiling curves of the different insulating liquids were plotted (see Figure 2-21 [32]), suggesting that the maximum temperature of mineral oil was 400 ºC and of ester liquids was 450 ºC. The results in this pool boiling curve are higher than the results in [31] but the differences between mineral oil and synthetic ester liquid are similar. When analysing the results in [32], the gas generation volumes were used to present the results, not concentrations. According to the results, a significant amount of carbon monoxide and carbon dioxide was generated in ester liquids due to the presence of oxygen atoms in the ester liquids' chemical structure. In the T2 fault level (> 300 ºC), the largest total gas volume was generated in synthetic ester liquid. Propane and propylene were only detected in synthetic ester liquid under the T2 thermal fault. Acetylene was only found in the high temperature thermal fault in mineral oil due to the heating element temperature in the mineral oil jumping to 1000 ºC and the high thermal fault hotspot causing the generation of acetylene.

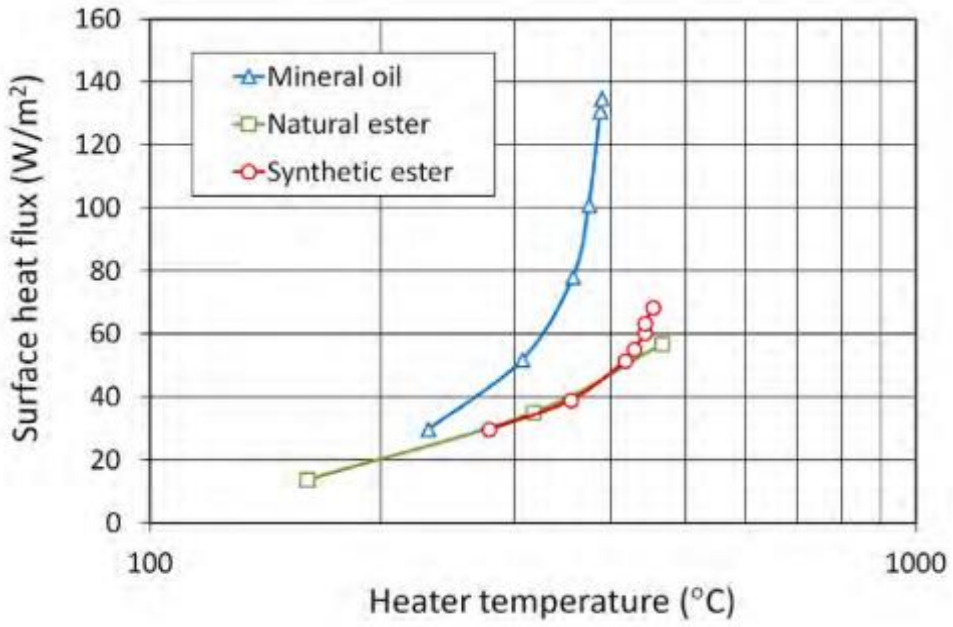

Figure 2-21 Pool boiling curves of the mineral oil, natural ester and synthetic ester investigated in [32]

2.4.1.2 Results based on the tube-heating method

The tube-heating setup in [33, 35] was used to investigate the gas generation characteristics of different insulating liquids under 250 ºC to 700 ºC thermal faults. 8 hours heating duration was applied for each thermal fault temperature. The insulating liquids used were soybean oil, sunflower oil and mineral oil. Both the generated amounts of gases in the oil phase and gas phase were considered. From Figure 2-22 to Figure 2-24 [35], the fault gases generated in the different insulating liquids are presented. It is worth noting that the fault gas values exceeding 1,000,000 ppm were not an error, as the free gases were largely generated by high temperature thermal faults. There were approximately 100 L of free gases generated in ester liquids under a 700 ºC thermal fault.

There were a negligible amount of fault gases generated in all insulating liquids when the thermal fault temperature was lower than 400 ºC. Carbon oxide gases started being clearly generated from 400 ºC in soybean oil and from 450 ºC in sunflower oil. In mineral oil, carbon dioxide started being generated from 600 ºC, with carbon monoxide generated in a small amount from 700 ºC. For hydrocarbon gases, methane,

ethane and ethylene started being generated from 450 ºC in both soybean oil and sunflower oil. The amounts of fault gas generated in soybean oil were higher than those in sunflower oil under the same thermal fault temperature. On the other hand, methane, ethane and ethylene started being clearly generated from 600 ºC in mineral oil. Acetylene started being generated in all insulating liquids when the thermal fault temperature reached 700 ºC and can be used as indicator of the occurrence of high temperature thermal faults above 700 ºC. The thermal fault temperatures when hydrogen started being generated in soybean oil, sunflower oil and mineral oil were 450 ºC, 500 ºC and 550 ºC, respectively. In addition, the concentrations of all fault gases increased with the increasing thermal fault temperatures.

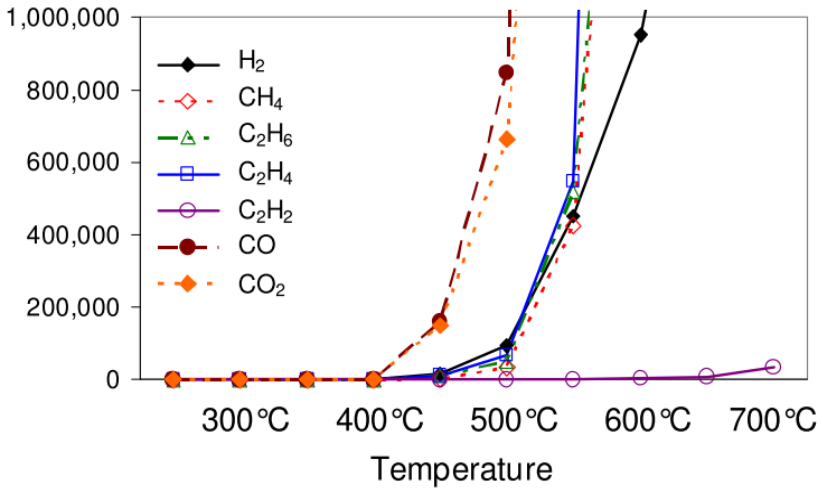

Figure 2-22 Fault gases generated in soybean oil under 300 ºC to 700 ºC thermal faults in [35]

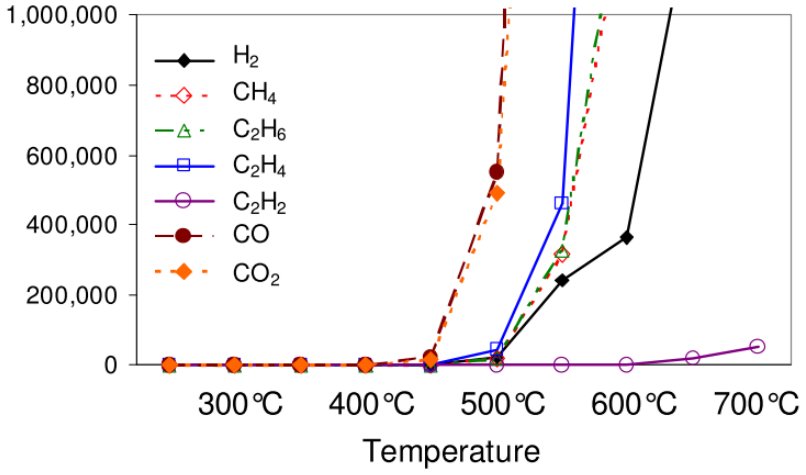

Figure 2-23 Fault gases generated in sunflower oil under 300 ºC to 700 ºC thermal faults in [35]

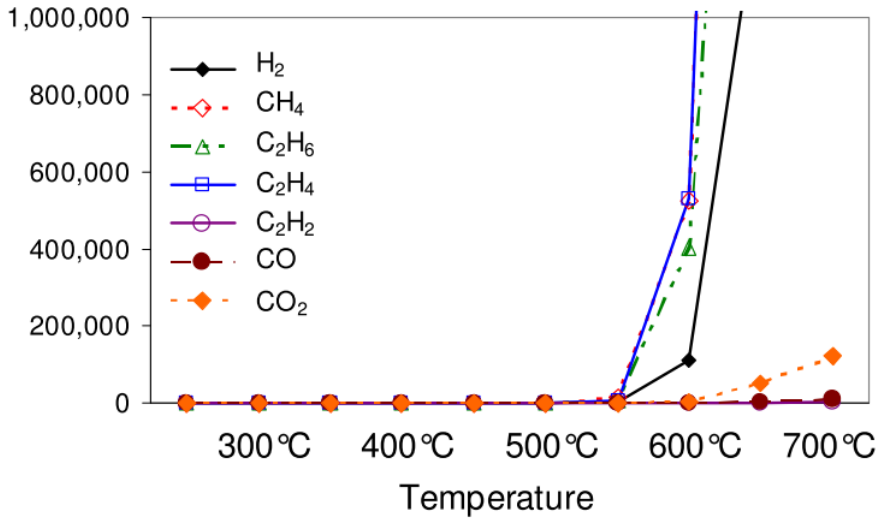

Figure 2-24 Fault gases generated in mineral oil under 300 ºC to 700 ºC thermal fault [35]

The study in [36] used a tube-heating experimental setup to replicate thermal faults from 300 ºC to 800 ºC for different insulating liquids. The insulating liquids included a conventional naphthenic-based mineral oil and two types of natural ester liquids, FR3 and camellia oil. The relative percentages of the fault gases, except carbon oxide gases, are shown in Figure 2-25 [36]. In camellia oil, ethane was the dominant gas for all thermal fault temperatures. The relatively percentage of hydrogen showed a decreasing tendency with the increase in thermal fault temperature, while methane and ethylene showed an increasing tendency. In FR3, the dominant fault gas for all the thermal fault temperatures was still ethane. Different from camellia oil, there were very small relatively percentages of other gases. In mineral oil, methane was the dominant fault gas when the thermal fault temperature was between 300 ºC and 700 ºC. Ethylene was the dominant fault gas when the thermal fault temperature reached 800 ºC. Meanwhile, there were small relatively percentages of acetylene in mineral oil under 700 ºC and 800 ºC thermal faults.

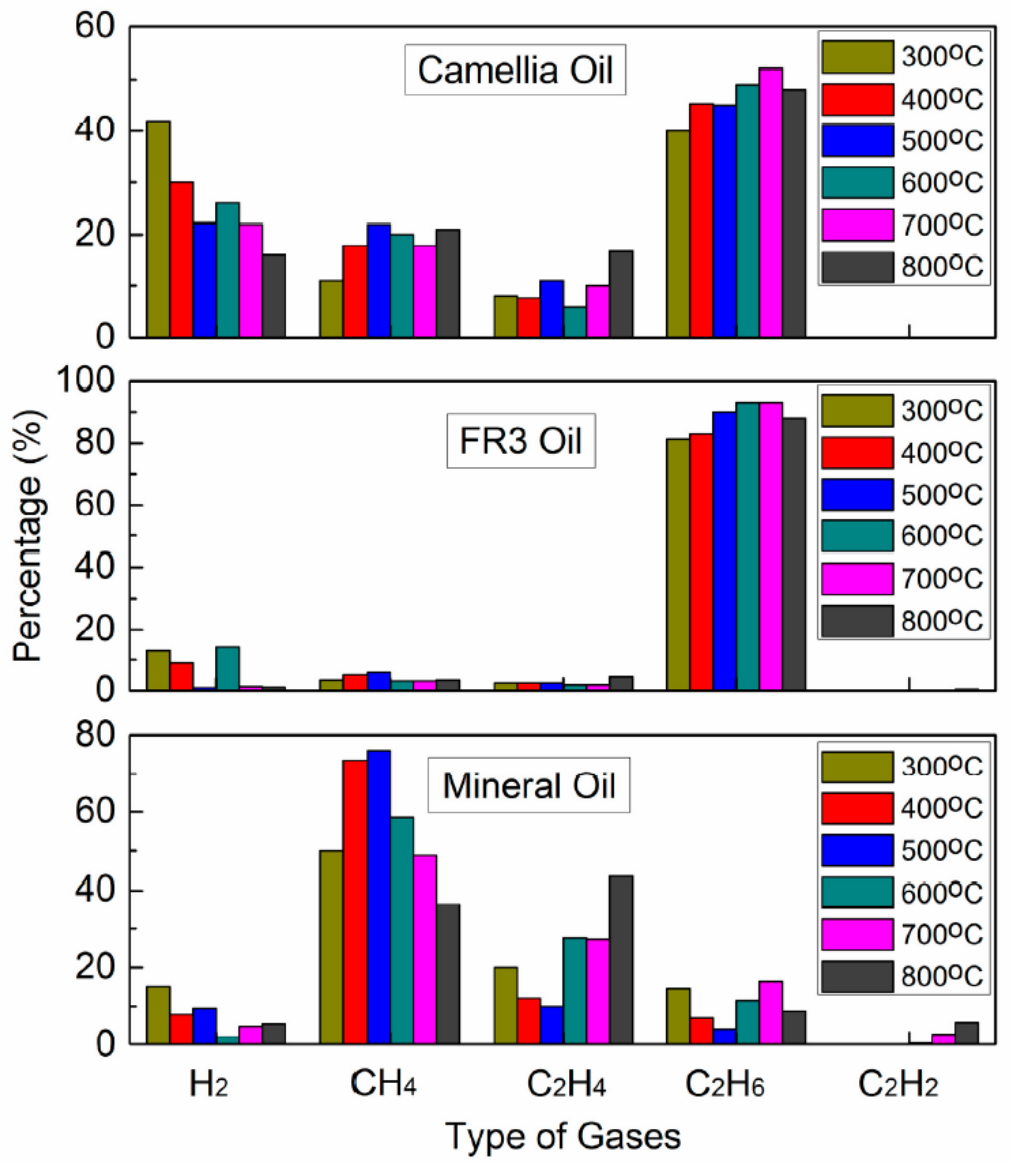

Figure 2-25 Relative percentages of dissolved gases between 300 ºC and 800 ºC thermal faults in [36]

2.4.2 DGA studies in an oil-paper insulation system

The study in [87] conducted lower temperature overheating experiments to examine the correlation between the degradation degree of insulating paper and generated gases. Two insulating paper degradation conditions were used including badly degraded insulating paper with a DP of 390 and new insulating paper with a DP of 1010. The paper samples were cut into 5 mm × 5 mm sections and immersed in new mineral oil. The heating temperature was from 75 ºC to 200 ºC, with 25 ºC intervals and a heating time of 12 hours. The dissolved gases generated included hydrogen,

methane, carbon monoxide and carbon dioxide. Oil only experiments under the same fault conditions were also conducted, finding that carbon oxide gases were not generated. Therefore, the generation of carbon oxide gases was from the paper samples. The relationships of carbon dioxide, carbon monoxide and the CO_2/CO ratio as a function of temperature are shown from Figure 2-26 [87] to Figure 2-28 [87], separately.

Figure 2-26 [87] presents the relationship between generated carbon dioxide and temperature. The generation of carbon dioxide by the new insulating paper showed a decrease tendency with the increase in temperature, with there being no remarkable difference for the badly degraded paper. However, the generation of carbon monoxide showed an increasing tendency for both paper samples under a temperature increase (see the results in Figure 2-27 [87]). For the CO_2/CO results shown in Figure 2-28 [87], the insulating paper started to degrade between 75 ºC and 100 ºC. With a temperature increase, the ratio decreased, indicating that a worse fault has occurred. Moreover, the new insulating paper degraded faster than the badly degraded insulating paper under a temperature increase.

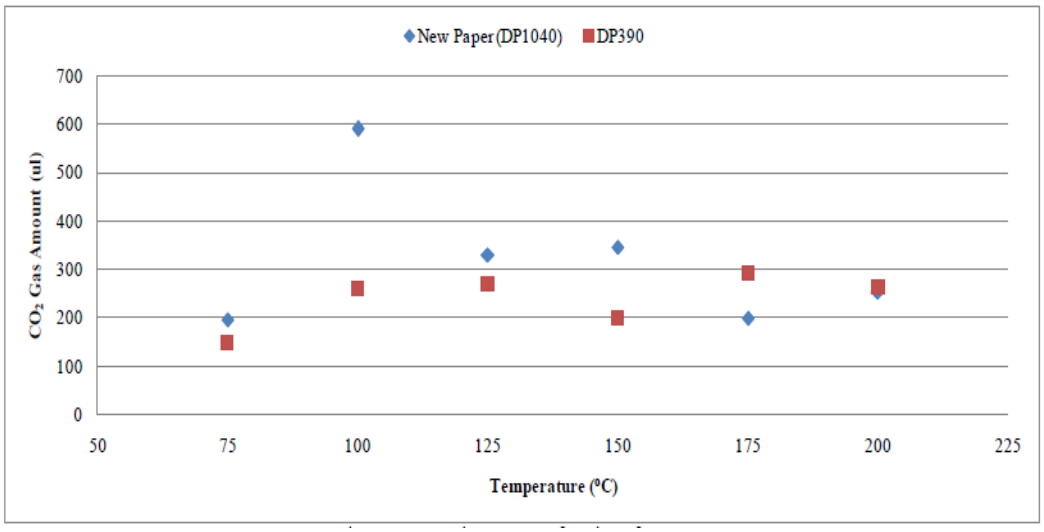

Figure 2-26 Generated carbon dioxide as a function of temperature in a mineral oil-paper insulation system between 75 ºC and 200 ºC thermal faults in [87]

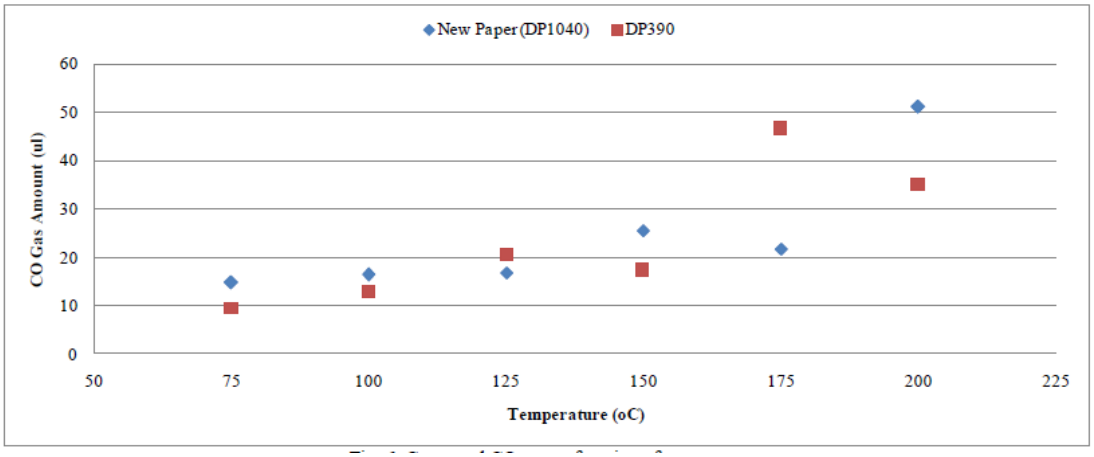

Figure 2-27 Generated carbon monoxide as a function of temperature in a mineral oil-paper insulation system between 75 ºC and 200 ºC thermal faults in [87]

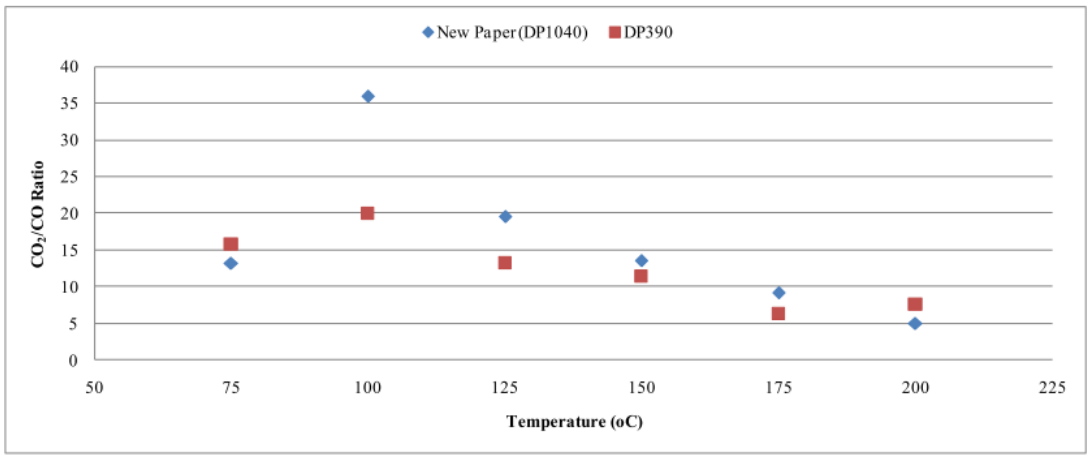

Figure 2-28 CO_2/CO ratio as a function of temperature in a mineral oil-paper insulation system between 75 ºC and 200 ºC thermal faults in [87]

The study in [88] simulated the overheating degradation of a mineral oil-paper insulation system. There were three types of pressboard used including new pressboard, aged pressboard with a DP of 672 and aged pressboard with a DP of 449. The size of the pressboard was 5mm square, with the heating temperature varying from 150 ºC to 225 ºC, with intervals of 25 ºC and a heating time of 8 hours. The results of the relationship between the generated carbon oxide gases and temperature are shown in Figure 2-29 [88] and Figure 2-30 [88]. The amounts of carbon monoxide and carbon dioxide increased with the increasing temperature but the amounts were different for the differently degraded pressboards.

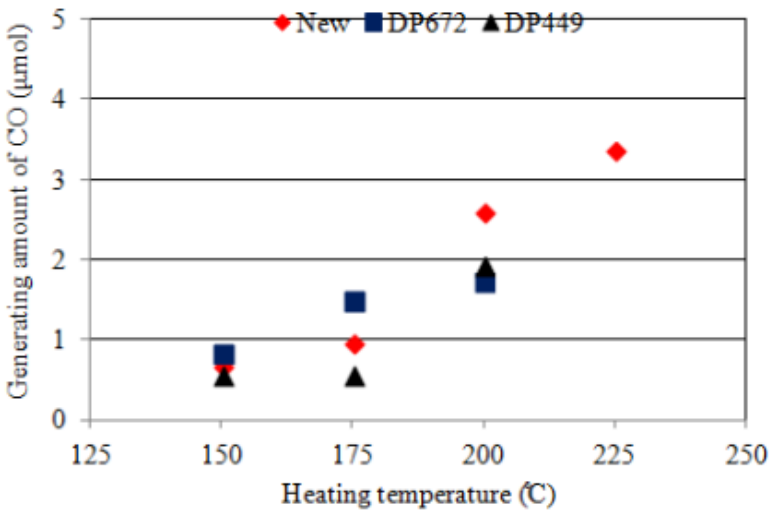

Figure 2-29 Relationship between the generated amount of carbon monoxide and temperature in a mineral oil-paper insulation system between 150 ºC and 225 ºC thermal faults in [88]

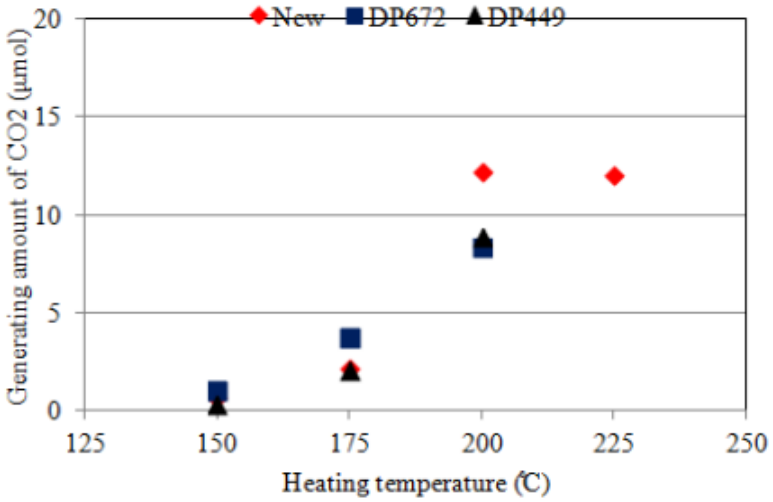

Figure 2-30 Relationship between the generated amount of carbon dioxide and temperature in a mineral oil-paper insulation system between 150 and 225 ºC thermal faults in [88]

The total generation of carbon monoxide and carbon dioxide in differently degraded pressboards under 150 ºC, 175 ºC and 200 ºC thermal faults are summarised in Figure 2-31 [88]. When the thermal fault temperatures were 150 ºC and 175 ºC, the pressboard with a DP of 672 generated more carbon oxide gases than the new pressboard. The reason could be the higher possibility of carbon monoxide and carbon dioxide being generated during the degradation of the new pressboard. However, less carbon monoxide and carbon dioxide were generated by the pressboard with a DP of 449 due to the carbon monoxide and carbon dioxide having already been generated by

prior degradation.

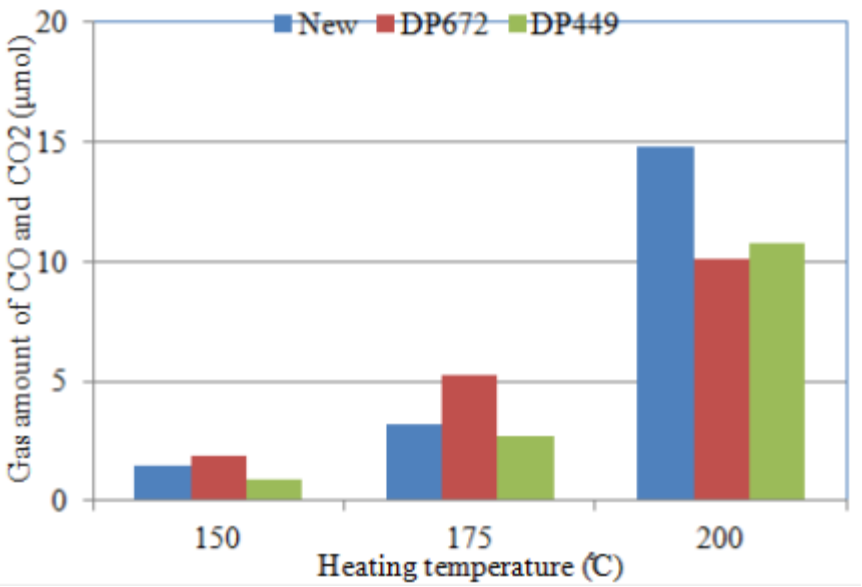

Figure 2-31 Total generation of carbon monoxide and carbon dioxide in different degraded pressboards under 150 ºC, 175 ºC and 200 ºC thermal faults in [88]

2.5 Summary

DGA has been used for monitoring transformer health status for decades. Seven fault gases (hydrogen, methane, ethane, ethylene, acetylene, carbon monoxide and carbon dioxide) are commonly used to identify electrical and thermal faults. The DGA technique can not only be applied using the traditional laboratory measurement method but also in real time using commercial online DGA monitors. Meanwhile, the standards related to the DGA technique in IEEE and IEC have been published and revised to help apply and normalise the use of the DGA technique in industry.

In order to investigate fault gas generation characteristics in different insulating liquids under thermal faults, different experimental setups using different heating methods, including oven-heating method, immersed-heating method and tube-heating method, have been designed. Among these three heating methods, the oven-heating method can only simulate temperatures in the T1 thermal fault range. The most common used method is the immersed-heating method but the heating temperature is limited by pool boiling theory. The tube-heating method is a better method for

covering the whole temperature range defined by thermal faults. In addition, the hotspot temperatures simulated by using the tube-heating method are comparable with the conditions in real transformers. However, there is a lack of tube-heating experiment setup designs.

According to the published results testing thermal faults in mineral oil, hydrogen is commonly generated by electrical faults. Methane, ethane and ethylene are normally generated by T2 thermal faults. Acetylene can be an indicator of both high energy electrical and thermal faults. Generally, carbon oxide gases are generated from paper related faults. Ester liquids have been considered as an alternative insulating liquid to replace mineral oil. It has been found that carbon oxide gases are generated in higher amounts in ester liquid when compared to mineral oil under the same fault conditions. The characteristics of generated hydrocarbon gases are almost the same as in mineral oil. However, published DGA thermal studies rarely focus on an insulating liquid-paper insulation system. Therefore, it is of key importance to develop a tube-heating experimental setup to investigate and compare fault gas generation characteristics in different transformer insulations, including oil only and oil-paper insulation systems under thermal faults.

Chapter 3 Experimental Descriptions

3.1 Introduction

In order to investigate fault gas generation characteristics in liquid only and liquid-paper insulations, an experimental setup that can achieve a wide range of thermal fault temperatures up to the T3 thermal fault level is designed and assembled. This chapter initially introduces the basic information about the liquid and solid insulation materials under investigation. Secondly, the experimental platform, which features a tube-heating loop and an online DGA monitor, is described in detail. This experimental platform was firstly employed for DGA studies of insulating liquids in [89]. In the present study, the experimental platform is further developed to conduct experiments not only in liquid only insulation but also in oil-paper insulation system. Then, several designing related tests including oil filling test, heating tube temperature profile test and sealing performance test are presented. Finally, the calculation of the DGA data and the method used to report the results are given.

3.2 Materials under Investigation

3.2.1 Liquid insulation

Mineral oil has been used in power transformers for over a century due to its reliable features, including high dielectric strength, high heat dissipation efficiency and low price. Mineral oil is a refined product separated from petroleum crude oil during a distillation procedure by selecting the boiling range of the mineral oil fraction [90]. Mineral oil is a naturally occurring mixture of molecules formed by carbon and hydrogen, and also a small amount of nitrogen and sulphur [1]. There are three main kinds of hydrocarbon molecules that form mineral oil: paraffinic ($C_{2n}H_{2n+2}$), naphthenic ($C_{2n}H_{2n}$) and aromatics (C_nH_n) [91]. Figure 3-1 presents examples of the hydrocarbon molecule structures of mineral oil. Hydrogen (H) and carbon (C) in these

molecules link together to form carbon-carbon (C-C) bonds and carbon-hydrogen (C-H) bonds [92]. Since carbon and hydrogen molecules form hydrocarbon compounds in mineral oil, several types of hydrocarbon gas can be generated under transformer electrical or thermal faults. Naphthenic or intermediate crude oils have been manufactured as insulating liquids in the UK for at least 60 years [1].

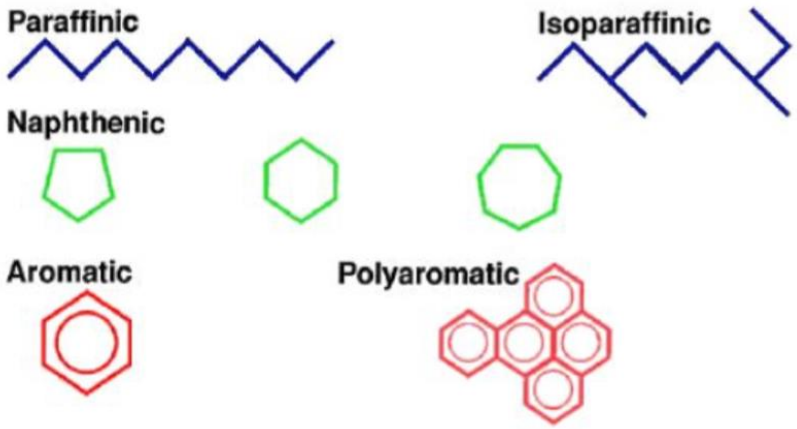

Figure 3-1 Basic hydrocarbon structures in mineral oil molecules [91]

For the paraffinic structure, the molecules can be branched or straight. Compared with naphthenic and aromatic structures, paraffinic molecules have lower thermal stability [1]. For the naphthenic structures, they have five, six or seven carbons in the ring structure, and six rings predominates. Concerning the advantages when compared to the other two structures, naphthenic structure has excellent low-temperature properties and better solvency power. The aromatic structure is the most important group, with the mineral oil used in a transformer most likely to contain some aromatic molecules. They have at least six carbon atoms with alternating double and single bonds in one ring, and have different characteristics when compared to the other two structures chemically and physically [93]. The tested mineral oil used in this current study is Gemini X from Nynas.

With increasing awareness of environmental impact and safety considerations, the disadvantages of mineral oil are exposed more than ever. The use of mineral oil is not

environmentally friendly and is a hazard to the environment, especially when there is leakage since mineral oil is not readily biodegradable. In the past decade, ester liquids, including synthetic esters, are considered as the alternative dielectric liquids to replace the mineral oil in power transformers and tap-changers [1]. Organic compounds form the synthetic ester liquid during an esterification reaction between polyvalent alcohols and fatty acids (as shown in Figure 3-2 [94]). Synthetic esters have the advantages of high flash point, good biodegradability and good tolerance to moisture [95].

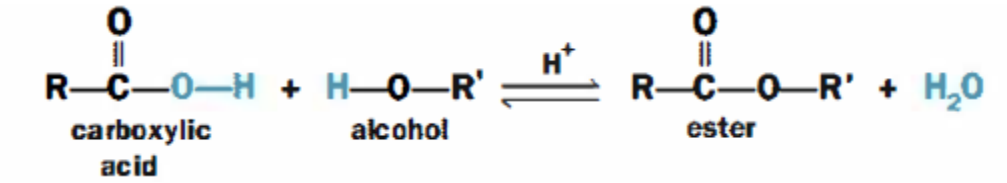

Figure 3-2 Esterification reaction [94]

Figure 3-3 shows the molecule structure of a synthetic ester, which has four fatty acid chains. The longer chain structure and larger weight of ester molecules mean a higher flash point, density and viscosity than mineral oil [96]. A higher flash point means that esters are more flame-retardant and safer when applied in transformers. However, the viscosities of synthetic ester liquid are higher, leading to a reduction in cooling efficiency when the power transformer is operating in natural cooling mode [97]. Compared to mineral oil, it has organic compounds (-OH) and unsaturated hydrocarbon compounds (-R). Accordingly, carbon oxide gases are easier to generate in synthetic ester liquid than mineral oil under the same thermal faults. Ester liquids have been used in transformers rated up to 400 kV [98]. The tested synthetic ester liquid used in this current study is MIDEL 7131 from M&I Materials.

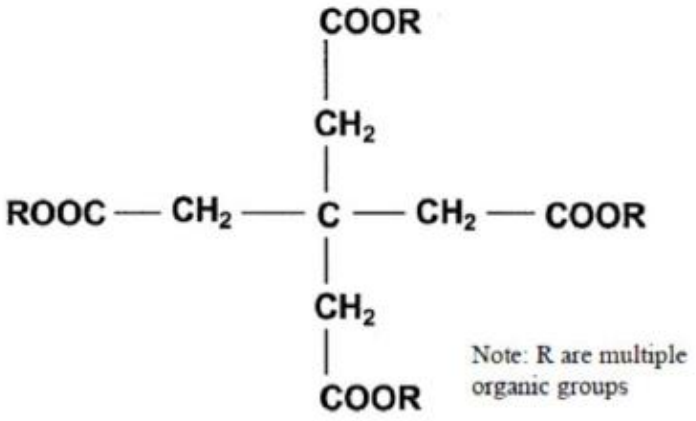

Figure 3-3 The chemical structures of a synthetic ester [99]

3.2.2 Solid insulation

Cellulose paper and pressboard form the solid insulation system used in transformers. Both cellulose paper and pressboard are formed by fibres that include 70-80% cellulose, 10-20% hemicelluloses and 2-6% lignin [46, 100]. Figure 3-4 shows the chemical formula for cellulose [1]. Cellulose is a high-polymer carbohydrate chain consisting of glucose units [1]. The number of glucose units is identified as the degree of polymerization, which is related to the aging process of the solid materials. Normally, the DP of brand new Kraft paper is between 1000-1200. With the ageing process, the Kraft paper degrades and the DP reduces. The mechanical strength of the solid material can reduce to 20-25% of its original value when the DP reduces to 200, which is referred to as the end-of-life for transformer insulation system [101]. Unbleached softwood pulp is used to produce Kraft paper and is processed by sulphate to make sure the electrical properties of the Kraft paper will not decay. Non-thermally upgraded Kraft paper from Weidmann is used in this study.

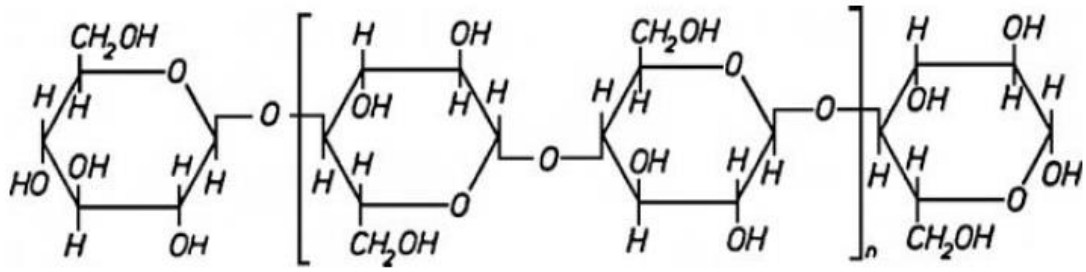

Figure 3-4 The chemical structure of cellulose [1]

3.3 Tube-heating Based Experimental Setup

3.3.1 Design and construction

A schematic diagram of the experimental setup and a 3D plot are shown in Figure 3-5. The overall tube-heating experimental setup can be divided into three parts: the oil circulation system, heating system and DGA measurement system.

The oil circulation system has five parts: oil tank, system pump, expansion tank, pressure gauge and tubes. The oil tank and tube material is 316 stainless steel that has higher hardness and better corrosion resistance. The diameter of the tubes is 10 mm. The fittings and valves used to assemble the system are from Swagelok® and have the advantages of gas tight performance and high pressure resistance. The oil tank contains the bulk liquid under investigation, with the system pump used to circulate the liquid inside the system. An expansion system with pressure monitoring is incorporated for safety reasons in case there is a pressure increase in the system.

For the heating system, a furnace with a maximum set temperature of 1200 ºC is used to maintain the heating tube at expected temperatures. A small amount of liquid (or liquid-paper insulation system) inside the heating tube will be heated by the furnace in the hotspot area, which is also defined as the fault area. The heating tube is fully filled with liquid before heating. It needs to be noted that the heating tube is part of the oil circulation system that connects with other tubes. After the expected fault period, the liquid with fault gases will be circulated using the system pump and diluted in bulk liquid.

For the DGA measurements, an online DGA monitor TM8 is employed to undertake the DGA measurements before and after the heating process. The main advantages compared with offline measurement in a laboratory are avoiding the sampling process, the leakage during transportation and the delay measurement. Meanwhile, the DGA results can be reported in real-time through the online monitor's supporting software installed in a computer.

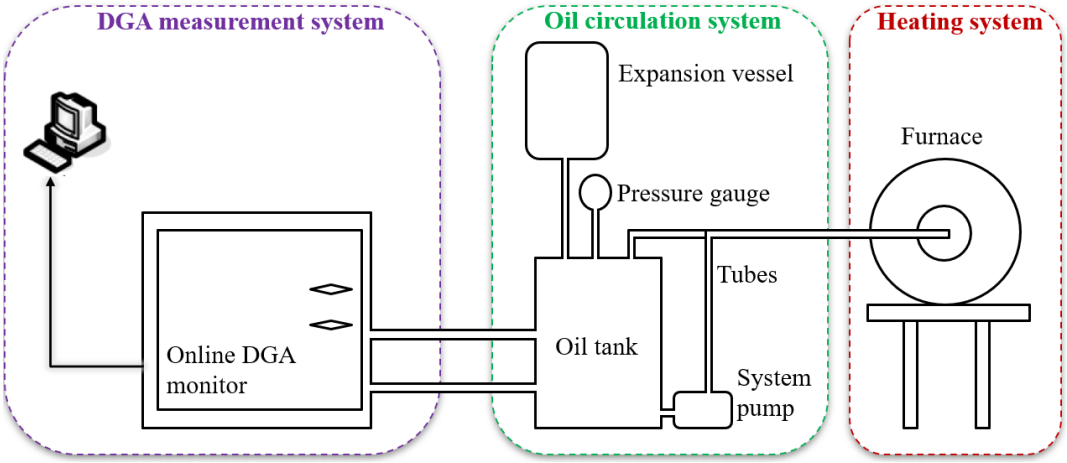

(a)

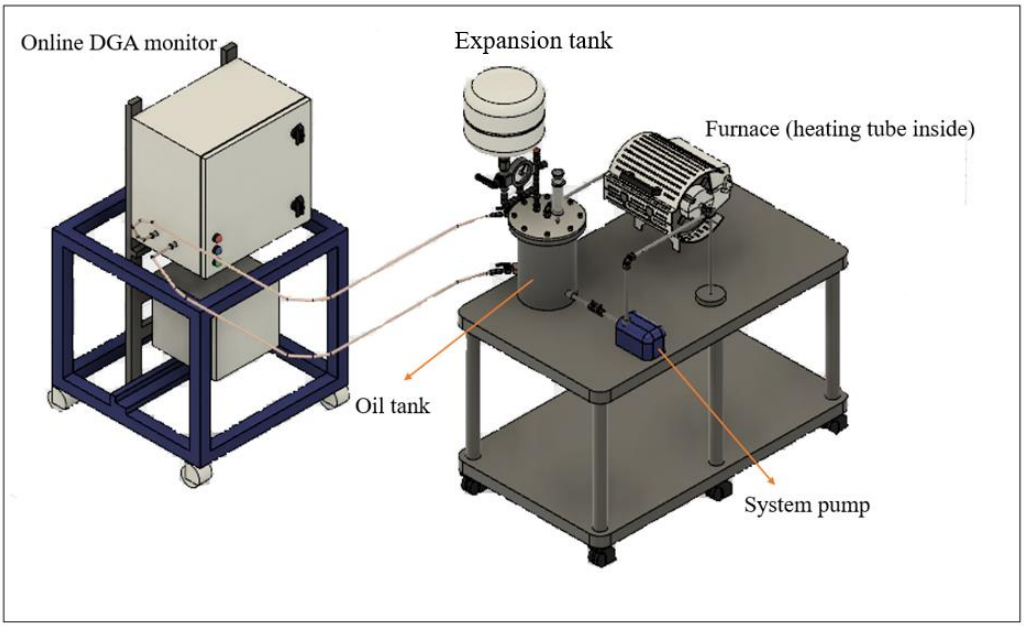

(b)

Figure 3-5 a) Schematic diagram of the tube-heating experimental setup and b) 3D plot the tube-heating experimental setup

3.3.2 Fault generation

To simulate the thermal fault temperature, one of the horizontal tubes in the oil circulation system is used as the heating tube. A furnace made by Carbolite Gero LTD is employed to heat up the tube. The maximum set temperature of the furnace is up to 1200 ºC so that the temperature range from 250 ºC to 750 ºC in this study is covered. The set temperature of the furnace is controlled by a control panel directly connected to the furnace. The controller uses a PID control system, allowing a stable thermal fault temperature to be created on the heating tube during the experiments (Figure 3-6 presents the photos of the furnace and control panel).

Figure 3-6 Furnace and control panel

The length of the heating tube is 34 cm, of which only 15 cm is located within the central heating zone of the furnace (see Figure 3-7). This 15 cm length area is regarded as the localised fault area in this study. The heating tube is fully filled with the insulating liquid under investigation during the heating process. The fault area is quite small and the simulated thermal fault condition is similar to a localised hotspot in transformers. Two thermocouples are installed on both sides of the fault area using two clips to monitor the simulated temperature and ensure it is maintained at the expected setpoint.

Figure 3-7 Photo of the heating tube within the furnace and the position of the thermocouples on the heating tube held by two clips

3.3.3 Oil tank with circulation loop

The dimension of the oil tank and functions of the ports are shown in Figure 3-8. During the experiments, there is a total of 6.6 L of insulating liquid in the overall experiment setup, including 6 L of liquid in the oil tank and 0.6 L of liquid in pipework. The oil tank volume is 7.6 L. A stainless steel lid is fitted on top of the oil tank and a rubber gasket is installed between the lid and oil tank to improve the sealing performance. Two connection ports are designed on the same side of the oil tank to form the oil circulation loop between the main tank and online DGA monitor. Moreover, another port is on the top part of the oil tank for vacuuming the headspace of the system. On the other side of the oil tank, a port is used to enable the insulating liquid to circulate in the oil circulation system from the port to the system pump, and then pass through the return tube welded on the oil tank lid to return back to the oil tank. The system pump is a Totton® magnetic coupled centrifugal pump NDP 14/2. The oil circulation path in the oil circulation system is shown in Figure 3-9. The insulating liquid is pumped from the oil tank and passes through the oil injection tube to fill the heating tube, then returns back to the oil tank by passing through the oil return tube. Moreover, another two ports are embedded on the lid for different functions, one for releasing nitrogen during the degassing process and the other one for connecting safety components.

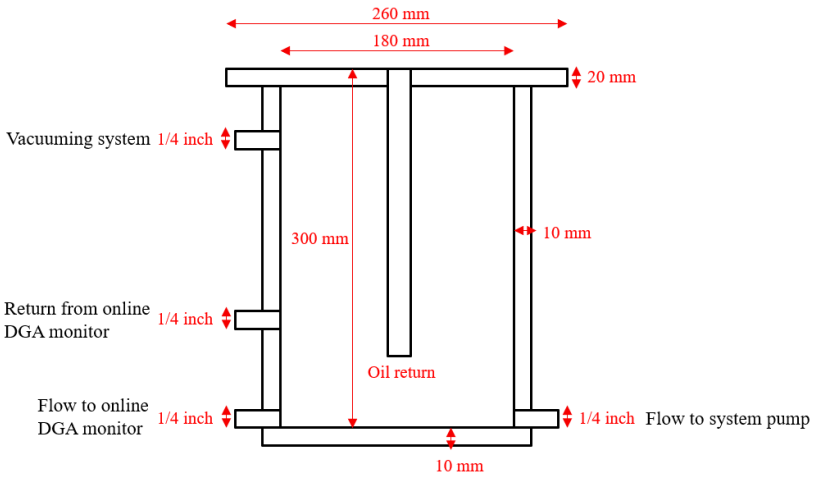

Figure 3-8 Dimension of the oil tank and functions of the ports

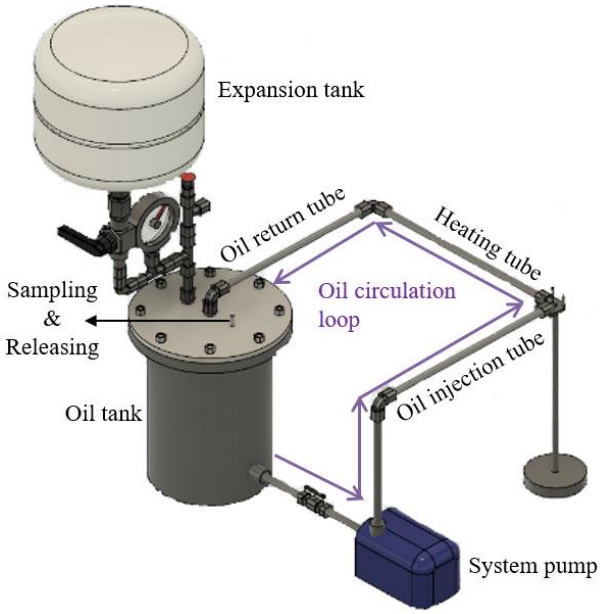

Figure 3-9 Oil circulation path in the oil circulation system

3.3.4 Expansion system

Since free gases can be generated under higher thermal fault levels, three safety components are installed in parallel through the port embedded on the lid (as shown in Figure 3-10). The parallel equipped safety components are an expansion tank, pressure relief valve and pressure gauge. The expansion tank volume is 15 L and there is a bladder with a maximum volume of 3 L inside the expansion tank. The bladder material is synthetic rubber, which has a low gas permeability characteristic (see Figure 3-11 for the structure and appearance). To control the pressure inside the

expansion tank, a Schrader valve is welded on top of the expansion tank. The valve core is a poppet valve with a spring inside. This design has the ability to maintain positive pressure and balance the pressure naturally from negative pressure when the pressure inside the expansion tank is lower than outside. The working principles of the Schrader valve are similar to the valves used on bicycles or basketballs. Another component employed as a secondary safety component is a pressure relief valve, which has the feature of automatically releasing pressure when pressure in the system is higher than 10 psi (68.95 kPa). Moreover, a pressure gauge is used to monitor system pressure during the experiments.

Figure 3-10 Safety components

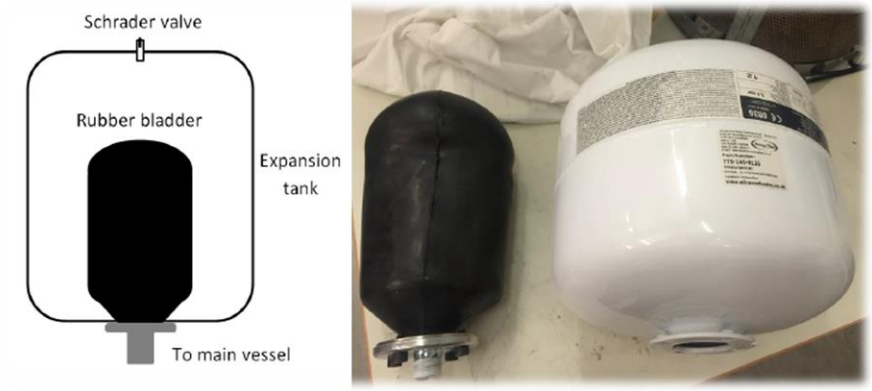

Figure 3-11 Structure and appearance of the expansion tank and bladder

3.3.5 Online DGA measurement

The online DGA monitor used in the DGA measurement system is a commercial product from QUALITROL, named the SERVERON TM8. The appearance and the inner structure of the TM8 is shown in Figure 3-12. It can detect all seven fault gases (hydrogen, methane, ethane, ethylene, acetylene, carbon monoxide and carbon dioxide) and the atmosphere gases (oxygen and nitrogen). The measurement accuracy and detection range of each gas are shown in Table 3-1. During the measurements, TM8 continues circulating the insulating liquid between itself and the oil tank by using its self-equipped oil pump to avoid consuming the insulating liquid.

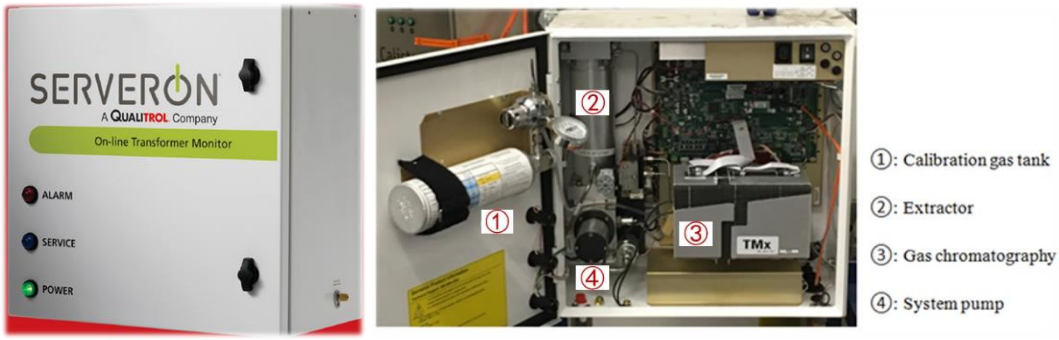

Figure 3-12 Appearance and structure of the online DGA monitor

Table 3-1 Accuracies and detection ranges of online DGA monitor (LDL, lower detection limit)

Gas	**CO_2**	**CO**	**H_2**	**CH_4**	**C_2H_6**
Accuracy	± 5% or ± LDL	± 5% or ± LDL	± 5% or ± LDL	± 5% or ± LDL	± 5% or ± LDL
Range (ppm)	5-30,000	5-10,000	3-3,000	5-7,000	3-5,000
Gas	**C_2H_4**	**C_2H_2**	**O_2**	**N_2**	
Accuracy	± 5% or ± LDL	± 5% or ± LDL	± 10% or +30/-0 ppm	± 10% or ± LDL	
Range (ppm)	5-5,000	1-3,000	30-25,000	5,000-100,000	

The detection technology of the TM8 is gas chromatography (GC). A schematic diagram of the TM8 operation principles is shown in Figure 3-13 [102]. Firstly, the

sampled insulating liquid from the oil tank flows into the oil phase of the gas extractor, with the gas extractor then extracting the dissolved gases from the insulating liquid through a semi-permeable membrane installed in the middle of the extractor. Secondly, the extracted dissolved gases are carried by the carrier gas helium (He) to flow into the GC. Different chemical substances are in the GC columns to retain different types of dissolved gases. The shape of the GC columns is designed as a spiral to guarantee the dissolved gases fully contact with the chemical substances inside the columns. The flow speed of weakly retained dissolved gases in the GC columns is faster than the strongly retained dissolved gases. Finally, the separated dissolved gases flow into the detector. The detector used in the TM8 is a thermal conductivity detector (TCD). The final results reported by the TM8 supporting software are gas-in-oil concentrations, representing the concentrations of dissolved gases in the oil phase of the oil tank. However, the TM8 will initially obtain gas-in-gas results from the detector, with the gas-in-gas results then calibrated to the gas-in-oil results through the embedded algorithm in the TM8.

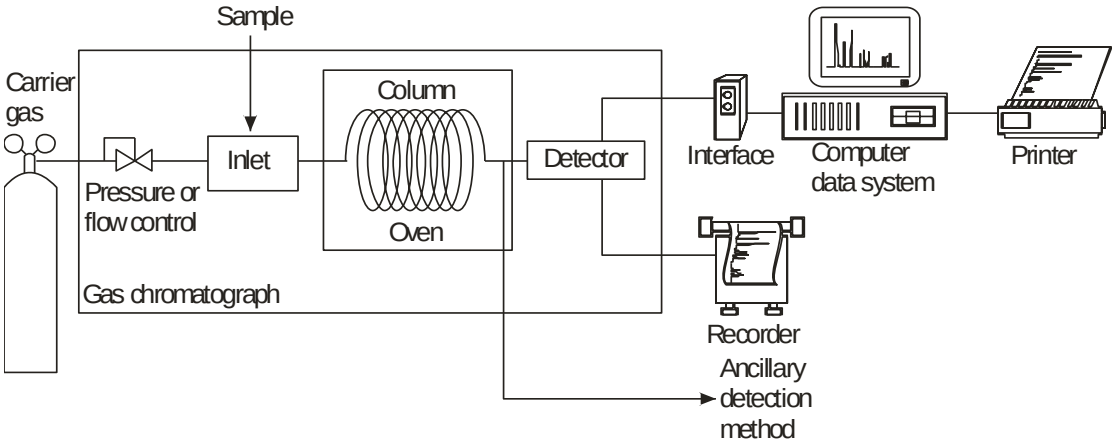

Figure 3-13 Schematic diagram of the operation principles [102]

In previous study [89], the DGA measurement results from online DGA monitor TM8 were compared with laboratory GC based DGA measurements. As the extraction method used in TM8 was the same as laboratory headspace extraction method, the DGA measurement results were comparable between these two methods. The differences between online results and laboratory results were within 20%.

3.4 Liquid Filling Procedure

When filling the system with the insulating liquid being tested, the pump embedded in the online DGA monitor is used to pump 6.6 L of insulating liquid from an oil container into the oil tank. The insulating liquid is then circulated in the oil circulation system using the system pump. The tubes are fully filled with the insulating liquid during circulation. Once circulation is stopped, the tubes need to be fully filled with the insulating liquid to ensure the insulating liquid truly experiences the simulated thermal fault during the heating process. In order to validate this, a specific test was conducted.

Since a stainless steel tube is not transparent, the stainless steel heating tube in the oil circulation system is replaced by transparent rubber tube (as shown in Figure 3-14). Moreover, silica gel was used to seal the junction points to maintain a gastight performance. The insulating liquid was initially circulated in the oil circulation system through the system pump to guarantee the transparent rubber tubes being filled with insulating liquid. The pump was then switched off and the system was left for 24 hours. The result showed that the transparent rubber tube was fully filled with insulating liquid without any empty space or bubbles forming during the test period.

Figure 3-14 Photo of a transparent rubber tube replacing the heating tube

In high temperature thermal fault experiments, free gases are generated after the fault period. To investigate the flow path of free gases in the system, a T-connector was installed in the middle of the transparent rubber tube (as shown in Figure 3-15). A

syringe was used to inject air into the system through one of the T-connecter's terminals to simulate the generation of free gases during the heating process. The experimental phenomenon showed air bubbles flowing to the oil tank directly, with the air bubbles finally released into the system's headspace. Meanwhile, the tube was still fully filled with insulating liquid.

Figure 3-15 Photo of a T-connector installed in the middle of the transparent rubber tube

3.5 Temperature Profile Measurement

During the heating process, the heating system's furnace heats up the heating tube directly and maintains its temperature at the expected thermal fault level. The heating tube is regarded as the conductor of the transformer so that the insulating liquid (or liquid-paper insulation system) is thermally stressed by the heated tube. A smaller temperature difference between the heating tube and insulating liquid indicates a better performance of the simulated thermal fault. Accordingly, the temperature distribution characteristics inside the heating tube need to be investigated.

The method used to measure the insulating liquid temperature at different positions inside the heating tube can be conducted by installing thermocouples inside the heating tube. To hold the thermocouples at specific positions inside the heating tube, several small components have been designed (see Figure 3-16). There are three holes inside the small components to vertically hold three thermocouples inside the heating tube. Moreover, a PTFE disc is installed inside the T-connector to hold the thermocouples in place and avoid oil leakage.

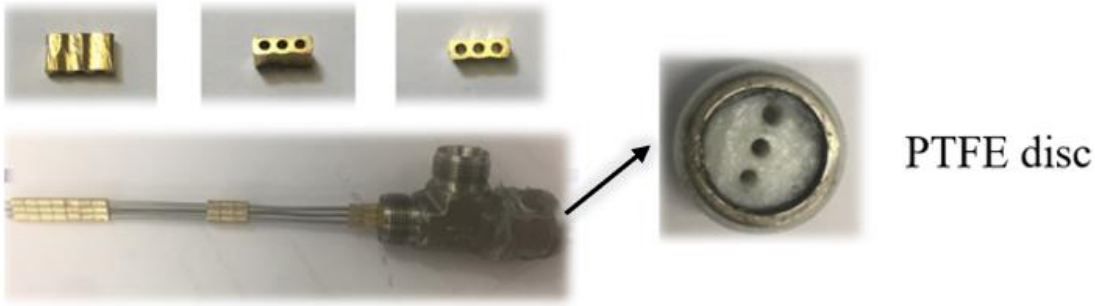

Figure 3-16 Designed components and PTFE disc to hold the thermocouples in place

The temperature profiles of both insulating liquids investigated in this study inside the heating tube were measured at different temperatures, ranging from 150 ºC to 350 ºC with 50 ºC incremental steps. 6.6 L of mineral oil or 6.6 L of synthetic ester liquid was filled into the system to conduct the experiments. The dimensions of the components and the positions of the three thermocouples inside the heating tube are shown in Figure 3-17 as a sectional drawing. The temperature distribution of the insulating liquid inside the heating tube in the middle of the fault area was measured. The thermocouples inside the heating tube are positioned vertically from top to bottom, named top, middle and bottom, respectively. In addition to these three thermocouples inside the heating tube, there are another five thermocouples used to measure outer surface temperatures at different positions (shown in Figure 3-17). Two thermocouples are installed on the outer top surface and bottom surface of the heating tube at the same position as the three thermocouples inside the heating tube. Another two thermocouples are used to measure the outer top surface of the oil injection tube and oil return tube near the heating tube. In addition, the surface temperature near the system pump is also monitored to check whether the temperature will exceed the maximum operational temperature of the system pump. During the heating process, the furnace heated the outer top surface of the heating tube to the expected temperature quickly and maintained stability for 2 hours to generate steady-state temperature results.

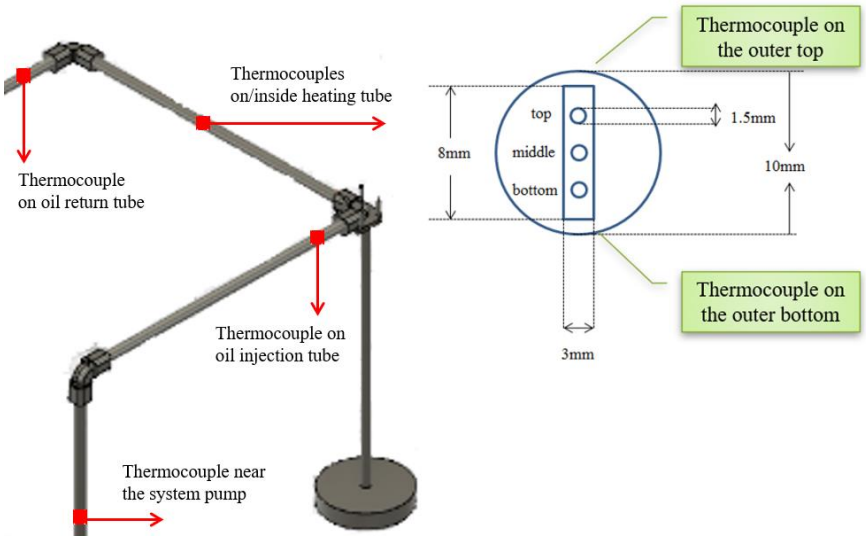

Figure 3-17 Component dimensions and thermocouple positions

Figure 3-18 and Figure 3-19 show the heating tube temperature profile results of mineral oil and synthetic ester liquid at different controlled thermal fault temperatures. In both figures, temperatures on the red line are the baseline showing the controlled thermal fault temperatures. During the tests, the outer top surface temperature of the heating tube was heated to the baseline temperature but had a few degrees centigrade higher, marked as a bold number in the figures. It can be seen that there is a temperature gradient within the liquid inside the heating tube for both insulating liquids. The temperature is the highest inside the heating tube at the top position and the lowest in the bottom position. However, the temperature differences between the outer surface and inside the heating tube are lower when the heating tube is filled with synthetic ester liquid. This indicates that a higher temperature inside the heating tube is achieved when filled with synthetic ester liquid at the same thermal fault temperature. The average molecular weight of ester liquids is higher than mineral oils, which in turn gives higher viscosity than mineral oils. Higher ester liquid viscosity slows the oil flow and increases the temperature in real transformers, especially in naturally cooled transformers [97].

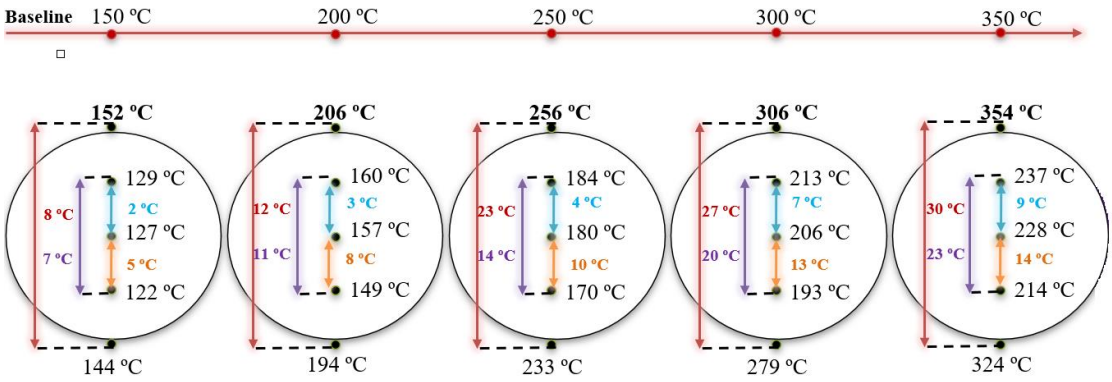

Figure 3-18 Temperature profile results when filled with mineral oil

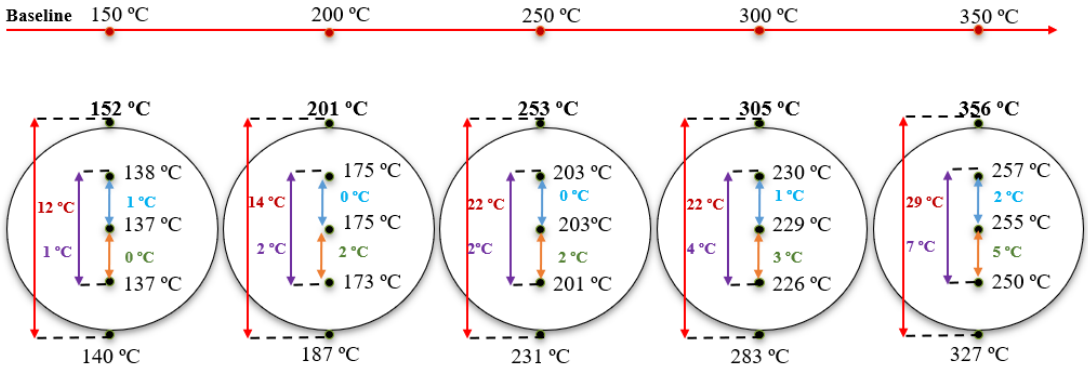

Figure 3-19 Temperature profile results when filled with synthetic ester liquid

When consider the temperature difference inside the heating tube, the difference inside the heating tube when filled with synthetic ester liquid is also lower In addition, for both insulating liquids, the temperature difference between top and middle is lower than the difference between middle and bottom, suggesting that the hotter insulating liquid stays in the top part of the heating tube. Also, the outer top surface temperature is higher than the outer bottom surface temperature for both insulating liquids. With the increase of the outer top surface temperature, the temperature differences between each position increase. As the temperature inside the heating tube is not uniform, there must be natural oil flow occurring within the heating tube.

The temperature results for the oil injection tube and oil return tube, together with the temperature near the pump when filled with mineral oil and synthetic ester liquid, are presented in Table 3-2. It can be seen for both insulating liquids, although the temperatures on these tubes are much lower than the temperature on the heating tube,

the temperature on the oil return tube is higher than the temperature on the oil injection tube. The results suggest that the heated insulating liquid flows more easily into the oil return tube than into the oil injection tube, leading to the natural oil flow being more violent in the oil return tube side. In addition, a high temperature heating process does not affect the normal operation of the system pump for both insulating liquids since the temperature near the system pump in each test is stable at an ambient temperature.

Table 3-2 Temperature results for the oil injection tube, oil return tube and near system pump when filled with mineral oil and synthetic ester liquid

Baseline temperature	**150 ºC**	**200 ºC**	**250 ºC**	**300 ºC**	**350 ºC**
Mineral oil					
Oil injection tube	18 ºC	50 ºC	61 ºC	75 ºC	89 ºC
Oil return tube	55 ºC	77 ºC	93 ºC	113 ºC	130 ºC
Near pump	21 ºC	21 ºC	21 ºC	21 ºC	21 ºC
Synthetic ester liquid					
Oil injection tube	27 ºC	57 ºC	70 ºC	83 ºC	101 ºC
Oil return tube	63 ºC	82 ºC	100 ºC	122 ºC	137 ºC
Near pump	21 ºC	21 ºC	21 ºC	21 ºC	21 ºC

For the tube-heating method, the hotspot is reached at the inner surface of the heating tube. The insulating liquid that has direct contact with the top inner surface of the heating tube will experience the highest temperature as expected. So, the smaller the temperature difference between the outer surface and inner surface of the heating tube, the better the system will be at achieving the simulated thermal fault. Fourier's Law is used to estimate this temperature difference [103]:

$$\Delta T = \frac{q\Delta x}{kA} = \frac{750 \times 1 \times 10^{-3}}{17 \times \pi \times 1 \times 10^{-2} \times 15 \times 10^{-2}} = 9.36 \qquad \textbf{(3-1)}$$

Where:

q: power transfer, 750 W

k: thermal conductivity 17 W/mºC

A: heat surface area, 0.00471 m^2

Δx: thickness of the pipe, 0.001 m

ΔT: temperature difference, 9.36 ºC

From the equation, the temperature difference is only affected by power transfer because all the other parameters are constant. The thermal conductivity of the 316 stainless steel is about 17 W/mºC and the maximum power of the furnace is 750 W. Assuming that the maximum power of the furnace is transferred to the heating tube, then the maximum temperature difference between the outer and inner surface of the heating tube will be 9.36 ºC. Under real conditions, the power provided by the furnace will be smaller than its maximum power due to the power loss, the temperature difference will be lower than 9.36 ºC. Accordingly, the insulating liquid in direct contact with the top inner surface of the heating tube will experience the expected fault temperature. The maximum error is around 3.7% when thermal fault temperature is set at 250 ºC.

To verify the accuracy of the calculation, a verification test without insulating liquid inside the heating tube was conducted. The test procedure and installed thermocouple positions are the same as the temperature profile test above but without insulating liquid filling the heating tube. Two temperatures were selected to conduct the experiments: 250 ºC and 750 ºC. The measurement results are shown in Table 3-3. Almost no temperature difference can be seen inside the heating tube. The temperatures inside the heating tube are around 10 ºC lower than the outer surface temperatures and the difference between outer surface and inner surface of the heating tube should be smaller than 10 ºC, indicating that the difference between the heating tubes' outer and inner surfaces are small, verifying the accuracy of the calculation.

Table 3-3 Temperature profile results without insulating liquid inside the heating tube

Baseline temperature	**250 ºC**	**750 ºC**
Outer top	248 ºC	752 ºC
Outer bottom	248 ºC	751 ºC

Inner top	239 ºC	744 ºC
Inner middle	240 ºC	743 ºC
Inner bottom	237 ºC	743 ºC

Figure 3-20 and Figure 3-21 show the temperature profile fitting results for the outer top surface and inside the heating tube when filled with mineral oil and synthetic ester liquid. Due to the withstanding ability of the PTFE disc, the temperature profile tests were conducted up to 350 ºC. Accordingly, linear fitting was used to fit the curve to the higher temperatures. The R-square of 0.99 indicates that the selected fitting curve is comparable to reality. It can be seen that the temperatures of both insulating liquids on the heating tube and inside the heating tube have a linearly increasing tendency. For both insulating liquids, when the outer top surface temperature increases by 50 ºC, the temperature difference between the outer top surface and the middle position inside the heating tube increases by around 25 ºC. Thus, the temperature gradient inside the heating tube is larger at higher temperatures. Meanwhile, it can be seen that the temperature difference inside the heating tube when filled with synthetic ester liquid is lower than filled with mineral oil.

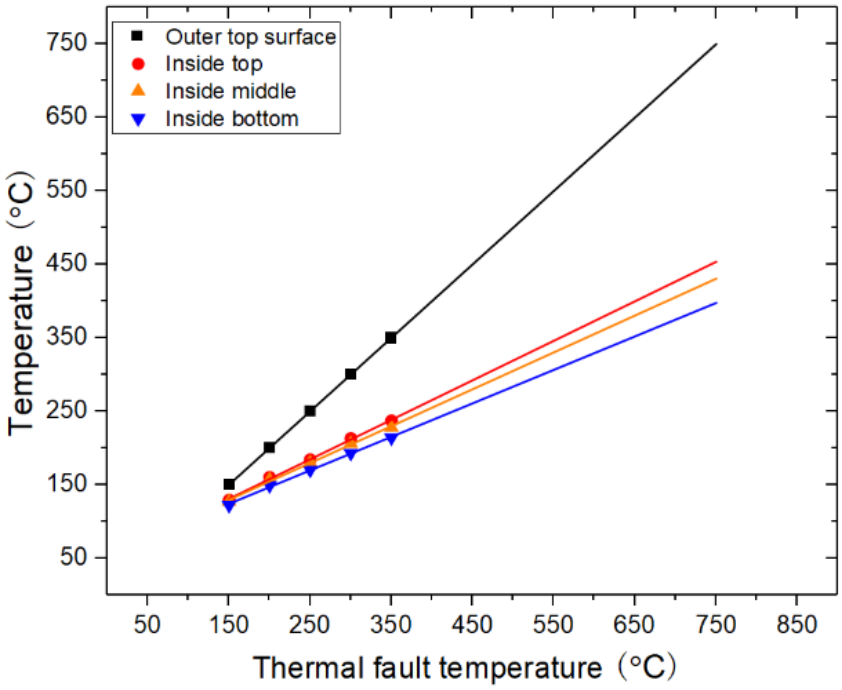

Figure 3-20 Linear fitting of mineral oil temperature profile

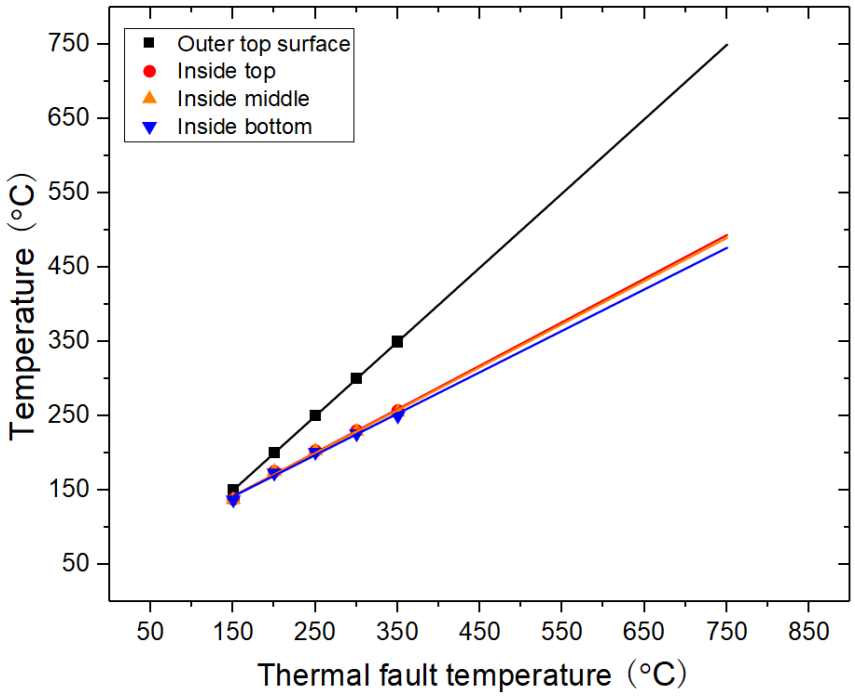

Figure 3-21 Linear fitting of synthetic ester liquid temperature profile

3.6 Sealing Performance Test

A pressure gauge is installed in the experimental setup. To check the sealing performance of the experimental setup, the retention time of pressure differences in the system was measured. 200 mbar of positive pressure was added into the system by using nitrogen. The overall experimental setup was left for 24 hours to monitor the pressure difference. There was less than 20 mbar (10%) decrease after 24 hours, indicating the sealing performance in the experimental setup to be in an acceptable range. The same tests were repeated several times by assembling and disassembling the system to ensure the same sealing conditions. For most of the formal experiments, the heating duration will be less than 24 hours. In addition, the formal experiments are conducted under atmosphere pressure and the pressure driving force of the leakage is even smaller, which reduces system leakage compared to the sealing performance test.

3.7 Sample Preparation

The investigated insulating liquids include a mineral oil, Gemini X and a synthetic ester liquid, MIDEL 7131. When conducting the experiments, the new insulating liquid was taken from the liquid barrel directly without any further filtration. The insulating liquid was then injected into the system. To control the moisture level and remove gases, the insulating liquid was purged by nitrogen for 3 hours. During the degassing process, the nitrogen was injected from the bottom of the oil tank and passed through the insulating liquid, and then released into the atmosphere. After the degassing process, both insulating liquids had moisture level less than 10% relatively humidity.

The investigated Kraft paper samples were firstly cut into 15 cm lengths and 3 cm widths. Three Kraft paper layer samples were inserted into the tubes. The tubes with Kraft paper samples were then dried in an air-circulating oven at 105 ºC for 48 hours. After the drying process, the samples were mixed with the insulating liquid that had already been pre-processed and put in a vacuum oven for another 48 hours at 60 ºC for full impregnation and to further remove moisture. After processing, the moisture content of the Kraft paper samples was less than 1% by weight.

3.8 Results Calculation Method

As mentioned in the working principles of the online DGA monitor TM8, insulating liquid will be continually sampled from the oil tank to the extractor inside the TM8 through an embedded oil pump. The dissolved gases are extracted by extractor and separated in GC system. The TCD detector is used to detect the separated dissolved gases. At this stage, the detected concentration of each dissolved gas is the concentration in the gas phase, which is defined as C_{gig}. In order to obtain the concentration in the oil phase, the software in TM8 will make a calculation based on equation (3-2) [23]:

$$C_{gio} = C_{gig} \times (K + \beta) \quad \textbf{(3-2)}$$

Where:

C_{gio}: concentration of dissolved gas in the oil phase

C_{gig}: concentration of dissolved gas in the gas phase

K: solubility coefficient of dissolved gas (Ostwald coefficient)

β: volume ratio of the gas phase and oil phase

During the operation of extractor, the temperature and pressure of the extractor could be different from the external environment and thus a correction to the standard atmospheric pressure (101,325 Pa) and temperature (25 ºC) is needed. Equation (3-2) will be improved by adding several parameters. These parameters are measured or embedded in TM8. Accordingly, the TM8 will use equation (3-3) to report the final gas-in-oil concentrations at standard conditions:

$$C_{gio}^{min} = C_{gig} \times (K_{min}^{act} + \beta) \times \frac{P^{act}}{P_s} \times \frac{T_s}{T^{act}} \quad \textbf{(3-3)}$$

Where:

C_{gio}^{min}: concentration of dissolved gas in the oil phase of mineral oil under standard conditions

C_{gig}: concentration of dissolved gas in the gas phase

K_{min}^{act}: solubility coefficient of dissolved gas in mineral oil (Ostwald coefficient) at the working temperature of the extractor

β: volume ratio of the gas phase and oil phase

P^{act}, T^{act}: pressure and temperature at the working conditions of the extractor (Measured by TM8)

P_s, T_s: pressure and temperature at the standard conditions

When using the TM8 to monitor the transformer with alternative insulating liquid, a calibration from mineral oil to alternative insulating liquid is required to ascertain the correct gas-in-oil results. The calibration is necessary as Ostwald coefficients embedded in the TM8 are based on the mineral oil. From the working principles of the

extractor in the TM8, the extracted dissolved gases in the gas phase are extracted from the oil phase, with these extracted gases detected by the TCD. They are the real amount of dissolved gases that can be extracted from the liquid phase and detected by the detection device. The detected gas-in-gas concentrations are not affected by the type of insulating liquid. This means that when the TM8 is conducting DGA measurements with alternative insulating liquids, the detected gas-in-gas concentration by the TCD can be used to calculate the gas-in-oil concentration of alternative insulating liquids based on equation (3-4):

$$C_{gio}^{a} = C_{gig} \times (K_{a}^{act} + \beta) \times \frac{P^{act}}{P_s} \times \frac{T_s}{T^{act}} \quad \textbf{(3-4)}$$

Where:

C_{gio}^{a}: concentration of dissolved gas in the oil phase of alternative insulating liquids at standard conditions

C_{gig}: concentration of dissolved gas in the gas phase

K_{a}^{act}: solubility coefficient of dissolved gas in alternative insulating liquid (Ostwald coefficient) at the working temperature of the extractor

β: phase ratio of the gas phase and oil phase

P^{act}, T^{act}: pressure and temperature at the working conditions of extractor

P_s, T_s: pressure and temperature at the standard conditions

From equation (3-4), the gas-in-gas concentration is unknow value which cannot be directly obtained, but the gas-in-gas concentration can be calculated by the reported gas-in-oil concentration based on mineral oil parameters using equation (3-3) as:

$$C_{gig} = \frac{C_{gio}^{min}}{(K_{min}^{act} + \beta) \times \frac{P^{act}}{P_s} \times \frac{T_s}{T^{act}}} \quad \textbf{(3-5)}$$

Then, the correct gas-in-oil concentration for alternative insulating liquid can be obtained by substituting equation (3-5) into equation (3-4) as:

$$C_{gio}^{a} = \frac{C_{gio}^{min} \times (K_a^{act} + \beta) \times \frac{P^{act}}{P_s} \times \frac{T_s}{T^{act}}}{(K_{min}^{act} + \beta) \times \frac{P^{act}}{P_s} \times \frac{T_s}{T^{act}}} = \frac{C_{gio}^{min} \times (K_a^{act} + \beta)}{(K_{min}^{act} + \beta)} = \frac{C_{gio}^{min} \times K_a^{act}}{K_{min}^{act}} \quad \textbf{(3-6)}$$

From equation (3-6), the C_{gio}^{min} can be directly obtained from reported results and the temperature and pressure will not affect the results. The only influential factors are the Ostwald coefficients of the mineral oil and alternative insulating liquid. In this study, the extractor is working at the atmosphere temperature, and the temperature is assumed as 25 ºC for all the experiments. The Ostwald coefficient reported in IEC 60567-2011 [23] at 25 ºC for both two types of insulating liquid are used for calculation. The Ostwald coefficients are listed in Table 3-4. Therefore, the gas-in-oil concentration reported by the software can be directly used when mineral oil is the test insulating liquid. When test insulating liquid is changed to synthetic ester liquid, a calculation is needed based on equation (3-6) to ascertain the correct gas-in-oil concentration.

Table 3-4 Ostwald coefficient of mineral oil and synthetic ester liquid in IEC 60567-2011 at 25 ºC [23]

Gas	CO_2	CO	H_2	CH_4	C_2H_6	C_2H_4	C_2H_2
Mineral oil	1.090	0.132	0.056	0.429	2.820	1.840	1.240
Synthetic ester liquid	2.050	0.127	0.051	0.381	2.190	1.870	4.380

3.9 Summary

This chapter has introduced the properties of the investigated insulating liquids and Kraft paper, and the preparation for the insulation samples. The tube-heating experimental setup has been introduced. Three tests, the liquid filling test, the temperature profile test and the sealing performance test, have been explained. The liquid filling test confirms that the heating tube can be fully filled with insulating

liquid and shows the flowing direction of free gases. Moreover, based on the investigation of the temperature profile test of the heating tube, the temperature distribution in the heating tube is obtained under five baseline temperatures. Also, the advantage of the tube heating method confirms that insulation can experience expected thermal faults in the heating tube's inner surface. The sealing performance of the experimental setup is checked by conducting a pressure retention test. Finally, the calculation method for the gas-in-oil concentration using alternative insulating liquids is given.

Chapter 4 Generation of Fault Gases in Mineral Oil and Synthetic Ester Liquid under Simulated Thermal Faults

4.1 Introduction

DGA related transformer thermal faults are classified as T1, T2 and T3 thermal faults with specific temperature ranges. The heating methods, such as oven-heating and immersed-heating, were mainly used to simulate thermal faults in previous studies [21, 25, 29-31]. However, the oven-heating method provides a uniform temperature profile to simulate thermal faults but only in the T1 temperature range, which is lower than 300 ºC. The immersed-heating method cannot achieve stable high temperatures (> 400 ºC) due to the pool boiling phenomenon [31]. To cover a wide range of stable thermal fault temperatures, the tube-heating method described in Chapter 3 is employed in this study. Meanwhile, synthetic ester liquid has been increasingly used as an alternative insulating liquid to mineral oil due to its non-toxic, environmentally friendly and high fire resistance. Therefore, it is of importance to study and compare fault gas generation characteristics between mineral oil and synthetic ester liquid.

In this chapter, a series of thermal faults with various temperatures up to 750 ºC are achieved to investigate the fault gas generation characteristics in both mineral oil and synthetic ester liquid. The experimental procedure is initially introduced, with the gas-in-oil generation results then reported. In addition, the fault gas generation characteristics between the two liquids will be compared.

4.2 Experimental Condition and Procedure

4.2.1 Sample preparation

The investigated insulating liquids include mineral oil, Gemini X, and a synthetic ester liquid, MIDEL 7131. Totally, around 6.6 L of insulating liquid (including 6 L of liquid in the main liquid tank, 0.6 L of liquid in the pipework) is injected into the experimental setup. During the experiments, around 0.013 L of insulating liquid is heated inside the heating tube and then largely diluted in the bulk liquid. Before conducting the formal experiments, both liquids are pre-processed to achieve moisture levels of less than 10% relative humidity. The system's headspace is filled with nitrogen. Five different fault temperatures, covering T2 to T3 thermal faults, are set with different heating durations to avoid excessive gas generation. It needs to be noted that the T1 fault range is not covered in this study since gas generation under a T1 thermal fault in the present setup is extremely slow. If using a longer heating duration (up to 1 week) to simulate T1 thermal faults, gas leakage during the long duration test may compete with the gas generation, potentially leading to confusing results. The conditions for the mineral oil and synthetic ester liquid experiments are listed in Table 4-1.

Table 4-1 Mineral oil and synthetic ester liquid experimental conditions

Fault temperature	350 ºC	450 ºC	550 ºC	650 ºC	750 ºC
Heating duration for mineral oil	72 h	10 h	4 h	10 mins	1 min
Heating duration for synthetic ester	30 h	10 h	4 h	10 mins	1 min
Liquid volume	6.6 L (6 L in the main tank + 0.6 L in the pipework)				
Headspace volume	2.3 L N_2 (1.6 L in the main tank + 0.7 L in the bladder)				

4.2.2 Test procedure

A flow chart of the test procedure is shown in Figure 4-1.

1) A system pump is operated to circulate liquid for 10 minutes to ensure that the liquid circulation loop, especially the heating tube, is totally filled with insulating liquid.

2) Three DGA background measurements are performed to obtain benchmark concentrations of dissolved gases before each thermal fault.

3) Once background measurements are finished, 100 ml of liquids are sampled from the liquid phase.

4) The furnace is switched on to create the expected thermal fault. During the heating process, both sides of the heating tube within the furnace are monitored using two thermocouples.

5) After a specific heating process duration (as shown in Table 1), the furnace is switched off and the system pump is switched on again for 10 minutes to cool down the system and re-mix the liquid in the system.

6) Post fault DGA measurements are taken until the concentration of dissolved gases reach a steady-state (regarded as reaching equilibrium).

7) Once post fault measurements are finished, another 100 ml of liquid is sampled from the liquid phase.

8) One extra step is required for thermal fault experiments with temperatures of 650 ºC and 750 ºC. In these two extremely high temperature experiments, free gases are largely generated. Therefore, the volume of free gases is measured at the end of the experiment and then the degassing procedure is performed before the next

experiment to decrease the benchmark.

After each thermal fault experiment, the heating tube is disassembled from the system. A new heating tube is reconnected to the system and 200 ml of pre-processed liquids are refilled into the system to start a new experiment.

It needs to be noted that the fault gases are measured from the liquid phase during the DGA measurements and thus the reported results are the gas-in-oil concentrations. Some of the dissolved gases will diffuse into the gas phase, with partitioning between the oil phase and gas phase existing in the experimental system. The gas-in-oil concentrations are, however, continuously measured after the fault until reaching a steady-state.

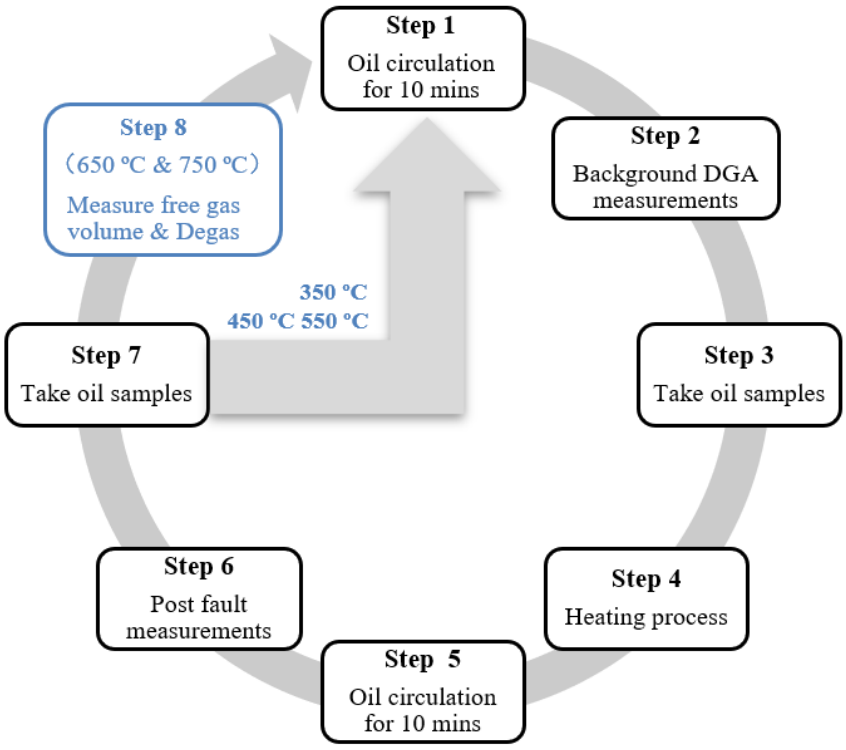

Figure 4-1 The procedure for the liquid oil thermal fault experiments

The volume of free gases in the headspace can be measured by using a 50 ml syringe after the equilibrium status of the system is reached. When measuring the volume of gas in the bladder inside the expansion vessel, the pressure in the expansion vessel is

increased to 200 mbar so that the bladder is squeezed to push the gas from the bladder to the liquid tank. A 50 ml syringe is connected to the gas sampling port welded on the lid via a three-way valve. Then, the positive pressure pushes the gas into the syringe until the pressure returns back to atmospheric pressure. The number of full 50 ml strokes is recorded until the final stroke that cannot be fully filled. The total volume of the headspace gas in the bladder can then be calculated. In order to ascertain the volume of free gases, the initial gas volume left inside the bladder after taking the liquid samples needs to be subtracted. As mentioned in the experimental conditions, 2.3 L of nitrogen is filled as the headspace including 1.6 L in the liquid tank and 0.7 L in the bladder. A total volume of 0.2 L liquid samples taken during the experiment leads to around 0.5 L of nitrogen keeping in the bladder which can be regarded as the initial gas volume left inside the bladder. The volume of free gases is then calculated as:

$$V = 50\ ml \times n + V_f - 500\ ml \quad \textbf{(4-1)}$$

where

V: the volume of free gases in ml.

n: number of full strokes of a 50 ml syringe.

V_f: the volume of gas in the final stroke of the syringe.

4.3 Generation of Fault Gases in Mineral Oil

4.3.1 Experiments without free gases generation

Thermal faults will result in the generation of fault gases due to the chemical decomposition of insulating liquid. Small unstable fragments are formed due to the scissions of chemical molecular bonds under different thermal fault temperatures. These small unstable fragments recombine rapidly into different gas molecules by complex reactions. These fault by-products are dissolved in oil as dissolved gases, or released into the headspace as free gases if the generation is in a large quantity [5].

There are no free gases generated in mineral oil experiments when the thermal fault

temperatures are set to be 350 ºC, 450 ºC and 550 ºC. Taking the 450 ºC thermal fault experiment as an example, Figure 4-2 shows the recorded temperature profile during the 4-hour heating duration. The temperature rises up quickly and remains stable for the entire heating period. Both sides of the heating tube inside the furnace are monitored using two thermocouples to make sure that the expected thermal fault temperature is achieved. Channel 1 which is near the pump side of the heating tube is controlled to be exactly 450 ºC, while Channel 2 is near the oil tank side and the temperature is slightly higher than 450 ºC. The temperature difference between two channels is within 10 ºC. The same temperature profile conditions are applied to the 350 ºC and 550 ºC thermal fault experiments.

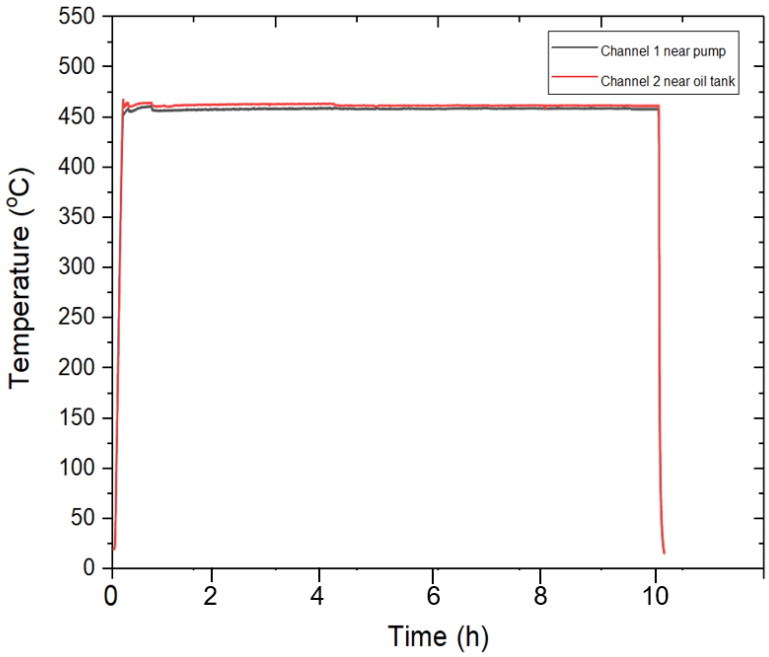

Figure 4-2 Temperature recording for the 450 ºC thermal fault experiment

Figure 4-3 shows the gas-in-oil DGA measurement results reported from the online DGA monitor. The results include three background measurements and five post fault measurements. Five different dissolved gases were detected including carbon dioxide, carbon monoxide, methane, ethane and ethylene. All the dissolved gases reach a steady status quickly after the heating process. In addition, the benchmark concentrations of dissolved gases before the heating process are higher than the detection limits of the online DGA monitor to guarantee measurement accuracy. The

gas-in-oil generations of dissolved gases are calculated as the differences between the average values of the last three post fault measurements and the average of the three background measurements. It can be indicated in Figure 4-3 that there is an approximate 26.8 ppm increase of carbon dioxide, 17.2 ppm increase of carbon monoxide, 16.5 ppm increase of methane, 19.9 ppm increase of ethane and 1.7 ppm increase of ethylene after experiencing a 450 ºC thermal fault for 10 hours.

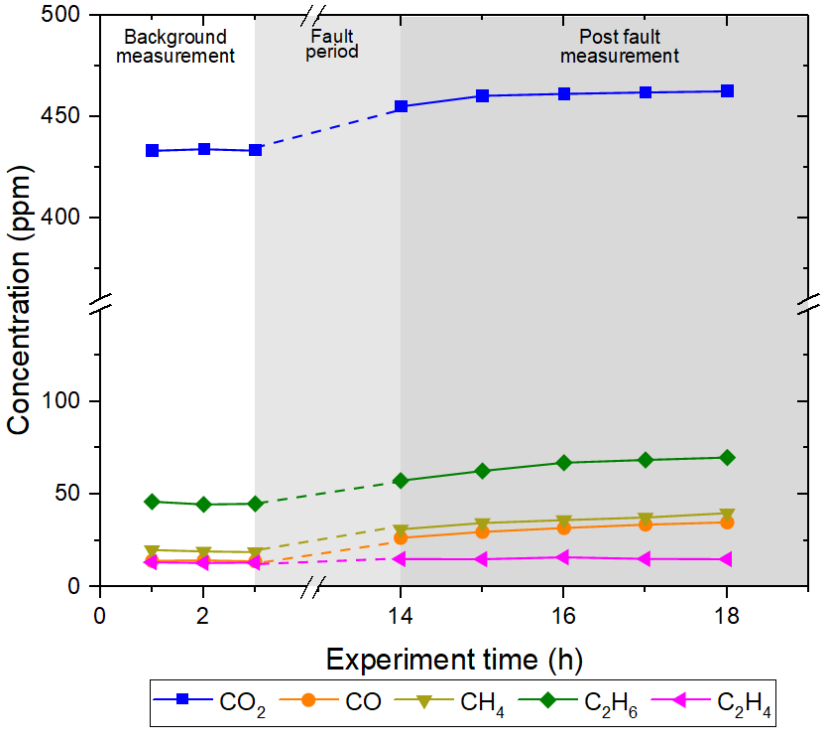

Figure 4-3 DGA measurement results for a 450 ºC thermal fault in mineral oil

4.3.2 Experiments with free gases generation

Free gases are generated in the mineral oil experiments when the thermal fault temperatures are set at 650 ºC and 750 ºC. Taking the 650 ºC thermal fault experiment as an example, Figure 4-4 shows its temperature recording. Around 16 minutes are taken to heat the heating tube from room temperature of 25 ºC to thermal fault temperature of 650 ºC. The time used to reach the expected thermal fault temperature is longer than previous tests at lower thermal fault temperatures. A temperature difference up to 100 ºC existed between channel 1 near the pump and channel 2 near the oil tank measurements when a 650 ºC thermal fault is reached. The reason is

probably due to the violent oil flow and free gases generation inside the heating tube, resulting in asymmetrical distribution of temperature inside the heating tube. It can be seen that the recorded temperatures of the two thermocouples fluctuate during the 10 minute heating duration. The furnace is switched ON and OFF intermittently to maintain the average values of the two thermocouples within 650 ºC ± 20 °C. After the heating process, the heating tube temperatures are naturally decreased to 150 ºC and the pump is switched on to further cool down the system. The same ON-OFF control method is also applied in the 750 ºC thermal fault experiments.

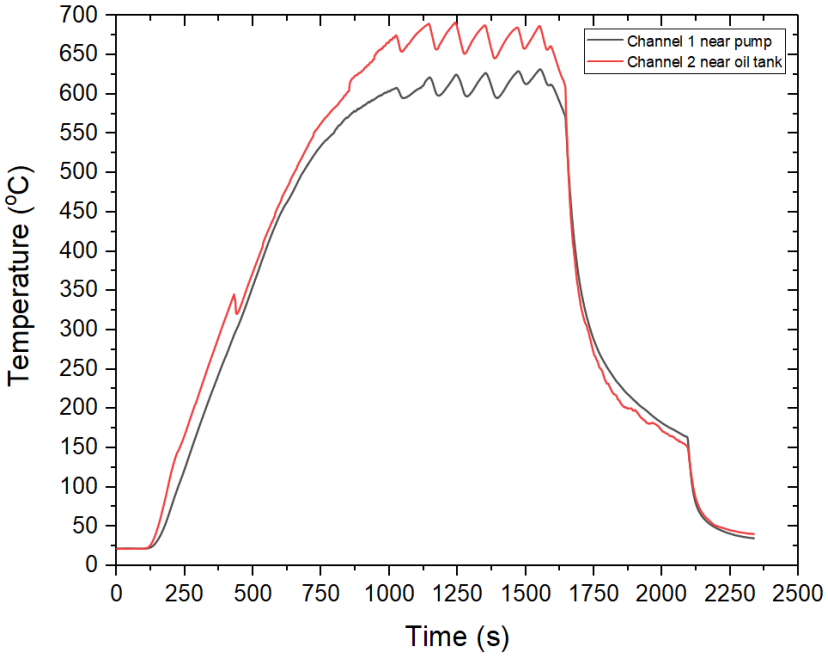

Figure 4-4 Temperature recording for a 650 ºC thermal fault experiment

The DGA measurement results for a 650 ºC thermal fault experiment are shown in Figure 4-5. Different from the post fault measurement results in the 450 ºC thermal fault experiment shown in Figure 4-3, the fault gases, after a 10-minute heating duration in a 650 ºC thermal fault, increase slowly and take approximately 24 hours to reach a steady-state. This is due to free gases being generated and released to the gas phase, with a longer time taken to dissolve back to the oil phase, resulting in equilibrium status being slowly reached. The volume of the generated free gases is around 220 mL in the 650 ºC thermal fault experiment. It can be seen that methane, ethane and ethylene are mainly generated, especially ethylene. Moreover, acetylene

starts to be generated in a 650 ºC thermal fault even though the generation amounts are quite small at 4 ppm. Meanwhile, hydrogen is also generated after heating process. There are negligible amounts of carbon oxide gases generated when compared to the large generation of hydrocarbon gases. To sum up, there is an approximate 122.5 ppm increase in hydrogen, 2709 ppm increase in methane, 1877 ppm increase in ethane and 3931 ppm increase in ethylene.

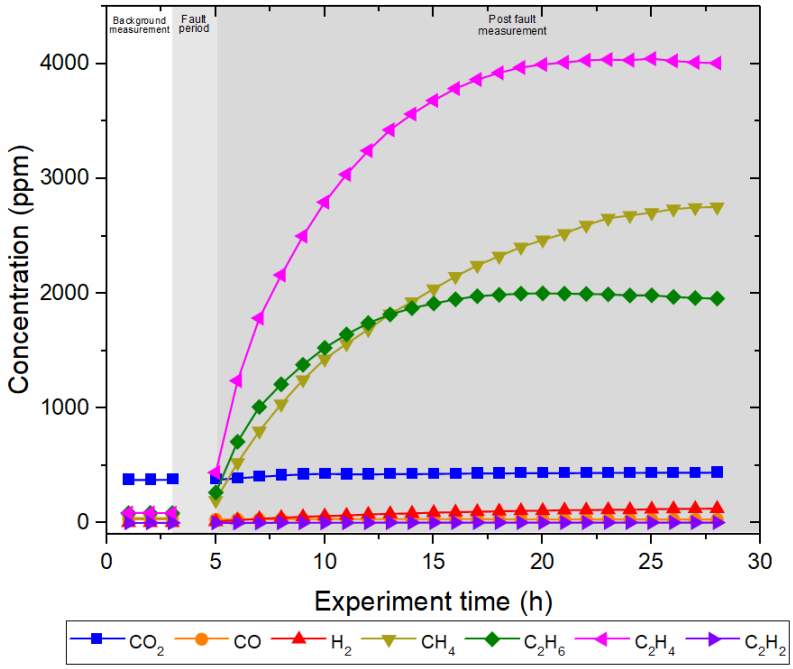

Figure 4-5 DGA measurement results for a 650 ºC thermal fault in a mineral oil insulation system

4.3.3 Gas generation characteristics under various fault temperatures

For mineral oil, a series of 11 experiments were conducted, including 3 experiments at 350 ºC, 2 experiments at 450 ºC, 3 experiments at 550 ºC, 1 experiment at 650 ºC and 2 experiments at 750 ºC. The repeating experiments at the thermal fault temperature show a reasonable repeatability when the relative differences are within 20%. The gas-in-oil fault gas generation results are listed in Table 4-2. It needs to be noted that the reported gas-in-oil generation results in Table 4-2 are based on the average values of the repeating experiments if there are any.

Table 4-2 Gas-in-oil generation results in mineral oil under various fault temperatures, ppm

Temperature (Heating duration)	H_2	CH_4	C_2H_6	C_2H_4	C_2H_2	CO_2	CO
350 ºC (72 h)	0.0	5.6	2.5	2.9	0.0	20.0	9.4
450 ºC (10 h)	0.0	16.1	18.1	1.8	0.0	25.0	17.5
550 ºC (4 h)	11.9	149.8	156.0	94.4	0.0	25.2	37.2
650 ºC (10 mins)	122.5	2708.6	1876.6	3931.1	3.8	62.3	0.0
750 ºC (1 min)	1367.9	21744.6	9379.6	32449.1	195.3	4.7	3.0

It can be seen that gas-in-oil fault gases are generated in higher amounts with the increase in thermal fault temperature. Carbon oxide gases are generated from a 350 ºC thermal fault. Hydrocarbon gases are clearly generated from a 450 ºC thermal fault and increase significantly from a 650 ºC thermal fault. Among these fault gases, hydrogen is not generated in the 350 ºC and 450 ºC thermal fault experiments but starts to be generated from the 550 ºC thermal fault experiment. In addition, there is no generation of acetylene in all thermal fault temperatures up to 550 ºC. Acetylene starts to be generated in the 650 ºC thermal fault experiment and largely generated in the 750 ºC thermal fault experiment. Free gases are generated in the 650 ºC and 750 ºC thermal fault experiments. The volume of free gases in the 650 ºC and 750 ºC thermal fault experiments is around 220 ml and 1050 ml, respectively.

The gas-in-oil generation rates of each fault gas under different thermal fault temperatures are calculated and shown in Figure 4-6. The gas-in-oil generation rates of most fault gases increase with the increasing thermal fault temperature. The overall increasing tendency of gas-in-oil generation rates of hydrocarbon gases and hydrogen is faster than that of carbon oxide gases, especially from 550 ºC onwards. In addition, the gas-in-oil generation rate of ethylene is lower than methane and ethane when the thermal fault temperature is lower than 550 ºC, and then exceeds all the other fault gases starting from 650 ºC and above. Almost the same gas-in-oil generation rates are observed between methane and ethane throughout the temperature range. The

increasing trends of carbon oxide gases are comparable with hydrocarbon gases at temperatures up to 550 ºC and become noticeably slower at higher temperatures of 650 ºC and 750 ºC.

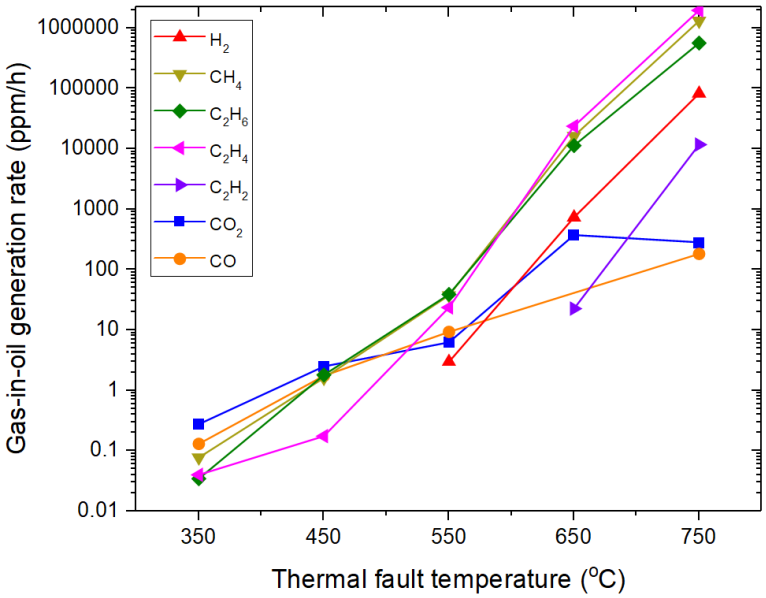

Figure 4-6 Gas-in-oil generation rates in mineral oil under different thermal fault temperatures

The chemical structure of mineral oil contains C-C and C-H molecular bonds, and there are no oxygen atoms in mineral oil molecules, with hydrocarbon gases more easily produced from the reactions of small unstable fragments formed by the broken C-C and C-H bonds [5]. However, the generation of carbon oxide gases can come from the reactions with dissolved oxygen or catalytic reactions with metal [22, 24]. In this study, the material of the experimental setup is stainless steel which is chemically stable with the insulating liquid. Therefore, the generation of carbon oxide gases is less likely due to the fewer reactions with the metal. However, although the degassing process is performed before each experiment, some oxygen is still dissolved in the oil, resulting in the generation of carbon oxide gases. With the increasing thermal faults, the reactions become more violent. Considering the limitation of oxygen dissolved in the oil, the carbon dioxide generation rates level off from 650 ºC (as shown in Figure 4-6).

Figure 4-7 shows the gas-in-oil generation pattern ratios of combustible gases under

different thermal fault temperatures in the mineral oil. The gas-in-oil generation pattern ratios of each combustible gas change with the increasing thermal fault temperatures. For hydrocarbon gases, the gas-in-oil generation pattern ratio of methane shows an increase tendency with the increasing temperature, reaching the maximum at the 750 ºC thermal fault with 34% of methane. The gas-in-oil generation pattern ratio of ethane increases from 350 ºC to 550 ºC and then decreases from 550 ºC to 750 ºC. The maximum gas-in-oil generation pattern ratio of ethane at the 550 ºC thermal fault is 35%. The overall gas-in-oil generation pattern ratio of ethylene shows an increase tendency from 350 ºC to 750 ºC. The maximum gas-in-oil generation pattern ratio of ethylene at a 750 ºC thermal fault is 50%. However, the gas-in-oil generation pattern ratio of acetylene is quite small that cannot be visible from the figure because the gas-in-oil generation amounts of acetylene are much smaller when compared with the other fault gases. There are very small gas-in-oil generation pattern ratios of hydrogen in the 550 ºC, 650 ºC and 750 ºC thermal faults. In addition, for carbon monoxide, there is a decreasing tendency in the gas-in-oil generation pattern ratio.

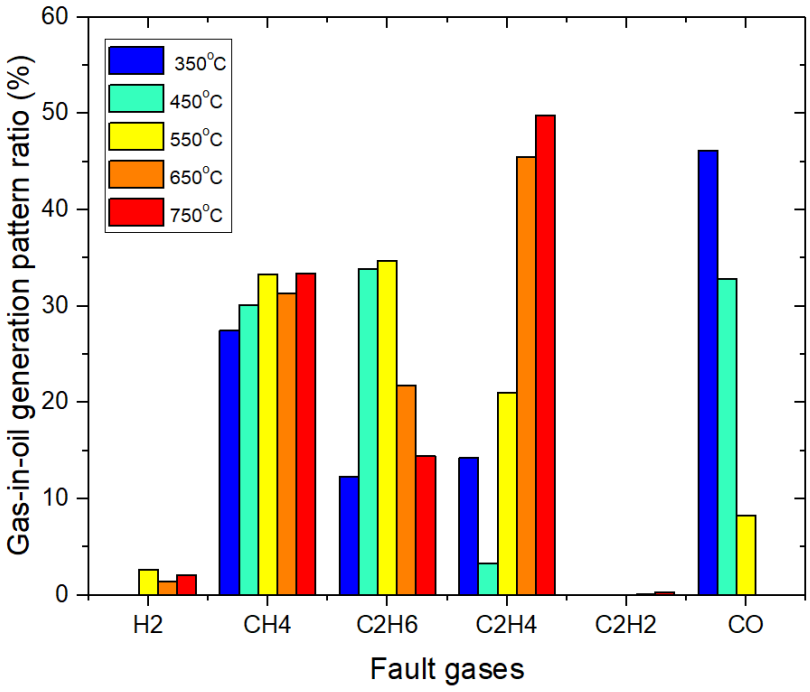

Figure 4-7 Gas-in-oil generation pattern ratios of combustible gas under different thermal fault temperatures in mineral oil

In order to use fault gas generation characteristics to indicate different thermal fault levels, the gas-in-oil generation pattern ratios of combustible gases under each thermal fault temperature in mineral oil are shown in Figure 4-8.

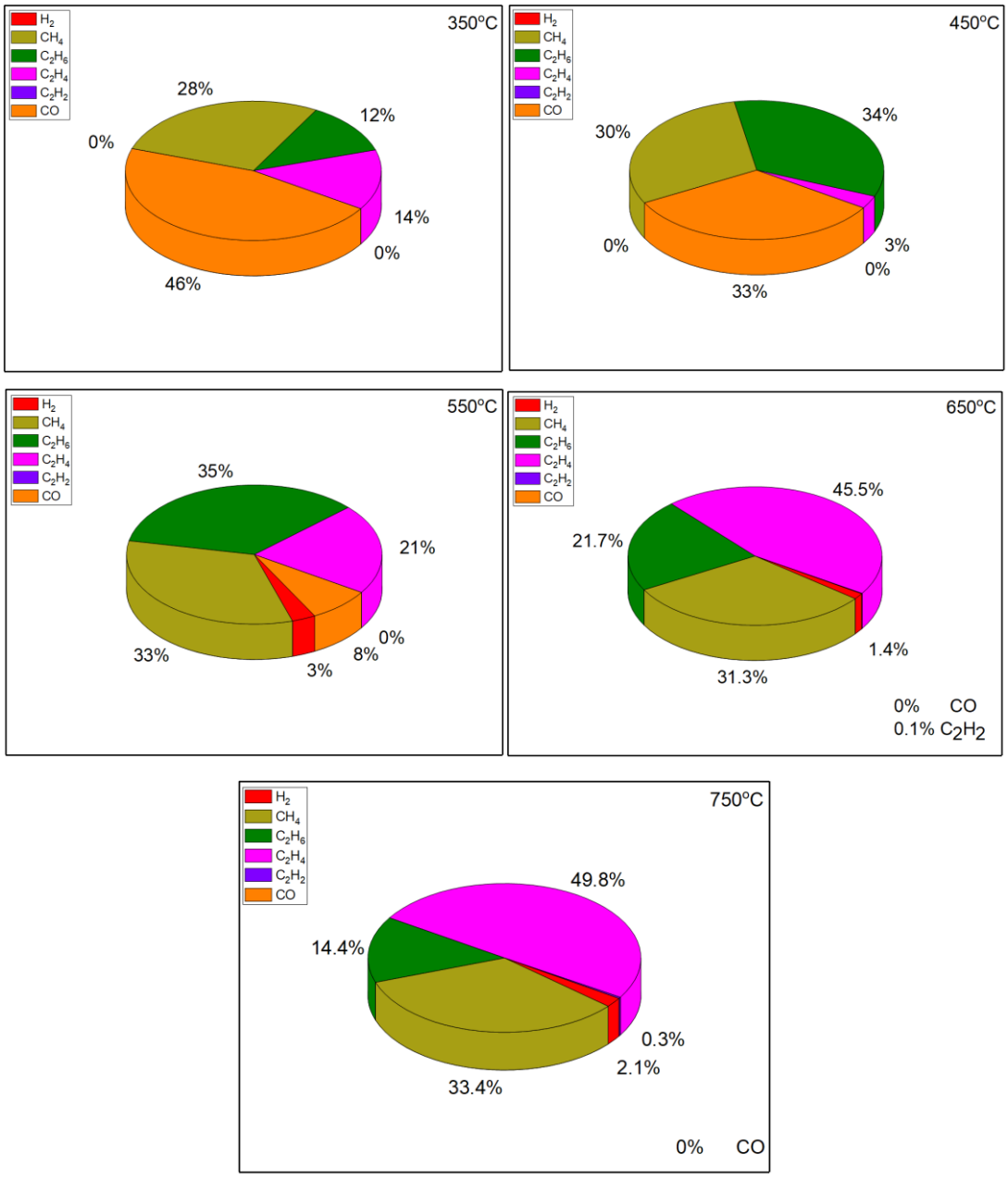

Figure 4-8 Gas-in-oil generation pattern ratios of combustible gases under each thermal fault temperature in mineral oil

In the 350 ºC thermal fault, the dominant fault gas is carbon monoxide it has a big gas-in-oil generation pattern ratio when compared with other fault gases. Methane is the dominant hydrocarbon gas. The presence of methane in the mineral oil has been considered as a suggestion for thermal fault occurrence [22, 47].

In the 450 ºC thermal fault, the hydrocarbon gas ethane has a big increase in the gas-in-oil generation pattern ratio when compared to the 350 ºC thermal fault. Ethane becomes the dominant fault gas.

When the thermal fault temperature increases to 550 ºC, the gas-in-oil generation pattern ratios of methane, ethane and ethylene all exceed the gas-in-oil generation pattern ratio for carbon monoxide, with ethane being the overall dominant fault gas. In addition, ethylene has a big increase in the gas-in-oil generation pattern ratio when compared to the lower thermal fault temperatures. When the temperature increases to modest temperatures in T2 thermal fault range, ethane and ethylene, the higher molecular weight gases, are largely generated [22, 47]. Moreover, hydrogen has a small gas-in-oil generation pattern ratio in the 550 ºC thermal fault.

In the 650 ºC thermal fault, the gas-in-oil generation pattern ratio of ethylene exceeds all the other fault gases, becoming the dominant gas. Hydrogen still has a small gas-in-oil generation pattern ratio. In addition, as shown in Table 4-2, acetylene starts to be generated at a 650 ºC thermal fault, although the gas-in-oil generation pattern ratio is quite small.

In the 750 ºC thermal fault, ethylene is still the dominant fault gas, with its gas-in-oil generation pattern ratio reaching the maximum value of 50%. The same as in the 550 ºC and 650 ºC thermal faults, hydrogen has small gas-in-oil generation pattern ratios, hence the presence of the hydrogen can suggest a thermal fault temperature of 550 ºC and above. Meanwhile, the presence of the acetylene can indicate an extremely high thermal temperature of 650 ºC and above [22, 47].

4.4 Generation of Fault Gases in Synthetic Ester Liquid

4.4.1 Experiments without free gases generation

The same as in the mineral oil thermal fault experiments, no free gases are generated

in the experiments when the thermal fault temperatures are set from 350 ºC to 550 ºC in synthetic ester liquid. It should be noted that the reported gas-in-oil results in synthetic ester liquid are already calibrated and converted to 25 ºC based on the equations in Chapter 3. The gas-in-oil generation of dissolved gases is calculated as the difference between the average values of the last three post fault measurements and the average values of the three background measurements. Meanwhile, the same temperature control is achieved as in the mineral oil experiments when conducting experiments in synthetic ester liquid from 350 ºC to 550 ºC. Figure 4-9 shows the DGA measurement results for the 450 ºC thermal fault experiment. The measurements include three background measurements and twelve post fault measurements. Different from the 450 ºC thermal fault experiment in mineral oil, the dissolved gases take 12 hours to reach a steady status in synthetic ester liquid after experiencing a thermal fault. Five different dissolved gases are detected including carbon dioxide, carbon monoxide, methane, ethane and ethylene. The generation of carbon dioxide and carbon monoxide are evident and much higher than hydrocarbon gases. Among these five different dissolved gases, there is an approximate 229 ppm increase in carbon dioxide, 107 ppm increase in carbon monoxide, 29 ppm increase in methane, 69 ppm increase in ethane and 37 ppm increase in ethylene after experiencing a 450 ºC thermal fault for 10 hours.

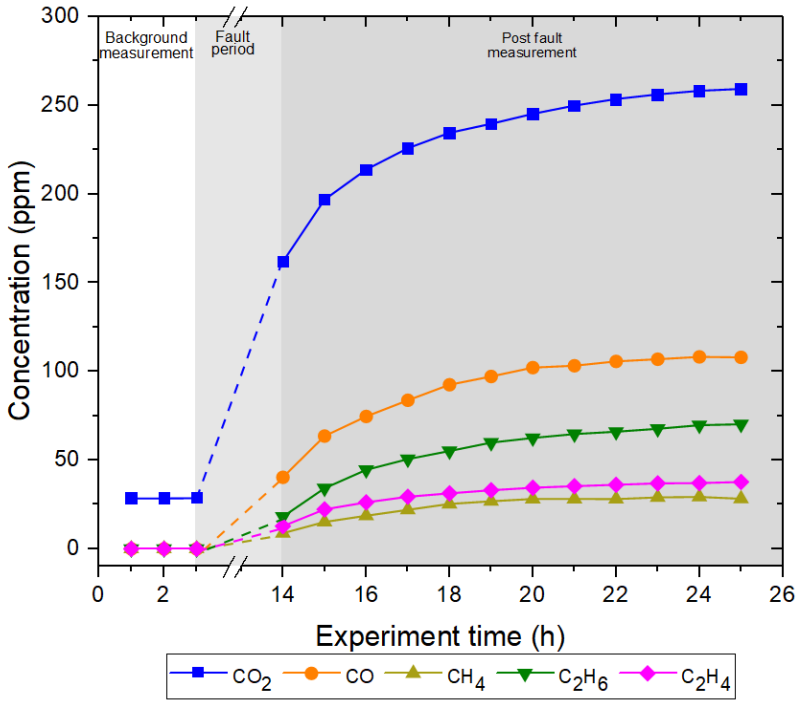

Figure 4-9 DGA measurement results for a 450 ºC thermal fault in synthetic ester liquid

4.4.2 Experiments with free gases generation

Free gases are also generated in synthetic ester liquid experiments when the thermal fault temperatures are set at 650 ºC and 750 ºC. The same temperature control is achieved as the experiments in mineral oil when conducting experiments in synthetic ester liquid at 650 ºC and 750 ºC. Figure 4-10 shows the gas-in-oil DGA measurement results for the 650 ºC thermal fault experiment in synthetic ester liquid. The volume of generated free gases is around 350 ml. As free gases are generated and released in the gas phase, a longer time is also needed in synthetic ester liquid thermal fault experiments to let fault gases dissolve back to the oil phase and reach equilibrium status. However, compared with the 650 ºC thermal fault experiment in mineral oil, 50 hours are needed in synthetic ester liquid to reach a steady-state. Six fault gases are generated including carbon dioxide, carbon monoxide, hydrogen, methane, ethane and ethylene. Among these gases, carbon dioxide is generated in the largest amount and is the dominant gas dissolved in liquid during a 650 ºC thermal fault. There is an approximate 163 ppm increase in hydrogen, 2546 ppm increase in methane, 6123 ppm increase in ethane, 3749 ppm increase in ethylene, 9683 ppm increase in carbon

dioxide and 4198 ppm increase in carbon monoxide.

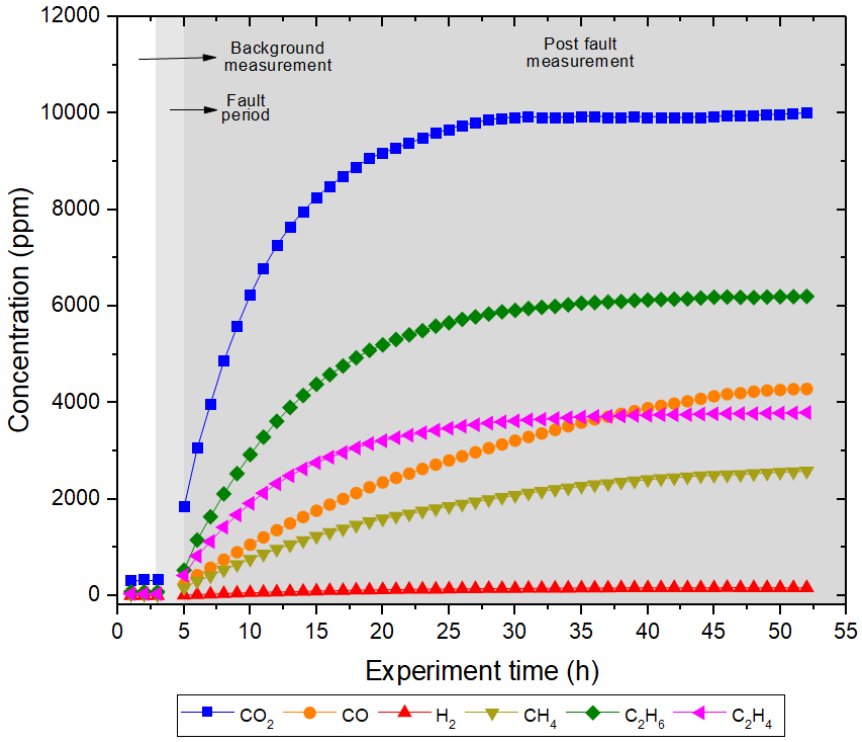

Figure 4-10 DGA measurement results for a 650 ºC thermal fault in synthetic ester liquid

4.4.3 Gas generation characteristics under various fault temperatures

In total, a series of five experiments were conducted on thermal fault temperatures from 350 ºC to 750 ºC in synthetic ester liquid. The gas-in-oil fault gas generation results are listed in Table 4-3. The gas-in-oil fault gases are generated in higher amounts with the increasing temperature of the thermal fault. Carbon oxide gases are generated in large amounts throughout the fault temperature range. Concerning the synthetic ester liquid, there are organic compounds and unsaturated hydrocarbon compounds that have oxygen atoms, with the scission of these compounds easily resulting in the generation of carbon oxide gases [22, 68].

Table 4-3 Gas-in-oil generation results between 350 ºC and 750 ºC thermal faults in synthetic ester liquid, ppm

Temperature (Heating duration)	H_2	CH_4	C_2H_6	C_2H_4	C_2H_2	CO_2	CO
350 ºC (30 h)	0.0	8.9	20.5	36.1	0.0	173.7	33.4
450 ºC (10 h)	0.0	28.9	69.2	37.2	0.0	229.4	107.7
550 ºC (4 h)	4.43	44.6	104.8	61.2	0.0	196.8	79.9
650 ºC (10 mins)	163.3	2545.8	6122.6	3749.3	0.0	9683.4	4198.2
750 ºC (1 min)	277.5	7364.9	6705.7	18594.6	90.9	12731.9	3283.9

Hydrogen is not generated in the 350 ºC and 450 ºC thermal fault experiments but starts to be generated from the 550 ºC thermal fault experiment. The hydrocarbon gases are generated in much larger amounts and in much shorter heating durations at 650 ºC and 750 ºC thermal fault temperatures. In addition, there is no generation of acetylene under the thermal fault temperatures up to 650 ºC, with it only being generated in the 750 ºC thermal fault experiment. The volume of free gases in the 650 ºC and 750 ºC thermal fault experiments is around 350 ml and 960 ml, respectively.

The gas-in-oil generation rates of each fault gas under different thermal fault temperatures are calculated and presented in Figure 4-11. The gas-in-oil generation rates of fault gases increase with the increasing thermal fault temperature. Different from the mineral oil results, the increasing trend of carbon dioxide is not slowed down at higher temperatures since the chemical structure of the synthetic ester liquid contains oxygen atoms that contribute to the generation of carbon oxide gases. Meanwhile, the fault gases have almost the same increasing trend when thermal fault temperature is lower than 650 ºC. When the temperature reaches 750 ºC, the gas-in-oil generation rate of ethylene exceeds all the other fault gases.

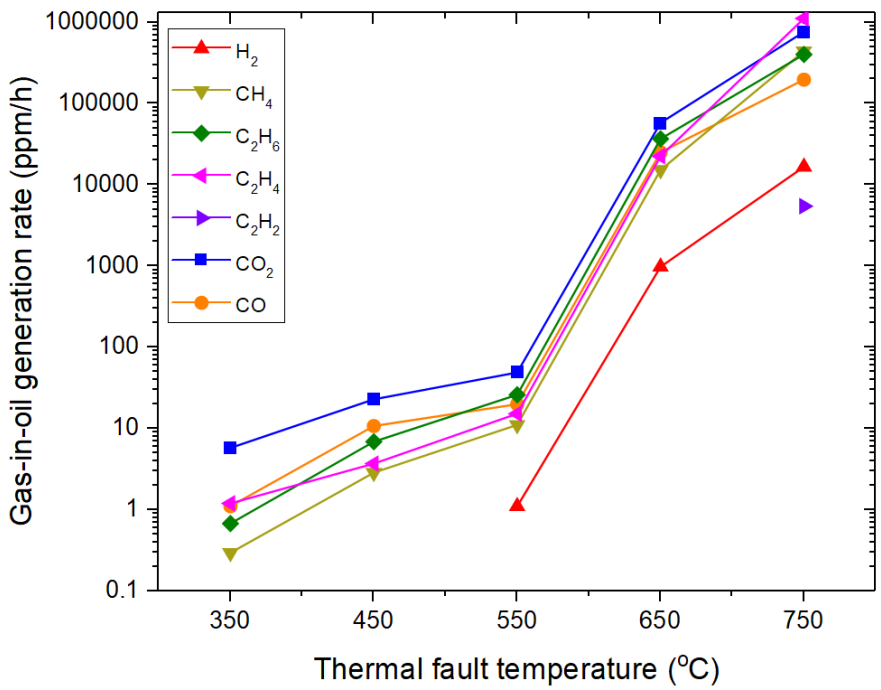

Figure 4-11 Gas-in-oil generation rates between 350 ºC and 750 ºC thermal faults in synthetic ester liquid

Figure 4-12 shows the gas-in-oil generation pattern ratios of each combustible gas under different thermal fault temperatures in the synthetic ester liquid. The gas-in-oil generation pattern ratios of each combustible gas change with the increasing thermal fault temperatures. Concerning the hydrocarbon gases, the gas-in-oil generation pattern ratio of methane increases with the increasing temperature and reaches the maximum value of 20% under the 750 ºC thermal fault. The gas-in-oil generation pattern ratio of ethane increases at the 350 ºC to 650 ºC thermal faults and then decreases from 650 ºC to 750 ºC thermal faults. The maximum gas-in-oil generation pattern ratio of ethane is 36% at the 650 ºC thermal fault. The overall gas-in-oil generation pattern ratio of ethylene has an increasing tendency. The maximum gas-in-oil generation pattern ratio of ethylene at the 750 ºC thermal fault is 50%. However, the gas-in-oil generation pattern ratio of acetylene is quite small and is not visible in the figure since the gas-in-oil generation amounts of acetylene are much smaller when compared with the other fault gases. There are very small gas-in-oil generation pattern ratios for hydrogen at 550 ºC, 650 ºC and 750 ºC thermal faults. In addition, for carbon monoxide, the gas-in-oil generation pattern ratio shows an overall

decreasing tendency.

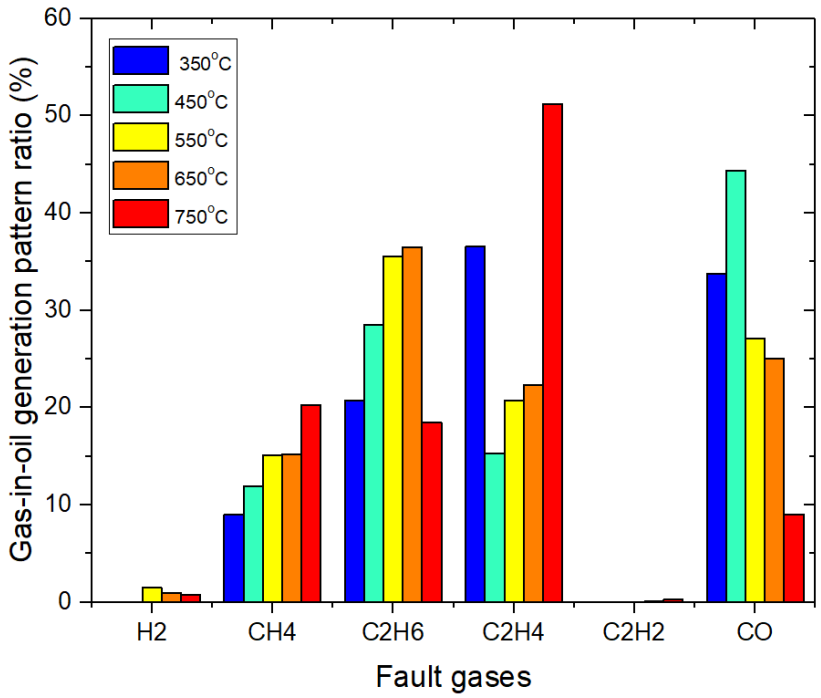

Figure 4-12 Gas-in-oil generation pattern ratios of each combustible gas under different thermal fault temperatures in synthetic ester liquid

Figure 4-13 shows the gas-in-oil generation pattern ratios of the combustible gases under each thermal fault temperature in synthetic ester liquid.

For the 350 ºC thermal fault, the dominant fault gas is carbon monoxide and the dominant hydrocarbon gas is ethylene. For the 450 ºC thermal fault, the dominant fault gas is still carbon monoxide but the dominant hydrocarbon gas changes to ethane. Moreover, the gas-in-oil generation pattern ratios of methane and ethane increase, while the gas-in-oil generation pattern ratio of ethylene decreases when compared with the 350 ºC thermal fault.

For both the 550 ºC and 650 ºC thermal faults, the gas-in-oil generation pattern ratios of carbon monoxide keeps decreasing. On the contrary, the gas-in-oil generation pattern ratios of methane, ethane and ethylene keep increasing. The dominant fault gas and hydrocarbon gas is ethane. It needs to be noted that hydrogen starts to have a small pattern ratio at the 550 ºC thermal fault.

When the thermal fault temperature increases to 750 ºC, the gas-in-oil generation pattern ratio of ethylene exceeds all the other fault gases, with ethylene becoming the dominant gas. Acetylene starts to be generated at the 750 ºC thermal fault, with its gas-in-oil generation pattern among the generated fault gases being very small.

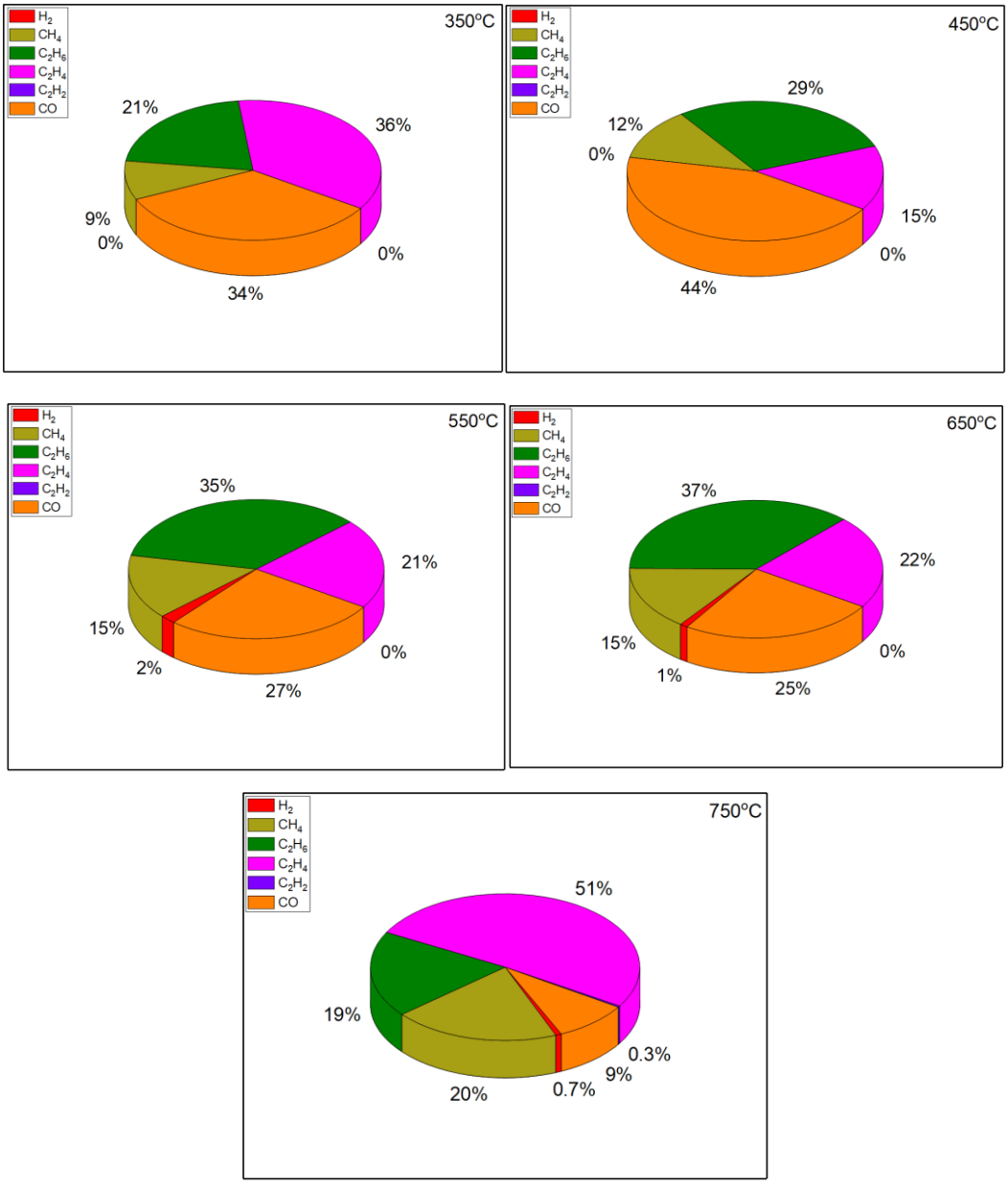

Figure 4-13 Gas-in-oil generation pattern ratios of combustible gases under each thermal fault temperature in synthetic ester liquid

4.5 Comparison of Fault Gas Generation Characteristics between Mineral Oil and Synthetic Ester Liquid

The comparisons of the gas-in-oil generation characteristics of fault gases between the mineral oil and the synthetic ester liquid are divided into two situations, the experiments without free gases generated and those with free gases generated.

4.5.1 Without free gases generation

There are no free gases generated when the thermal fault temperatures are between 350 ºC and 550 ºC for both insulating liquids. Figure 4-14 shows the compared results for the gas-in-oil generation pattern ratio of fault gases between mineral oil and synthetic ester liquid. When only considering the gas-in-oil generation pattern ratios of hydrocarbon gases, ethane is the dominant hydrocarbon gas at the 450 ºC and 550 ºC thermal faults for both insulating liquids. However, for the 350 ºC thermal fault, the dominant hydrocarbon gas is methane in mineral oil but ethylene in synthetic ester liquid. In addition, the gas-in-oil generation pattern ratio of methane is always higher than ethylene in mineral oil. On the contrary, the gas-in-oil generation pattern ratio of methane is always lower than ethylene in synthetic ester liquid. This is because ethylene is easily generated in synthetic ester liquid through natural ester specific reactions [68].

When considering all of the fault gases, carbon dioxide is the dominant fault gas for both insulating liquids at the 350 ºC and 450 ºC thermal faults. However, when the thermal fault temperature reaches 550 ºC, carbon dioxide is still the dominant fault gas for synthetic ester liquid but no longer the dominant fault gas for mineral oil. There is a faster decrease in the gas-in-oil generation pattern ratios for the carbon oxide gases as the temperature of the mineral oil increases compared to that in synthetic ester liquid. Hydrogen has a small gas-in-oil generation pattern ratio at the 550 ºC thermal fault for both insulating liquids. In a thermal fault, the presence of hydrogen can

indicate that the thermal fault temperature has already reached 550 ºC for both insulating liquids.

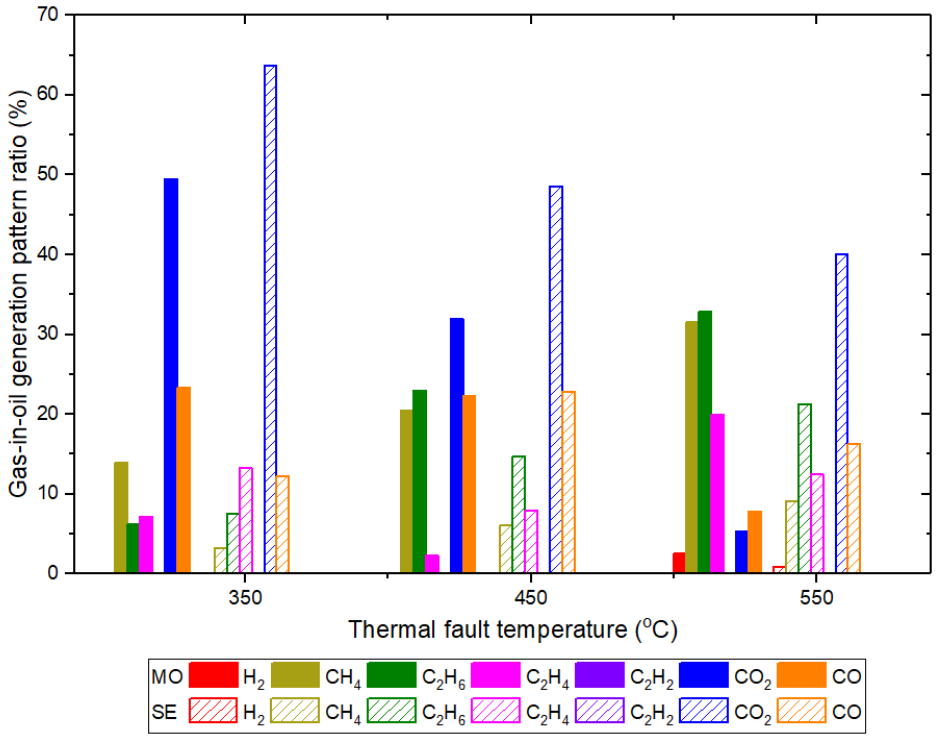

Figure 4-14 Comparison of gas-in-oil generation pattern ratios of fault gases in mineral oil and synthetic ester liquid between 350 ºC and 550 ºC thermal faults

4.5.2 With free gases generation

The free gases are generated in both insulating liquids at the 650 ºC and 750 ºC thermal faults. The free gases generated in the 650 ºC thermal fault in mineral oil is 220 ml, approximately 33% smaller than that in synthetic ester liquid which is 350 ml. The free gases generated by the 750 ºC thermal fault are comparable between two insulating liquids, which are 1050 ml in mineral oil and 960 ml in synthetic ester liquid. Figure 4-15 shows the compared results for the gas-in-oil generation pattern ratio of fault gases between mineral oil and synthetic ester liquid. It shows that carbon oxide gases already account for quite small gas-in-oil pattern ratios in mineral oil and are almost invisible. On the contrary, carbon oxide gases in synthetic ester liquid still have large gas-in-oil generation pattern ratios.

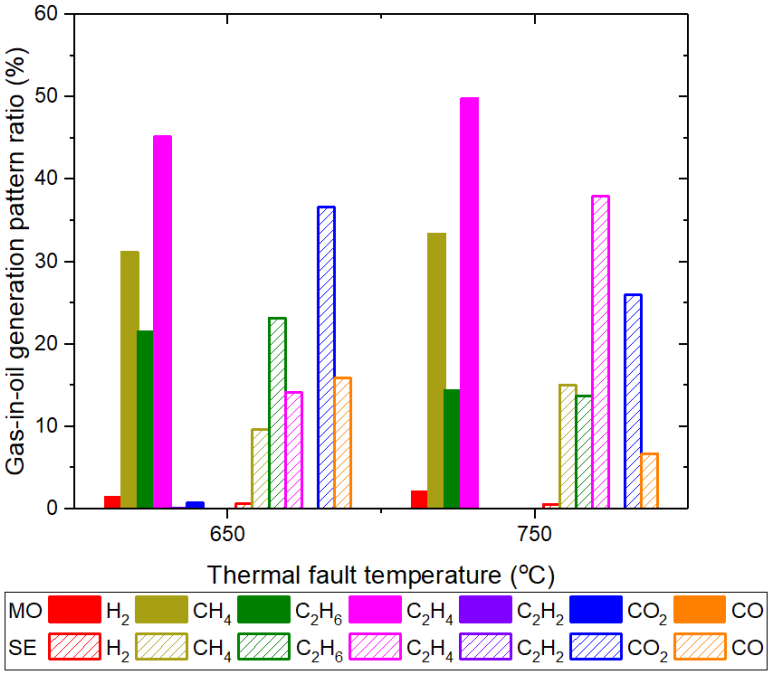

Figure 4-15 Comparison of gas-in-oil generation pattern ratios of fault gases in mineral oil and synthetic ester liquid under 650 ºC and 750 ºC thermal faults

Ethylene is the dominant fault gas among all the fault gases for mineral oil at the 650 ºC and 750 ºC thermal faults. However, ethylene is only the dominant fault gas for synthetic ester liquid at the 750 ºC thermal fault. The dominant fault gas for synthetic ester liquid during a 650 ºC thermal fault is still carbon dioxide and the dominant hydrocarbon gas is still ethane, which are similar findings to those under low temperature thermal faults. In addition, the gas-in-oil generation pattern ratio of ethylene is higher than methane for both insulating liquids at the 650 ºC and 750 ºC thermal faults. Meanwhile, there is also a small gas-in-oil generation pattern ratio of hydrogen at the 650 ºC and 750 ºC thermal faults for both insulating liquids, confirming that the presence of hydrogen in a thermal fault can suggest a thermal fault temperature of 550 ºC and above. Although the gas-in-oil generation pattern ratios of acetylene are not shown in the figure, the gas-in-oil generation results in section 4.3.3 and section 4.4.3 show that the acetylene starts to be generated at the 650 ºC thermal fault in mineral oil and at the 750 ºC thermal fault in synthetic ester liquid. Therefore, acetylene is the typical gas of high temperature thermal faults of 650 ºC and 750 ºC for mineral oil and of 750 ºC for synthetic ester liquid.

Comparing the results of the mineral oil and synthetic ester liquid with or without free gases generation, carbon oxide gases have the larger gas-in-oil generation pattern ratios in synthetic ester liquid, especially when the thermal fault temperature is higher than 550 ºC. In addition, the gas-in-oil generation pattern ratio of methane is higher than that of ethylene in mineral oil when the thermal fault temperature is between 350 ºC and 550 ºC, and lower than that of ethylene when the thermal fault temperatures are 650 ºC and 750 ºC. On the other hand, the gas-in-oil generation pattern ratio of ethylene is always higher than methane in synthetic ester liquid between 350 ºC and 750 ºC thermal faults.

4.6 Summary

In summary, a series of experiments simulating T2 and T3 thermal faults were conducted in mineral oil and synthetic ester liquid. Both insulating liquids generate the same types of fault gases. The gas-in-oil generation rates of all seven fault gases increase with the thermal fault temperature. When reaching 650 ºC and 750 ºC thermal fault temperatures, free gases are generated in both liquids. Compared to the mineral oil, carbon oxide gases are largely generated in synthetic ester liquid due to the oxygen atoms contained in its chemical structure.

When thermal faults are between 350 ºC and 550 ºC, carbon dioxide is the dominant fault gas in both insulating liquids at the 350 ºC and 450 ºC thermal faults. When the thermal fault reaches 550 ºC, carbon dioxide is still the dominant fault gas for synthetic ester liquid, while ethane becomes the dominant fault gas for mineral oil. If only considering hydrocarbon gases, ethane is the dominant fault gas for both insulating liquids at the 450 ºC and 550 ºC thermal faults. However, at the 350 ºC thermal fault, methane is the dominant fault gas in mineral oil, while ethylene is the dominant fault gas in synthetic ester liquid.

For 650 ºC and 750 ºC thermal faults, ethylene is the dominant faults gas in mineral oil. However, ethylene is only the dominant fault gas for synthetic ester liquid at the 750

ºC thermal fault. The dominant fault gas in synthetic ester liquid at the 650 ºC thermal fault is still carbon dioxide and the dominant hydrocarbon gas is still ethane. Meanwhile, the generation of hydrogen in a thermal fault can suggest thermal fault temperature has already reached 550 ºC for both insulating liquids. Acetylene can be the typical gas to suggest that the thermal fault temperature has already reached 650 ºC in mineral oil and reached 750 ºC in synthetic ester liquid.

Chapter 5 Generation of Carbon Oxide Gases in Mineral Oil and Kraft Paper Insulation System under Simulated Thermal Faults

5.1 Introduction

For a liquid-immersed transformer, the insulation system mainly consists of liquid and solid insulation materials. Cellulose paper and pressboard form the solid insulation, which has two main functions: to provide sufficient electrical strength to withstand the high voltage stresses and to provide sufficient mechanical strength to support the integrity of a transformer's winding structure. The representation of thermal faults in a transformer is normally a localised hotspot, which often occurs at the top part of the winding where cellulose insulation is used. Previously, many ageing studies were conducted on different oil-paper insulations at temperatures usually up to 130 ºC with varying ageing durations up to months [38-41, 104]. These accelerated ageing tests were usually undertaken in sealed containers placed in an air-circulating oven where a uniform temperature profile was applied to the oil-paper insulation. In addition, DGA was rarely conducted in these ageing studies due to the challenges associated with long-term sealing performance. Meanwhile, the thermal faults in real transformers are not only happened in insulating liquids but also in the area of oil-paper insulation. Therefore, it is of importance to study gas generation characteristics in oil-paper insulations under laboratory simulated localised thermal faults.

In this chapter, a series of thermal faults with various fault durations are simulated using the tube-heating method in a mineral oil-Kraft paper insulation system to investigate fault gas generation characteristics and, in particular, carbon oxide gases. The experimental procedure is initially introduced and the gas-in-oil generation results are then reported. In addition, conventional paper ageing indicators, like DP and 2-FAL, are measured and the relationship between different indicators are

analysed.

5.2 Experimental Condition and Procedure

5.2.1 Sample preparation

The investigated oil-paper insulation includes a mineral oil, Gemini X from Nynas and a non-thermally upgraded Kraft paper from Weidmann. The oil to paper ratio in the heating tube is 20:1, based on 12.0 g of mineral oil and 0.6 g of Kraft paper. In addition, the oil experiencing the thermal fault in the heating tube will be largely diluted in 6.6 L of bulk oil after the simulated faults. The size of the heating tube and fault area are shown in Figure 5-1 (a). The length of the heating tube is 34 cm, of which only 15 cm is heated by a furnace. This 15 cm long area is regarded as the thermal fault area. Three layers of Kraft paper samples are inserted only into this fault area and in a way that it is in tight contact with the inner surface of the heating tube. The insertion method ensures that the Kraft paper samples will experience the hotspot temperature and enables nature oil flow inside the heating tube. The 0.6 g Kraft paper samples are cut into three pieces of 15 cm in length and 3 cm in width. And then the Kraft samples are inserted into the defined fault area of the heating tube. A schematic diagram of the method used to insert the Kraft paper samples is shown in Figure 5-1 (b). Layer 1 is the layer of Kraft paper in direct contact with the inner surface of the heating tube (L1TMO), layer 3 is in contact with the oil (L3OMO) and layer 2 is in between layer 1 and layer 3 (L2MMO). The aim of this schematic diagram is to display the positions of the three layers in the fault area of the heating tube, with space deliberately left between each layer. In the experiments, these three layers are tightly touching each other with no visible gaps between them.

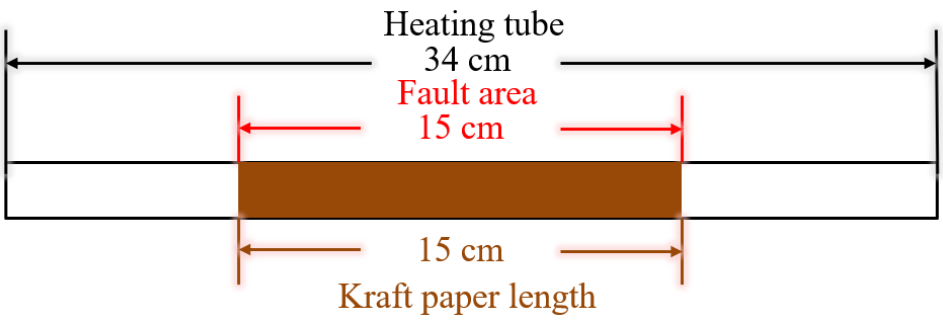

(a)

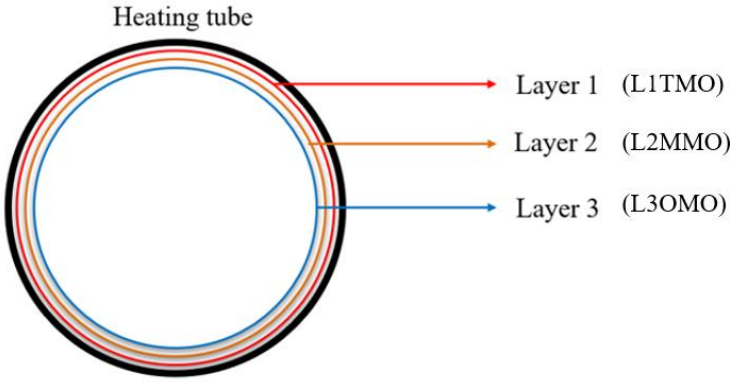

(b)

Figure 5-1 Position and length of Kraft paper inserted in the heating tube: (a) Front view and (b) Cross section view

Before conducting the formal experiments, the mineral oil and Kraft paper samples need to be pre-processed. 6.6 L of mineral oil (including 6 L of oil in the oil tank, 0.6 L of oil in the pipework) is initially injected into the oil tank through the embedded pump in the online DGA monitor TM8. Nitrogen is then used to purge the mineral oil for 3 hours to remove other gases and water content. After the degassing process, a vacuum pump is connected to the vacuum port on the oil tank to remove headspace gases, with 2.5 L of nitrogen then filled in the headspace through the gas sampling port on the lid. The Kraft paper samples are pre-processed following the procedure discussed in Chapter 3 section 3.7. Finally, the mineral oil and Kraft paper samples can achieve the moisture level of less than 10% relative humidity and less than 1% by weight, respectively. Moreover, the experiment conditions are summarised in Table 5-1. During the experiment, the thermal fault temperature is set at 250 ºC and 10 different heating durations from 0.5 to 24 hours are selected. Meanwhile, the

experiments are repeated for 2 times for each heating period to observe the repeatability of the experiments.

Table 5-1 Conditions for the mineral oil-Kraft paper experiments

Insulating liquid	Mineral oil (Gemini X)
Solid insulation	Non-thermally upgraded Kraft paper
Fault temperature	250 ºC
Heating period	0.5 h, 1 h, 2 h, 4 h, 6 h, 8 h, 12 h, 16 h, 20 h, 24 h
Oil weight in heating tube	12 g
Paper weight in heating tube	0.6 g
Liquid volume	6.6 L (6 L in the main tank + 0.6 L in the pipework)
Headspace volume	2.5 L N_2 (1.6 L in the main tank + 0.9 L in the bladder)

5.2.2 Test procedure

One of the 24-hour experiments is used as an example to introduce the test procedure and DGA measurements. The experiment procedure for the mineral oil-Kraft paper experiments is almost the same as the oil only experiments discussed in Chapter 4 section 4.2.2. The step 8 is not included as the free gases are not generated in oil-paper experiments. In addition, the volume of oil samples after each sampling process is 150 ml. After the experiment, the heating tube is disassembled from the system and the Kraft paper samples inside the heating tube are taken out for DP measurement. Oil samples before and after the heating process are used for 2-FAL measurement. To start a new experiment, a new heating tube with newly processed Kraft paper samples is reconnected to the system and 300 ml of newly processed oil is refilled into the system.

In order to simulate a specific fault temperature, both sides of the heating tube within the furnace are monitored. Figure 5-2 shows the recorded temperature profile during the 24-hour heating duration. It can be seen that the temperatures rise up quickly and remain stable for the entire heating duration. The side with the lower temperature

value is controlled to be exactly 250 ºC, while the other side of the heating tube is slightly higher than 250 ºC to ensure the oil-paper insulation inside the heating tube truly experiences the expected thermal fault temperature.

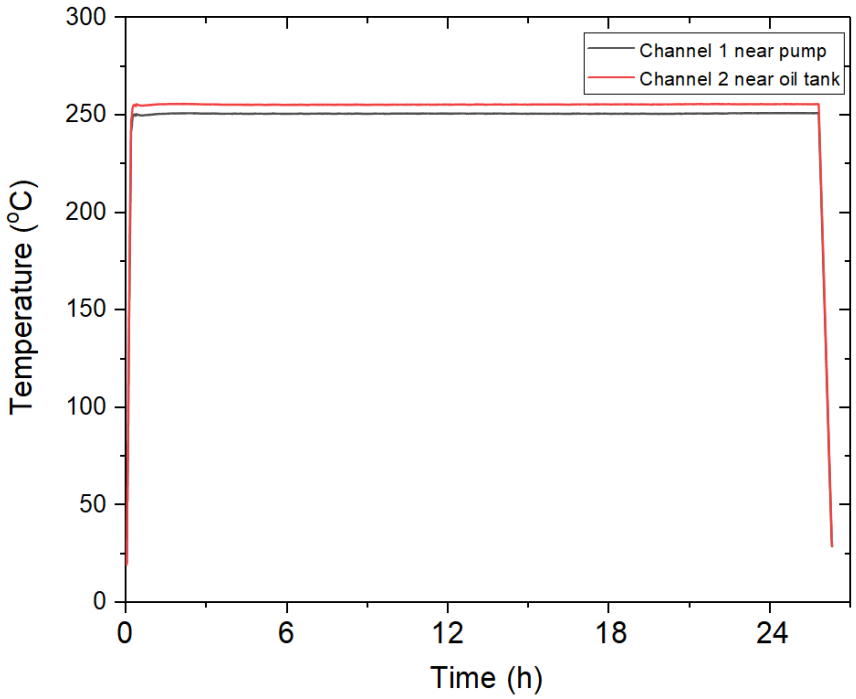

Figure 5-2 Temperature recording of a 24-hour heating duration for the mineral oil-Kraft paper experiment

Figure 5-3 shows the DGA results measured by the online DGA monitor TM8. The measurements include three background measurements and twelve post fault measurements. The concentrations of dissolved gases are measured from the oil phase and the reported results are gas-in-oil concentrations. Five different dissolved gases are detected by the online DGA monitor including carbon dioxide, carbon monoxide, methane, ethane and ethylene. Although methane, ethane and ethylene are detected in the background measurements, there is almost no generation of these three gases after 24 hours of simulated thermal fault. Moreover, the 24-hour fault duration is the longest fault period investigated in this chapter and the generated amounts of hydrocarbon gases in the longest fault period are inconspicuous, hence the generation of hydrocarbon gases can accordingly be neglected in all fault durations.

However, an increase in carbon oxide gases, the carbon dioxide and the carbon

monoxide, is evident. This is because that carbon dioxide and carbon monoxide are by-products of cellulose degradation under the simulated thermal fault. From the DGA measurement results, both carbon dioxide and carbon monoxide concentrations rapidly increase at the beginning and tend level off until reaching the steady-state. The gas-in-oil generations of carbon dioxide and carbon monoxide are calculated as the differences between the average values of the last three post fault measurements and the average of the three background measurements. Here, there is an approximate 240 ppm increase in carbon dioxide and 25 ppm increase in carbon monoxide after experiencing the 250 ºC thermal fault for 24 hours.

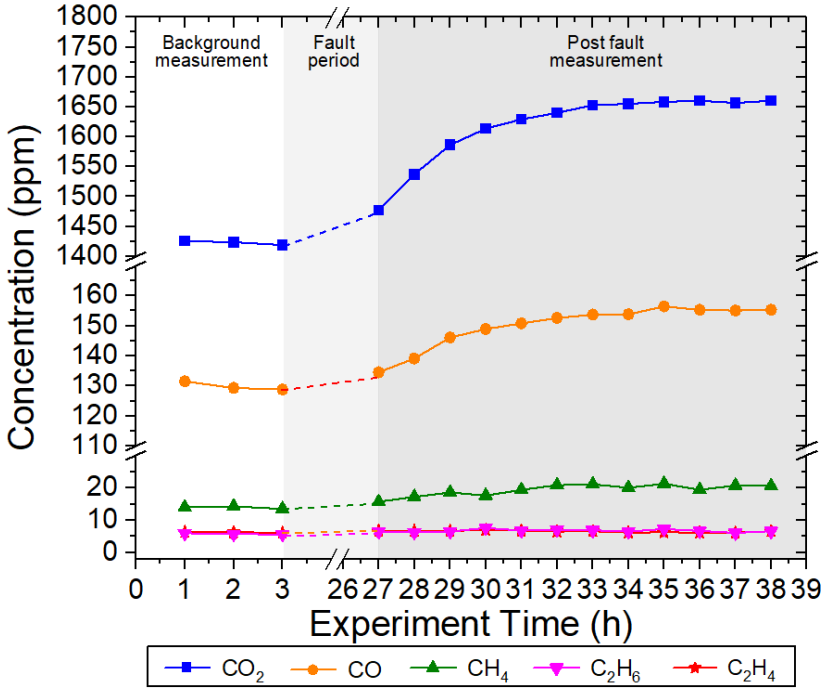

Figure 5-3 DGA measurement results for a 24-hour heating duration in the mineral oil-Kraft paper insulation system

5.3 Generation of Fault Gases

5.3.1 Mineral oil only experiment

The presence of faults will result in the generation of fault gases due to the chemical decomposition of the insulating materials, which includes both mineral oil and cellulose in this study. To investigate the generation of carbon oxide gases during the degradation of cellulose paper under thermal stress of 250 ºC, it is important to

understand the amounts of carbon oxide gases can be generated in the mineral oil when under the same thermal stress. The longest fault period of 24 hours is initially selected to perform the mineral oil only experiment because if negligible amounts of fault gases are generated, it is unnecessary to conduct shorter fault duration experiments.

The experiment procedure is the same as the oil-paper experiment, with the only difference being that there are no Kraft paper samples inserted in the heating tube. The DGA measurement results from the online DGA monitor are plotted in Figure 5-4, which clearly shows a negligible generation of dissolved gases after the 24-hour fault period. Since the generation of fault gases in the longest fault period are negligible, there is no need to perform shorter fault period experiments, with it being reasonable to assume that mineral oil will not contribute to gas generation in the following tests with both mineral oil and Kraft paper insulation.

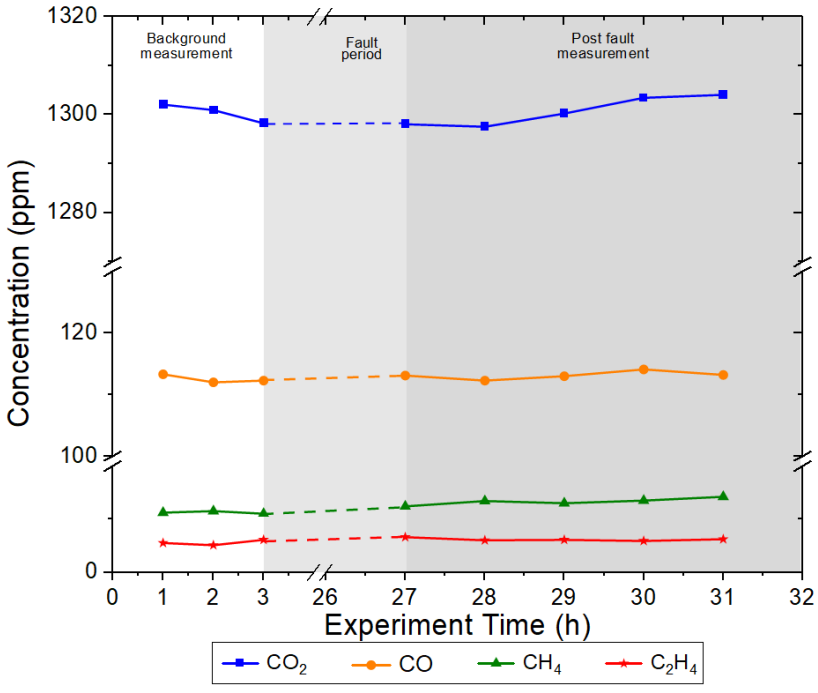

Figure 5-4 DGA measurement results for a 24-hour duration period in the mineral oil only experiment

5.3.2 Mineral oil-Kraft paper experiments

For the mineral oil-Kraft paper experiments, a series of 19 experiments, including

some repeating experiments, were conducted to investigate fault gas generation characteristics at a 250 ºC thermal fault with different heating durations. It needs to be noted that only one experiment was conducted for 20-hour heating duration. The experimental procedure follows the procedure introduced in section 5.2.2. When analysing gas generation results, two aspects need to be considered. First, the concentrations of gases in the post fault measurements need to reach a steady-state, which is assumed as equilibrium status; Second, the reported DGA measurement results are the gas-in-oil values that have been converted to 25 ºC. Only the gas-in-oil generation results of carbon dioxide and carbon monoxide for all the experiments are summarized in Table 5-2 since the generation of hydrocarbon gases is negligible. It is noted that the results of the two repeating experiments for each heating period show reasonable repeatability. Except for the cases with low absolution values, the relative difference for most cases is within 20%, which is reasonable for DGA measurements.

Table 5-2 Gas-in-oil generation results of carbon oxide gases for mineral oil-Kraft paper experiments under different heating durations at 250 ºC thermal fault

Heating duration	CO_2, ppm			CO, ppm		
	Test 1	Test 2	Average	Test 1	Test 2	Average
0.5 h	64.6	9.9	37.3	2.5	0.0	1.3
1 h	62.3	52.5	57.4	4.7	1.8	3.3
2 h	93.4	100.0	96.7	10.8	22.8	16.8
4 h	123.2	145.9	134.6	23.4	24.5	24.0
6 h	149.4	157.0	153.2	16.9	27.0	22.0
8 h	218.5	152.6	185.6	28.9	27.0	28.0
12 h	244.2	231.5	237.9	45.5	41.4	43.5
16 h	232.8	195.3	214.1	34.6	31.9	33.3
20 h	265.6	--	265.6	43.9	--	43.9
24 h	252.5	236.3	244.4	35.5	25.3	30.4

The gas-in-oil generation results against different heating durations are plotted in Figure 5-5 based on the data in Table 5-2. The fitting curve for each gas is based on the

average value at each heating duration. It can be seen that the generated amounts of carbon dioxide are much higher than carbon monoxide. With the increasing of the heating duration, the generated amounts of carbon dioxide and carbon monoxide rapidly increase before 8 hours of thermal fault duration and then slowly increase in a trend to reach stable status by 24 hours of thermal fault duration. Overall, both gases increase with the fault duration following an exponential trend. In consideration of no carbon oxide gases being generated in the mineral oil only experiment, it is confirmed that the generation of carbon oxide gases are from the decomposition of the cellulose paper samples. The main degradation mechanisms of cellulose include hydrolysis, oxidation and pyrolysis [71]. Pyrolysis at high temperatures can result in a significant formation of carbon oxide gases. In addition, carbon monoxide can also be dissociated from formic acid by hydrolysis and carbon dioxide is also the end product after oxidation [37]. To correlate the carbon oxide generation with the degradation of cellulose paper, the DP of the paper samples after each thermal fault duration is worthy of measurement.

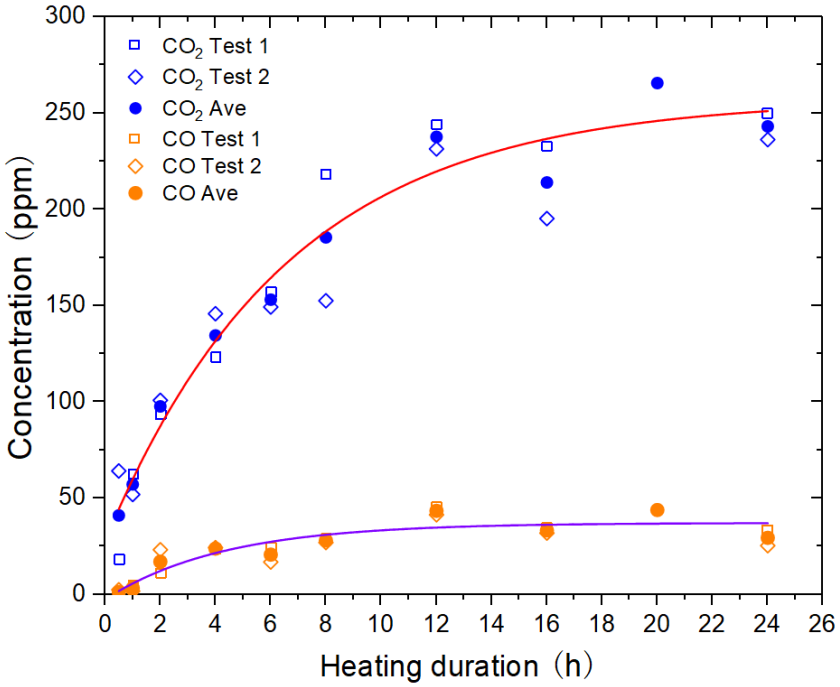

Figure 5-5 Gas-in-oil generation results of carbon oxide gases against different heating durations for mineral oil-Kraft paper experiments at 250 °C thermal fault

5.4 Correlation of Carbon Oxide Gas Generation with Paper Degradation

5.4.1 Paper degradation characterised by DP measurements

Cellulose is a polymeric chain of anhydrous-β-glucose joined by glycosidic bonds. DP represents the average number of glycosidic rings per cellulose macromolecule and is the most important direct indicator for assessing the ageing status of cellulose insulation directly related to the mechanical properties of cellulose [105, 106]. The measured DP value is the average value of different chain lengths. In the transformer industry, DP values are commonly measured through viscometry [107]. The measurement of the DP value can directly suggest the degradation of cellulose paper samples. Normally, new paper has a DP value from 1000 to 1200, with the DP value reducing under thermal stress because of chain scission. The number of chain scissions is increased when the cellulose paper experiences high energy dissipation. The DP value can drop to 200, which is often regarded as the end-of-life of cellulose insulation [37, 106].

Since there are three layers of cellulose paper samples inserted in the heating tube, each of the paper sample layers will have separate DP measurements following the procedure described in ASTM D4243 standard [108]. Figure 5-6 shows the DP values for each paper sample layer as a function of heating duration. The measured DP value for the new Kraft paper without degradation is around 980. Figure 5-6 shows that the DP values of all three layers have a rapid decreasing tendency under shorter heating durations and then tend to slowly decrease with the increase in heating durations with a trend moving towards saturation level. There is no doubt that the reduction of the DP values of the Kraft paper samples indicates cellulose decomposition at a 250 ºC thermal fault.

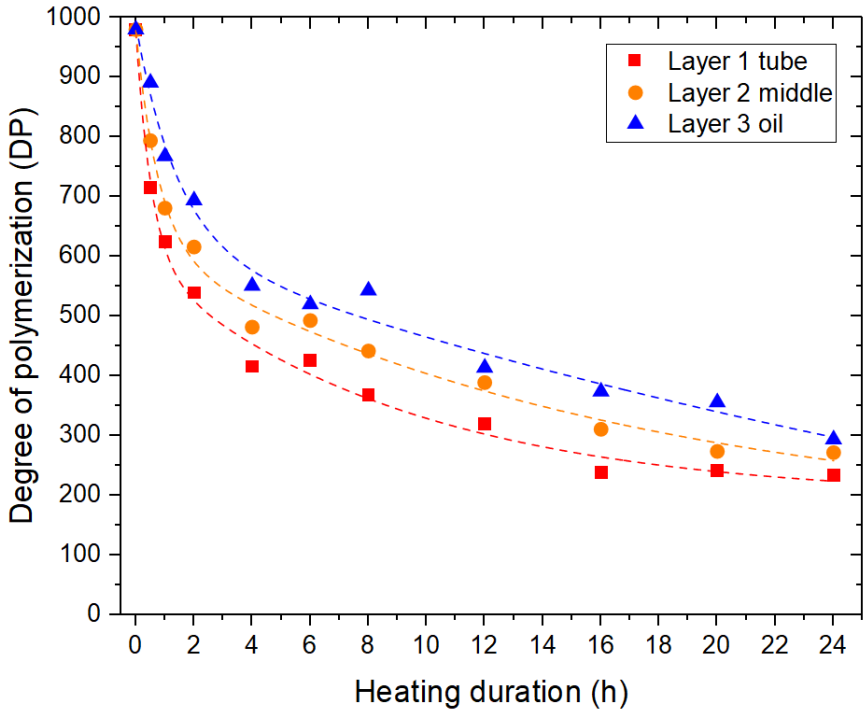

Figure 5-6 DP values of paper samples for each layer for mineral oil-Kraft paper experiments under different heating durations at 250 ºC thermal fault

The cellulose chains contain amorphous regions and crystalline regions that form microfibrils, which again form fibrils and finally fibres [37, 109]. The amorphous regions are irregular and more easily disordered and deteriorated. On the contrary, crystalline regions are compact and ordered [110]. In a cellulose chain, the disordered amorphous regions and crystalline regions are alternately joined together [111]. The mechanical strength of the paper is achieved by the ordered crystalline regions, which are hard to break. The amorphous regions of the cellulose are more easily cleaved than crystalline regions [37]. Hence, when paper degrades, amorphous regions are easily cleaved initially, resulting in a rapid reduction of the DP value in the early stage. On the other hand, crystalline regions degrade much more slowly, resulting in a slower reduction of the DP value at the later stage of paper ageing.

Meanwhile, it is clear that the DP values of layer 1 that is in direct contact with the inner surface of the heating tube are the lowest for all heating durations, while those of layer 3 in contact with the oil are the highest. The different DP values of the different layers suggest that a temperature gradient exists across the paper layers inside the

heating tube. Each Kraft paper sample layer must have experienced different thermal fault temperatures to some extent.

To characterise cellulose degradation, the determination of Chain Scission Number and Scission Fraction of Cellulose Unit (SFCU) as a function of DP are commonly used in ageing studies [106]. CSN represents the average number of chain scissions per cellulose chain unit during the course of degradation, given in equation (5-1) [106]:

$$CSN = \frac{DP_0}{DP_t} - 1 \qquad \textbf{(5-1)}$$

Where DP_0 represents the DP value of new Kraft paper samples before degradation and DP_t represents the DP value of Kraft paper samples at ageing duration.

SFCU represents the ratio of broken glucose units to the total glucose units of a cellulose chain, given in equation (5-2) [106]:

$$SFCU = \frac{CSN}{DP_0} = \frac{1}{DP_t} - \frac{1}{DP_0} \qquad \textbf{(5-2)}$$

Equations (5-1) and (5-2) are used in kinetic studies to predict the lifetime of transformers based on the condition of the cellulose insulation. The analysis of the kinetics of cellulose degradation can be followed by involving the determination of the SFCU as a function of degradation time t. The first kinetic model was developed by Ekenstam in 1936 and shown in equation (5-3) [106]:

$$\ln\left(1 - \frac{1}{DP_0}\right) - \ln\left(1 - \frac{1}{DP_t}\right) = kt \qquad \textbf{(5-3)}$$

Where k represents the rate of paper ageing. When the values of DP_0 and DP_t are large, the equation can be simplified as a proportional relationship between SFCU and ageing time. So equation (5-4) [106] is obtained:

$$\frac{1}{DP_t} - \frac{1}{DP_0} = kt \qquad \textbf{(5-4)}$$

In order to obtain the paper ageing rate for each layer, the SFCU as a function of heating duration is firstly plotted in Figure 5-7.The paper ageing rates for different layers are then obtained by linear fitting simplified kinetic model based on the points whose DP value is higher than 300.

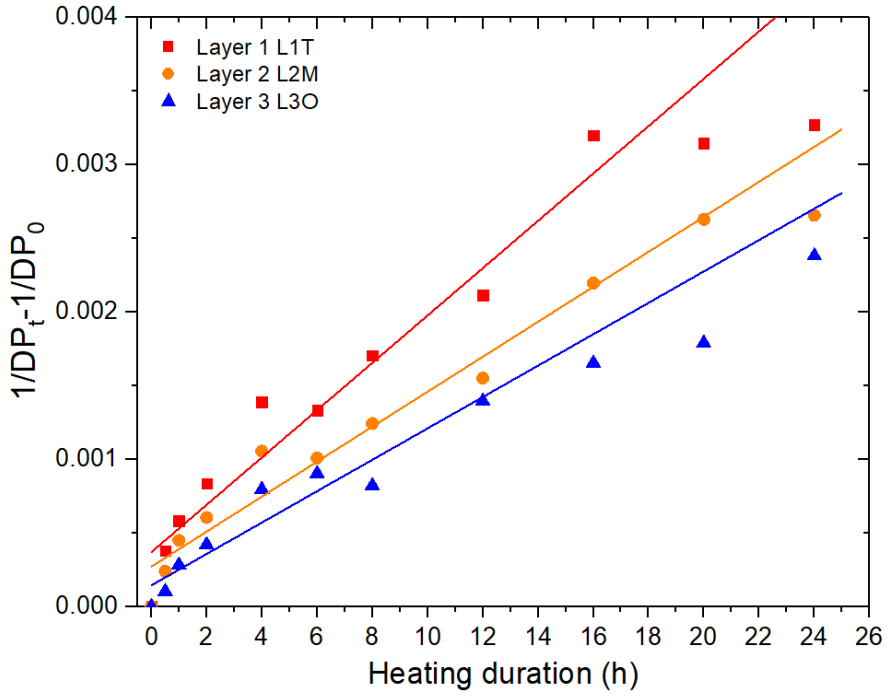

Figure 5-7 SFCU of different Kraft paper layers as a function of heating duration for mineral oil-Kraft paper experiments at 250 ºC thermal fault

It needs to be noted that the paper ageing rate in this experiment is much higher than in normal ageing studies since the cellulose insulation in this study experiences a high T1 thermal fault temperature of 250 ºC when compared with normal ageing studies using temperatures up to 130 ºC [38-41, 104]. Therefore, the degradation time in this study is much shorter and in the scale of hours rather than days or months in typical ageing studies. The paper ageing rates for is 1.61×10^{-4} for layer 1, 1.19×10^{-4} for layer 2 and 1.07×10^{-4} for layer 3. Layer 1 in direct contact with the inner surface of the heating tube has the highest paper ageing rate, corresponding to the lowest DP values of the three layers as shown in Figure 5-6. This indicates that layer 1 experiences the highest temperature, leading to the fastest degradation rate. In addition to the absolute DP values, the different paper degradation ageing rates also provide evidence of the

temperature gradient inside the heating tube.

5.4.2 Determination of temperature gradient across paper layers

In order to estimate the temperature difference between layers, the Arrhenius expression with activation energy and pre-exponential factor can be used, with the paper ageing rate k expressed as follows [112]:

$$k = Ae^{\frac{-E}{RT}} \quad \textbf{(5-5)}$$

Where A represents the pre-exponential factor, E represents the activation energy in J mol^{-1}, T is the temperature in Kelvin and R is the gas constant (8.314 J mol^{-1}K^{-1}). If the paper ageing rate k, activation energy E and pre-exponential factor A are known variables, the temperature difference (TF) between layers can be estimated by using equation (5-5) as:

$$TF_{L12} = \frac{-E}{Rln\frac{k_{L1T}}{A}} - \frac{-E}{Rln\frac{k_{L2M}}{A}} \quad \textbf{(5-6)}$$

$$TF_{L23} = \frac{-E}{Rln\frac{k_{L2M}}{A}} - \frac{-E}{Rln\frac{k_{L3O}}{A}} \quad \textbf{(5-7)}$$

$$TF_{L13} = \frac{-E}{Rln\frac{k_{L1T}}{A}} - \frac{-E}{Rln\frac{k_{L3O}}{A}} \quad \textbf{(5-8)}$$

The activation energy and pre-exponential factor are referred to the previous mineral oil-Kraft paper ageing study investigation [41], which are 111.9 kJ mol^{-1} for activation energy and 1.49×10^{9} mg kg^{-1}h^{-1} for pre-exponential factor, respectively. Then, the temperature difference between layer 1 and layer 2 (TF_{L12}) is 4.5 ºC, which is higher than that between layer 2 and layer 3 (TF_{L23}), 1.6 ºC. Hence, the maximum temperature difference between layer 1 and layer 3 (TF_{L13}) is 6.1 ºC.

Another method based on the lifetime estimation of cellulose insulation is also used to estimate the temperature gradient across the paper layers. The DP values of the Kraft

paper samples for each layer as a function of the heating duration is initially fitted as shown in Figure 5-6. After the fitting process, two DP values of the Kraft paper samples are selected to obtain the time used to reach the selected DP values. Mid-life criterion for the DP values of 400 and 300 are selected. The lifetimes corresponding to a DP of 400 and 300 are used to find the ageing temperature following equation (5-9) [113], which is based on mineral oil and Kraft paper.

$$Lifetime = \frac{150000}{2^{(\frac{T-98}{6})}} \quad \textbf{(5-9)}$$

The selected mid-life criteria of the DP values and corresponding lifetime, together with the temperature difference between layers, are listed in Table 5-3. It can be seen that in order to reach the same DP values of the Kraft paper samples, a shorter lifetime is used for layer 1 when compared with the other two layers. The temperature difference between layer 1 and layer 2 is higher than the temperature difference between layer 2 and layer 3.

Table 5-3 Estimation of temperature difference between each layer using a lifetime equation in a mineral oil-Kraft paper insulation system

		DP 400	DP 300
Lifetime	**Layer 1 (L1T)**	6 h	12 h
	Layer 2 (L2M)	10 h	18 h
	Layer 3 (L3O)	15 h	24 h
$\boldsymbol{TF_{L12}}$		5 ºC	4 ºC
$\boldsymbol{TF_{L23}}$		3 ºC	2 ºC
$\boldsymbol{TF_{L13}}$		8 ºC	6 ºC

Two different methods are used to estimate the temperature gradient across paper layers. The method using Arrhenius expression is based on the paper ageing rates of different layers when DP values are higher than 300. The method using lifetime estimation of cellulose insulation is based on lifetimes of different layers corresponding to the DP of 400 and 300. The results from both methods accord with

each other. The temperature difference between layer 1 and layer 2 is slightly higher than layer 2 and layer 3. The temperature profile results in Chapter 3 section 3.5 also provide the evidence that the temperature gradient inside the heating tube exists.

In addition, the experiments in [114] using the immersed-heating method to age oil-paper insulation also indicated different Kraft paper layers experiencing different temperatures during the heating process. Twelve layers of paper were wrapped around the heating element, with the heating element temperature raised continually from 100 ºC to 400 ºC with a 50 ºC increment each time. Under each temperature, 8-hour heating was applied. After a 56-hour heating duration, the DP values of the outside three layers were between 318 and 229, with all the other layers seriously burnt, resulting in the DP determination not being possible. Meanwhile, the thermal modelling work in [115, 116] presented that the temperature gradient existed for the paper layers wrapped around the conductors, with the temperature gradient ranging from 2-10 ºC. Accordingly, the temperature differences between each layer estimated in this current study are reasonable.

5.4.3 Correlation between carbon oxide generation and DP reduction

To correlate the generation of carbon oxide gases with the paper degradation, the average DP value of the 3-layer paper samples is used to represent the degradation of the paper samples, as shown in Figure 5-8. The first point represents the DP value of new Kraft paper, which is around 980. With the increase of heating duration, the DP value of the Kraft paper samples decreases exponentially to 266. It is noted that the DP value of the Kraft paper samples falls from 980 to 482 after a 4-hour heating duration. In addition, the chain scission number against the increase of heating duration is also plotted in Figure 5-8. It shows that chain scission number increases with the heating duration increase, along with the reduction of the DP value. More chain scissions are required to decrease the DP value further when the DP value is already low.

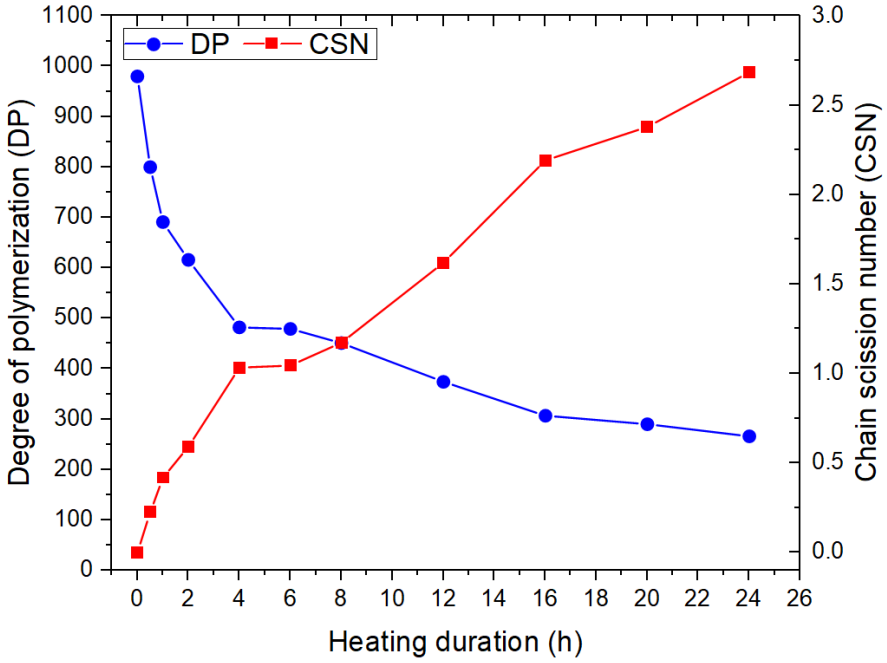

Figure 5-8 Average DP value and chain scission number of 3-layer Kraft paper samples versus heating duration in a mineral oil-Kraft paper insulation system at 250 ºC thermal fault

According to the degradation of the Kraft paper samples and negligible generation of carbon oxide gases in the mineral oil only experiment, there is no doubt that the decomposition of cellulose resulted in the observed generation of carbon oxide gases in the mineral oil-Kraft paper experiments. Figure 5-9 shows the relationship between the generation of carbon oxide gases and the reduction of DP. It can be seen that the generation of carbon oxide gases shows an exponential increase with the reduction of DP. The degradation of Kraft paper mainly has three processes, which are hydrolysis, oxidation and pyrolysis, depending on the temperature experienced and concentration of dissolved oxygen [71]. In ageing experiments, the ageing temperature is much lower when compared with the simulated thermal fault temperature in this study, so hydrolysis and oxidation are the main mechanisms considered. However, in this study, under a high thermal fault temperature of 250 ºC, pyrolysis is the dominant degradation mechanism of cellulose paper.

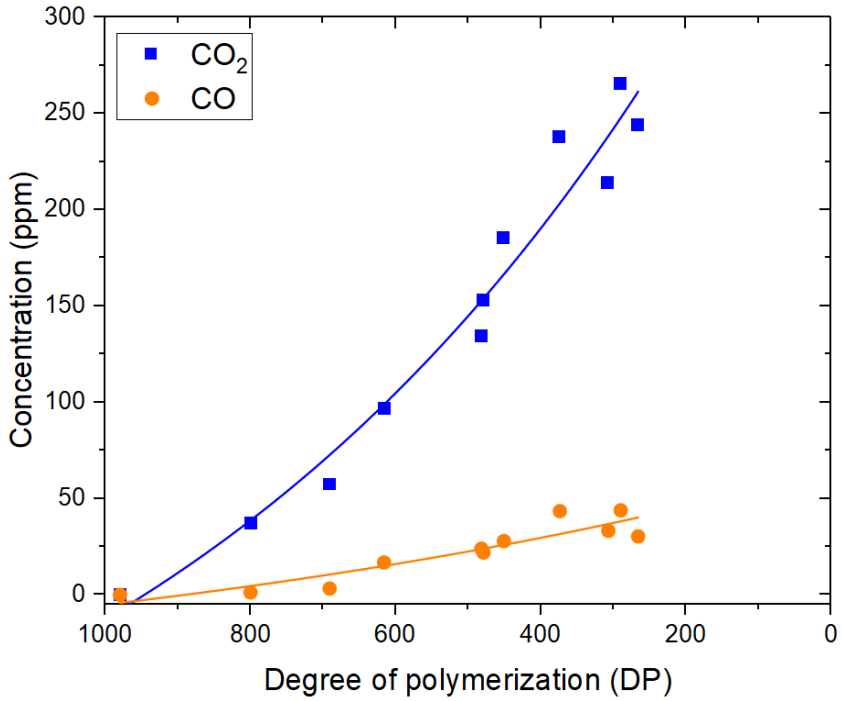

Figure 5-9 Generation of carbon oxide gases as a reduction of DP in a mineral oil-Kraft paper insulation system at 250 °C thermal fault

Figure 5-10 shows the generation of carbon oxide gases as a function of the chain scission number of the Kraft paper samples. It is important to note that there is a linear relationship between the generation of carbon oxide gases and chain scission numbers. With the increase in chain scissions in the Kraft paper samples, more carbon oxide gases were generated. The large number of anhydroglucose rings and weak C-O molecular bonds in polymeric chains of solid cellulosic insulation can be decomposed at lower temperatures. More polymer chain scissions can occur with the increase in temperature, leading to the formation of carbon oxide gases [24, 117]. The relationships between the generation of carbon dioxide/carbon monoxide and the chain scission number can be represented as:

$$C_{CO_2} = 130.98 \times CSN \quad \textbf{(5-10)}$$

$$C_{CO} = 21.55 \times CSN \quad \textbf{(5-11)}$$

Where C_{CO_2}, C_{CO} represent the generation concentration of carbon dioxide and carbon monoxide, respectively.

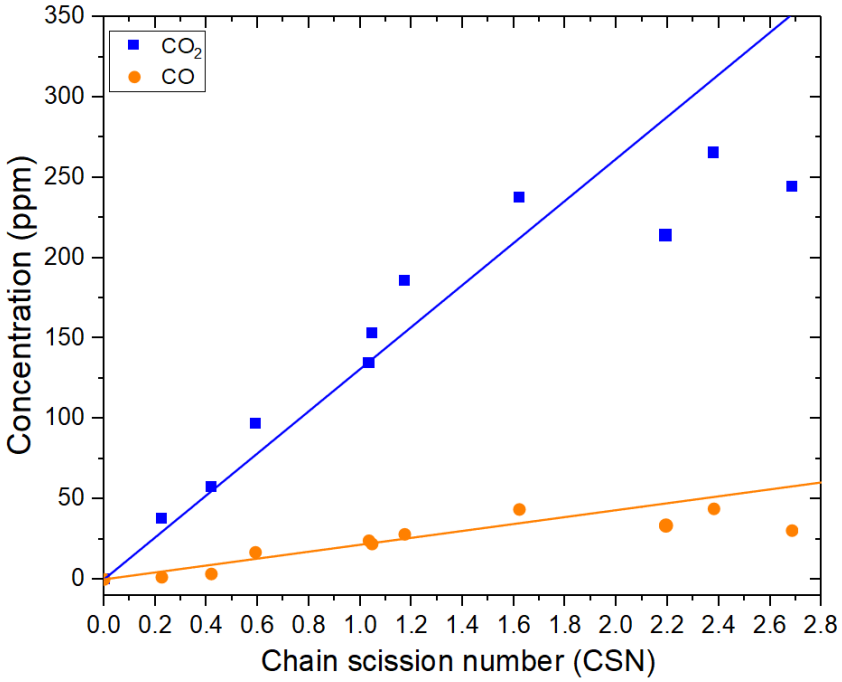

Figure 5-10 Generation of carbon oxide gases as a function of chain scission number in a mineral oil-Kraft paper insulation system at 250 ºC thermal fault

5.5 Comparison between Carbon Oxide Gases and 2-FAL

5.5.1 Generation of 2-FAL from paper degradation

To assess the condition of transformer insulation, furan concentration in oil is used as an indirect indicator of paper ageing. Furans were first confirmed to be related to paper ageing in the early 1980s [41]. Furan compounds are generated from the components in paper, which include cellulose, hemicellulose, lignin and degradation by-products of cellulose, such as glucose and laevoglucosan [118]. Different furan compounds relate to different faults in transformers [119]. 2-FAL is mainly generated from the decomposition of cellulose and pentosan caused by Kraft paper ageing [120]. During the present experiment, the concentration of 2-FAL in oil is measured before and after each thermal fault, between which the difference is used to indicate the concentration of 2-FAL concentration for each heating duration.

The concentrations of 2-FAL in oil corresponding to different thermal fault durations are presented in Table 5-4. It is necessary to note that for the first round of experiments,

the 0.5h, 12h and 20h samples did not measure the 2-FAL concentration. After the simulated thermal faults, around 0.013 L of stressed mineral oil in the heating tube is mixed with 6.6 L bulk oil in the main tank, creating a large dilution and leading to the detected amounts of 2-FAL in the oil being quite small.

Table 5-4 2-FAL concentration for mineral oil-Kraft paper experiments under different heating durations at 250 ºC thermal fault

Heating duration	2-FAL concentration, ppb		
	Test 1	Test 2	Average
0.5 h	--	0.0	0.0
1 h	1.5	0.0	0.8
2 h	11.0	21.0	16.0
4 h	17.0	26.0	21.5
6 h	43.0	31.0	37.0
8 h	53.0	35.0	44.0
12 h	--	62.0	62.0
16 h	66.0	50.0	58.0
20 h	--	87.0	87.0
24 h	74.5	97.0	86.0

Figure 5-11 shows the concentration of 2-FAL results as a function of heating duration. The average value of the two repeated experiments is used to plot the curve. It is clear that the concentration of 2-FAL in oil increases almost linearly with the increase in heating duration. Since the 2-FAL is related to the degradation of Kraft paper, the correlation between 2-FAL and DP of the Kraft paper samples is plotted in Figure 5-12. It can be seen that when DP is higher than 600, there is negligible increase of 2-FAL. However, when DP is lower than 600, a smaller DP decrease can lead to a large 2-FAL increase. Overall, the tendency shows that the 2-FAL exponentially increases with the reduction of DP. The similar exponential increase of the concentration of 2-FAL in oil as a reduction of the DP value was also observed in [39, 104, 121]. This conforms to previous understanding that the 2-FAL is best able to indicate the late paper ageing

stage [105, 122]. The 2-FAL is hardly generated during the early ageing stage, while is considerably generated at the late paper ageing stage, especially when the DP value of paper is lower than 400 [40].

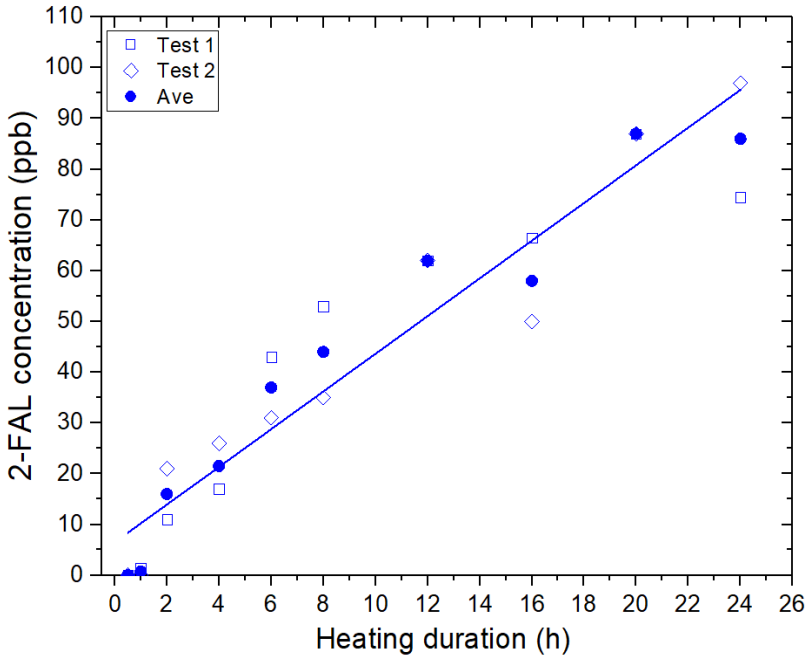

Figure 5-11 2-FAL concentration as a function of heating duration in a mineral oil-Kraft paper insulation system at 250 ºC thermal fault

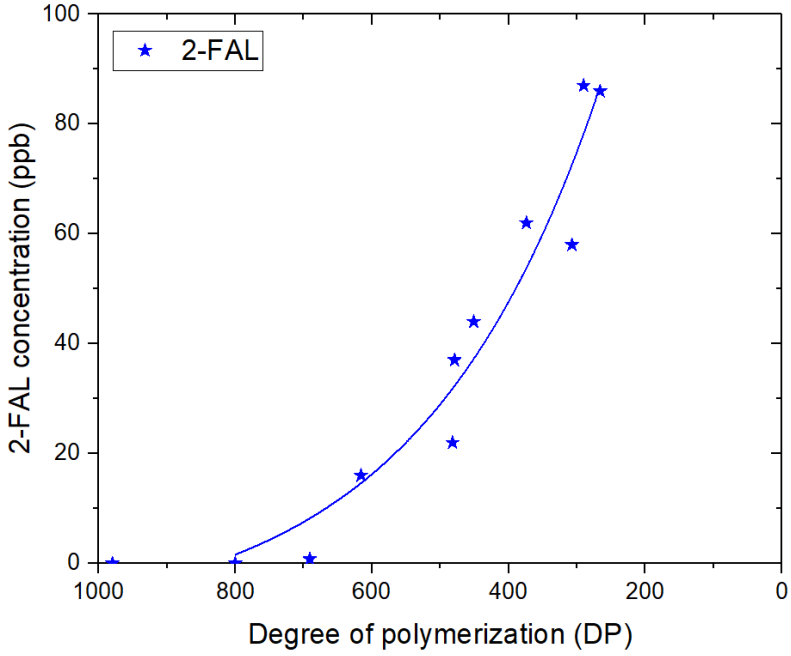

Figure 5-12 2-FAL concentration as a reduction of DP in a mineral oil-Kraft paper insulation system at 250 ºC thermal fault

5.5.2 Correlation between carbon oxide gases and 2-FAL

Figure 5-13 shows the correlation between the generation of carbon oxide gases and the concentration of 2-FAL in oil. Carbon oxide gases and 2-FAL are ageing products from the degradation of the Kraft paper samples. In addition, both the carbon oxide gases and the 2-FAL show an exponential increasing trend as the DP values of the Kraft paper samples reduce, as already shown in Figure 5-9 and Figure 5-12. Accordingly, it can be seen that there is a linear relationship between the generation of carbon oxide gases and the concentration of 2-FAL in oil. The linear correlation between carbon oxide gases and 2-FAL once again provides evidence that the generation of carbon oxide gases and 2-FAL are all caused by the decomposition of the cellulose paper samples.

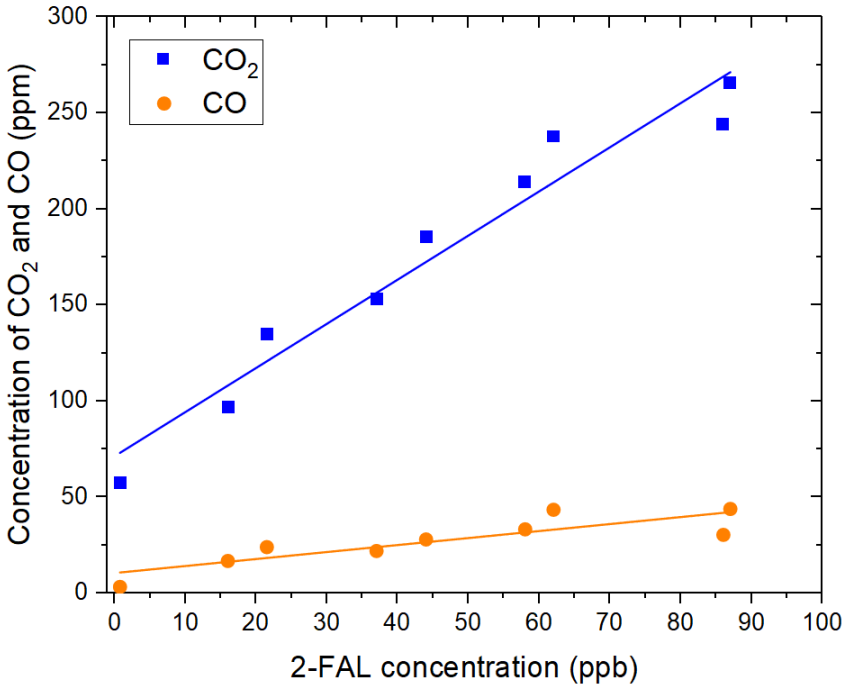

Figure 5-13 Correlation between the generation of carbon oxide gases and 2-FAL in oil in a mineral oil-Kraft paper insulation system at 250 ºC thermal fault

5.6 Comparison of Carbon Oxide Gases Generation with the Literature

Ageing experiments were conducted in [39] to investigate the effect of oil type on the

thermal degradation of Kraft paper by measuring several ageing indicators, such as the generation of carbon oxide gases, the DP of paper samples and the 2-FAL in oil. Glass ampoules were used to contain 150 ml of mineral oil and 0.5 g of Kraft paper samples or only 150 ml of mineral oil and heated in an air circulating oven. The headspace of the glass ampoules was filled with nitrogen. The ageing temperature was initially set at 70 ºC for one week, with the temperature then raised to 110 ºC for another week. The same procedure was repeated at 130 ºC, 150 ºC and 190 ºC.

The results showed that negligible amounts of carbon oxide gases and hydrocarbon gases were generated in oil only tests. On the contrary, large amounts of carbon oxide gases were generated in the experiments with the presenting of the Kraft paper samples, especially when the ageing temperature was higher than 110 ºC. In addition, the DP showed a decreasing trend with the increase in the ageing temperature. For the 2-FAL in oil results, there was little 2-FAL detected when the ageing temperature was lower than 110 ºC. On the other hand, a rapid 2-FAL increase was seen when the ageing temperature was higher than 110 ºC.

Compared with the studies in literature, the experiment temperature and the experiment conditions are different. In order to compare with the results in [39], the generation of carbon oxide gases for both studies is normalised to the generation per gram of Kraft paper sample to eliminate the influence of the oil to paper ratio as equation (5-12) and (5-13). Moreover, the calculation is also based on the assumption that the partitioning of carbon oxide gases between oil and Kraft paper is negligible. In addition, the generation of carbon oxide gases by weight is correlated with the chain scission number which eliminates the influence of the experiment temperature.

$$C_{CO_2\ weight} = \frac{C_{CO_2\ volume} \times V}{W} \quad \textbf{(5-12)}$$

$$C_{CO\ weight} = \frac{C_{CO\ volume} \times V}{W} \quad \textbf{(5-13)}$$

Where:

$C_{CO_2\ weight}$, $C_{CO\ weight}$: normalised generation of carbon dioxide/carbon monoxide

based on the Kraft paper sample weight (ul/g)

$C_{CO_2\ volume}$, $C_{CO\ volume}$: generation of carbon dioxide/carbon monoxide based on oil volume (ul/l)

V: investigated oil volume (l)

W: investigated Kraft paper sample weight (g)

Figure 5-14 and Figure 5-15 show the comparison results for the concentration of carbon dioxide and carbon monoxide as a function of the increased chain scission number, respectively. Figure 5-14 shows that the generation of carbon dioxide per gram of paper increases with the increasing of the chain scission number and the results are comparable between two studies. On the other hand, the generation of carbon monoxide per gram of paper in this study is clearly higher than that in [39]. The results indicate that carbon monoxide is largely generated under high temperature thermal faults when compared with normal ageing experiments. Both IEC 60599-2016 [24] and IEEE C57.104-2019 [22] mention that carbon monoxide is more easily generated under thermal faults when paper is presented in the insulation system. The comparisons imply that there are different mechanisms involved in carbon monoxide generation under different temperatures, which is worthy to research further.

According to [123], the generation of carbon oxide gases can also be influenced by moisture levels in Kraft paper samples. A series of ageing experiments were conducted with different ageing temperature (80 ºC, 100 ºC, 120 ºC, 140 ºC, 160 ºC and 180 ºC), ageing period and moisture levels. At the same ageing temperature and ageing period, the generation rate of carbon dioxide showed an increasing tendency with increasing moisture levels. For carbon monoxide, the generation rate showed a decreasing tendency with increasing moisture levels at temperatures lower than 160 ºC. There is lack of results on the effect of moisture at higher temperatures like 250 ºC used in the present study. In addition, it is hard to compare the moisture levels of paper samples used in [39], and the present study. Therefore, further research on carbon oxide gases generations at different temperatures and moisture levels of paper

is needed.

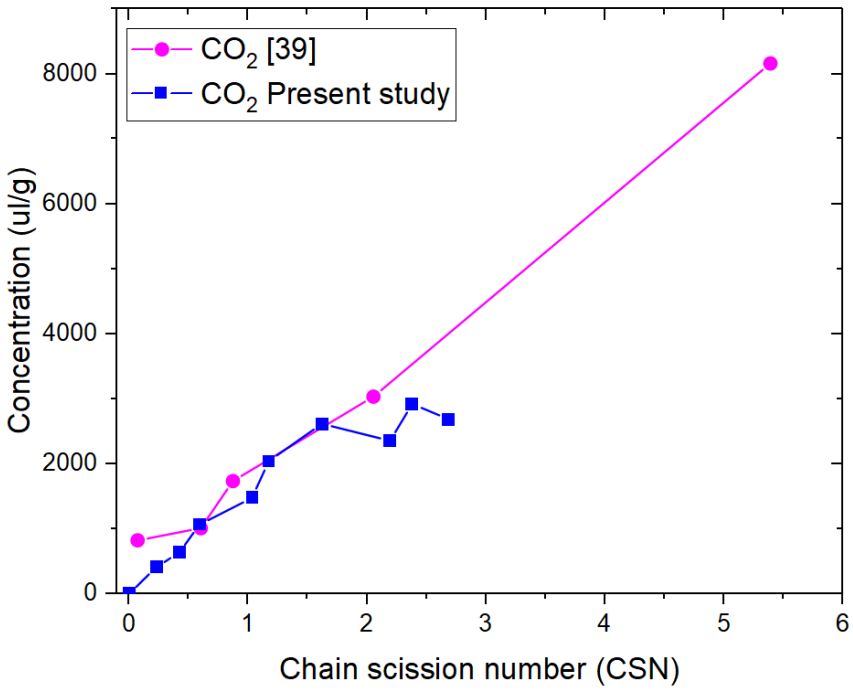

Figure 5-14 Comparison of the generation of carbon dioxide in a mineral oil-Kraft paper insulation system

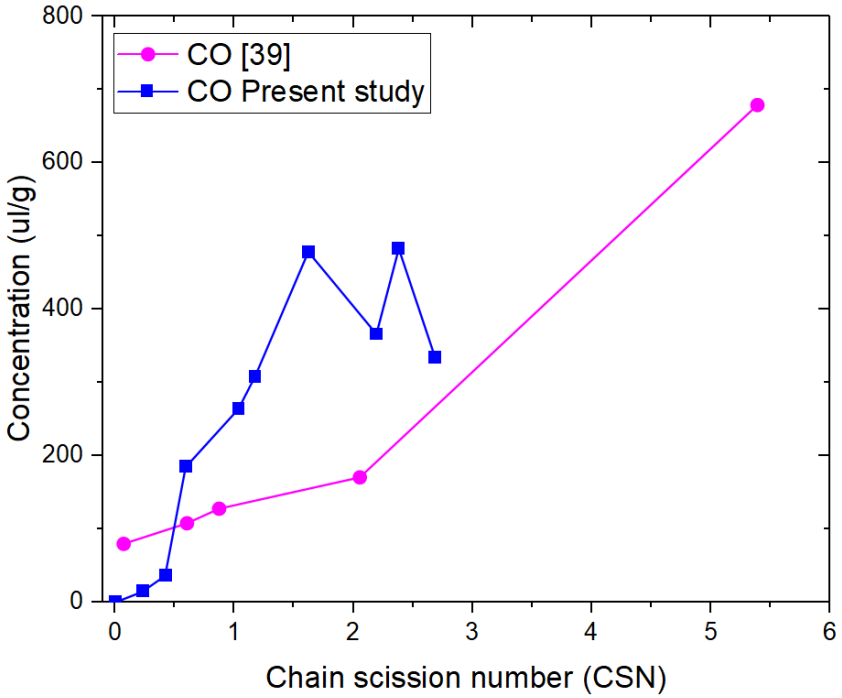

Figure 5-15 Comparison of the generation of carbon monoxide in a mineral oil-Kraft paper insulation system

5.7 Discussion on the Practical Implications of Carbon Oxide Gases Generation

5.7.1 Carbon oxide gases generation in a practical situation

In general, the generation of carbon oxide gases can be an indicator of the decomposition of the cellulose and further evidences that the overheating of cellulose under thermal faults can be provided by other paper ageing indicators. Moreover, both the IEEE standard and IEC standard suggest that the CO_2/CO ratio can be used to identify whether transformers are experiencing paper related thermal faults. The current IEC 60599-2016 [24] suggests that the accepted range of the CO_2/CO ratio for a normal transformer is between 3 and 10. When the CO_2/CO ratio is lower than 3, together with the concentration of carbon monoxide being higher than 1,000 ppm, it can be an indication of a paper related fault. When the CO_2/CO ratio is higher than 10, together with the concentration of carbon dioxide being higher than 10,000 ppm, it can be an indication of mild paper overheating (< 160 ºC) or oil oxidation.

However, in IEEE C57.104-2019 [22], more indicators are taken into account when using the CO_2/CO ratio to interpret paper related faults. When the CO_2/CO ratio is lower than 3 and the concentration of carbon monoxide is higher than 1,000 ppm, together with the formation of significant amounts of hydrocarbon gases, it can be an indication of a paper related fault. Meanwhile, when the CO_2/CO ratio is higher than 20 and the concentration of carbon dioxide is higher than 10,000 ppm, together with the concentration of furans being higher than 5 ppm, it can indicate slow paper degradation at relatively low temperatures (< 140 ºC).

Different from high benchmark concentrations of carbon oxide gases defined in IEEE and IEC standards to distinguish paper related faults when using the CO_2/CO ratio, the benchmark concentrations of carbon oxide gases before and after thermal faults in this study are much lower. This is due to the small fault size controlled in the heating tube.

In this study, the mineral oil-Kraft paper insulation system only experiences a thermal fault in a small fault area. After the fault, the stressed oil will be mixed with a large volume of bulk oil in the main oil tank, and the concentration of carbon oxide gases are largely diluted. This situation is similar to a localised thermal fault happened in a real transformer. However, the challenge is to estimate a reasonable insulation weight ratio between the fault area and the bulk oil.

Therefore, the gas-in-oil generations of carbon oxide gases in this study are scaled up to the gas-in-oil generation of carbon oxide gases in a practical case. It should be noted that this scale-up analysis is a scenario study and it is not the measured data in a real transformer. Two challenges need to be overcame. Firstly, a reasonable insulation weight ratio between the fault area and the bulk oil in a real transformer needs to be estimated. Secondly, a calculation method needs to be derived to calculate the generation of carbon oxide gases in a real transformer. In order to solve the first challenge, a reference power transformer is selected according to IEC standard 62332-1-2011 [124]. The details of the chosen reference power transformer are listed in Table 5-5. It needs to be noted that the hot insulation in the reference transformer is assumed to be Kraft paper and the reference transformer is regarded as a closed type transformer.

Table 5-5 Details of the reference power transformer [124]

Hot insulation volume (cm^3)	269,000
Mineral oil volume (cm^3)	8,325,000
Oil density (kg/dm^3)	0.87
Paper density (g/cm^3)	0.75

Equation (5-12) and (5-13) normalise the generation of carbon oxide gases by volume to the generation per gram of Kraft paper sample. Therefore, the equation (5-14) and (5-15) are used to scale up the gas-in-oil generation of carbon dioxide and carbon monoxide in the reference transformer. It needs to be noted that when scaling up the gas-in-oil generation of carbon oxide gases, the partitioning of carbon oxide gases

between solid insulation and insulating liquid is ignored, meaning that the generated carbon oxide gases totally dissolve in the bulk oil.

$$C_{CO_2\ volume\ real} = (C_{CO_2\ weight} \times W_{paper\ fault})/V_{oil\ real} \quad \textbf{(5-14)}$$

$$C_{CO\ volume\ real} = (C_{CO\ weight} \times W_{paper\ fault})/V_{oil\ real} \quad \textbf{(5-15)}$$

Where:

$C_{CO_2\ weight}$, $C_{CO\ weight}$: generation of carbon dioxide/carbon monoxide based on the Kraft paper sample weight in this study (ul/g)

$C_{CO_2\ volume\ real}$, $C_{CO\ volume\ real}$: generation of carbon dioxide/carbon monoxide based on oil volume in the reference transformer (ul/l)

$W_{paper\ fault}$: hot insulation weight in the fault area (g)

$V_{oil\ real}$: oil volume in the reference transformer (l)

A flow chart of the calculation method is shown in Figure 5-16. The concentrations of the generation of carbon oxide gases by volume can be directly obtained from TM8 in the present study. Then, the concentrations of carbon oxide gases by weight can be calculated by using equation (5-12) and (5-13). Once the volume of oil and weight of paper in fault area in a real transformer are confirmed, the scale up can be performed by using equation (5-14) and (5-15). Two scenarios are investigated when scaling up the gas-in-oil generation of carbon oxide gases in the reference transformer. Scenario 1 assumes that one of the six windings is suffering from a thermal fault corresponding to 1/6 hot insulation being in the fault area. On the other hand, Scenario 2 assumes that only the top part/pass of one winding is experiencing a thermal fault corresponding to 1/36 hot insulation being in the fault area.

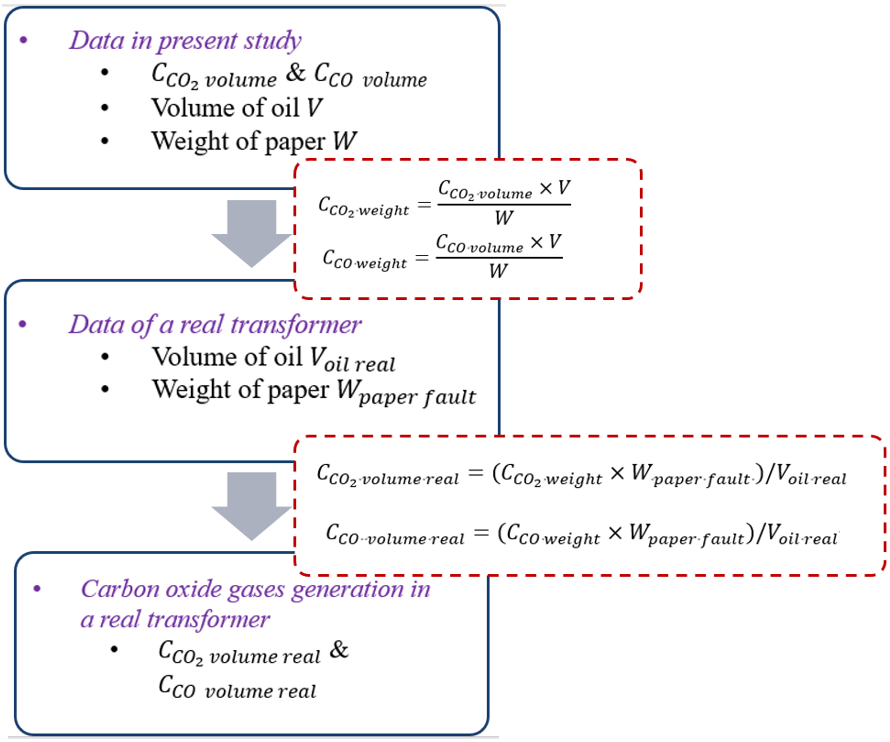

Figure 5-16 Flow chart of scaling up DGA results towards a real transformer

Table 5-6 lists the gas-in-oil generation of carbon dioxide and carbon monoxide for each heating duration in this study, to gather with their related scaled-up generation in the two defined scenarios. It can be seen that the gas-in-oil generation of carbon dioxide and carbon monoxide have been scaled up to much bigger values in the reference transformer. In addition, the gas-in-oil generation amounts of carbon oxide gases in scenario 1 indeed exceed the minimum concentration limits required in IEEE and IEC standards [22, 24].

Table 5-6 Gas-in-oil generation of carbon dioxide and carbon monoxide in this study and two scenarios, ppm

	Small-scale experimental setup		Scenario 1		Scenario 2	
Fault period	**CO_2**	**CO**	**CO_2**	**CO**	**CO_2**	**CO**
0.5 h	37.3	1.3	1,657.2	57.8	276.2	9.6
1 h	57.4	3.3	2,550.2	146.6	425.0	24.4
2 h	96.7	16.8	4,296.3	746.4	716.1	124.4

4 h	134.6	24.0	5,980.2	1066.3	996.7	177.7
6 h	153.2	22.0	6,806.6	977.4	1,134.4	162.9
8 h	185.6	28.0	8,246.1	1244.0	1,374.4	207.3
12 h	237.9	43.5	10,569.8	1932.7	1,761.6	322.1
16 h	214.1	33.3	9,512.3	1479.5	1,585.4	246.6
20 h	265.6	43.9	11,800.4	1950.4	1,966.7	325.1
24 h	244.4	30.4	10,858.6	1350.7	1,809.8	225.1

5.7.2 Practical implication of carbon oxide gases as indicators

When using the CO_2/CO ratio method to identify the paper related thermal faults, the total concentrations of carbon dioxide and carbon monoxide dissolved in oil are used to calculate the ratio, rather than the gas-in-oil generation of carbon dioxide and carbon monoxide. Therefore, the benchmark concentrations of carbon dioxide and carbon monoxide in the reference transformer need to be added from the gas-in-oil generation of carbon dioxide and carbon monoxide from the two scenarios in Table 5-6 to obtain the total gas concentrations. In this study, a new transformer (1 year of age) is considered in both scenarios. The benchmark concentrations of carbon dioxide and carbon monoxide of a power transformer at the age of 1 year are chosen as 190 ppm and 35 ppm, respectively, according to a DGA database study [125].

Figure 5-17 and Figure 5-18 show the gas-in-oil concentrations of carbon dioxide and carbon monoxide, and the related increasing rates of gas-in-oil generation caused by fault period in both scenarios. It needs to be noted that the points at zero represent the benchmark concentrations of carbon dioxide and carbon monoxide corresponding to the moment that the thermal fault has not happened. It can be seen from both figures that the total gas-in-oil concentrations of carbon oxide gases increase rapidly in a shorter fault period and tend to reach a steady status in a longer fault period. The overall tendency shows an exponential increase with the increasing fault period. In scenario 2, the total concentrations of carbon oxide gases do not exceed the minimum concentration limits as described in the standards since the fault area size is small. On

the contrary, the concentrations of carbon oxide gases in scenario 1 do exceed the minimum concentration limits after a 4-hour fault duration due to the relatively large fault size.

The increasing rates of carbon oxides in the gas-in-oil generation for both scenarios decrease exponentially with the increase of the fault duration. For scenario 1, the increasing rate of carbon dioxide decreases from 1663.3 ppm/h at a 0.5-hour fault duration to 30.2 ppm/h at a 24-hour fault duration, and the increasing rate for carbon monoxide decreases from 345.3 ppm/h at a 0.5 hour fault duration to 1.9 ppm/h at a 24-hout fault duration. For scenario 2, the increasing rate of carbon dioxide decreases from 277.2 ppm/h at a 0.5-hour fault duration to 5.0 ppm/h at a 24-hour fault duration, and the increasing rate of carbon monoxide decreases from 57.5 ppm/h at a 0.5 hour fault duration to 0.3 ppm/h at a 24-hout fault duration. There is no doubt that when the fault initially occurs, the increasing rates of both carbon dioxide and carbon monoxide are high, and when the paper is further degraded, the increasing rates of both carbon dioxide and carbon monoxide are reduced.

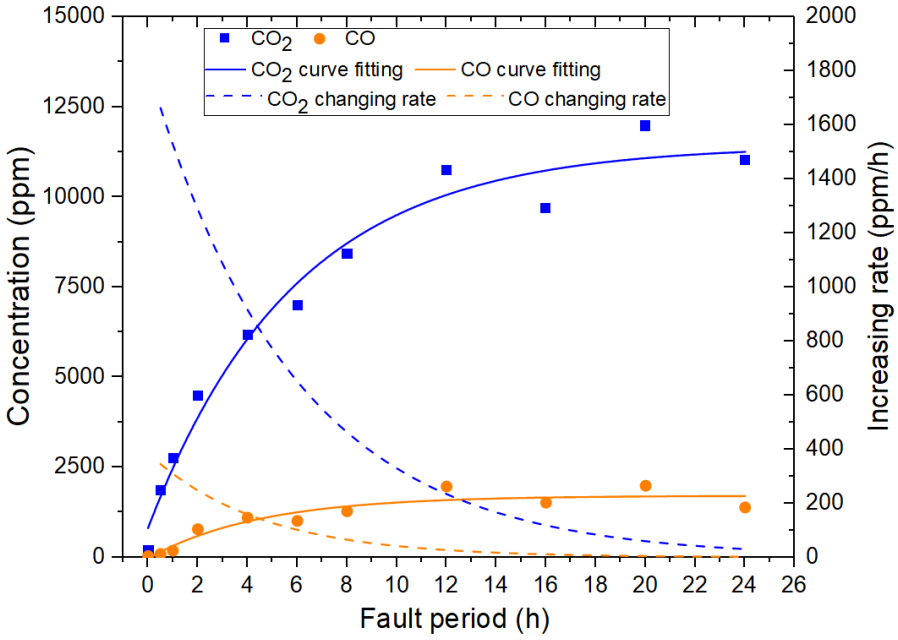

Figure 5-17 Gas-in-oil concentrations of carbon oxide gases and the increasing rate in a new transformer under thermal faults in scenario 1

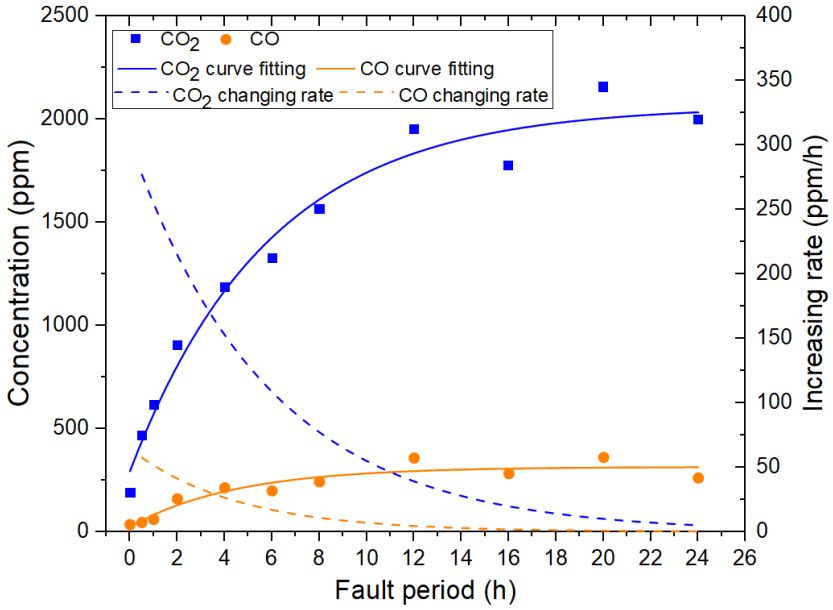

Figure 5-18 Gas-in-oil concentrations of carbon oxide gases and the increasing rate of a new transformer under thermal faults in scenario 2

Figure 5-19 presents the results of the CO_2/CO ratios in both scenarios. The first few points up to time zero in both scenarios represent the CO_2/CO ratio before the start point of the thermal fault. It can be seen that the CO_2/CO ratio is around 5.4 when there is no thermal fault, which means it is normal according to both IEC and IEEE standards [22, 24]. A sharp increase in the CO_2/CO ratio is observed once the thermal fault starts to happen. With the increase of the fault period, the CO_2/CO ratio reduces quickly, before fluctuating between 5 and 7. In addition, when the fault area size is small corresponding to the scenario 2, the sharp increase in the CO_2/CO ratio is less obvious compared with the scenario 1. This indicates that when more solid insulations degrade in a large fault area, the variation of the CO_2/CO ratio is more violent. Meanwhile, there is no sign of the CO_2/CO ratio going below 3 even when the paper has been seriously degraded. This is contradictory to what is suggested in IEC 60599-2016 [24] and IEEE standard C57.104-2019 [22].

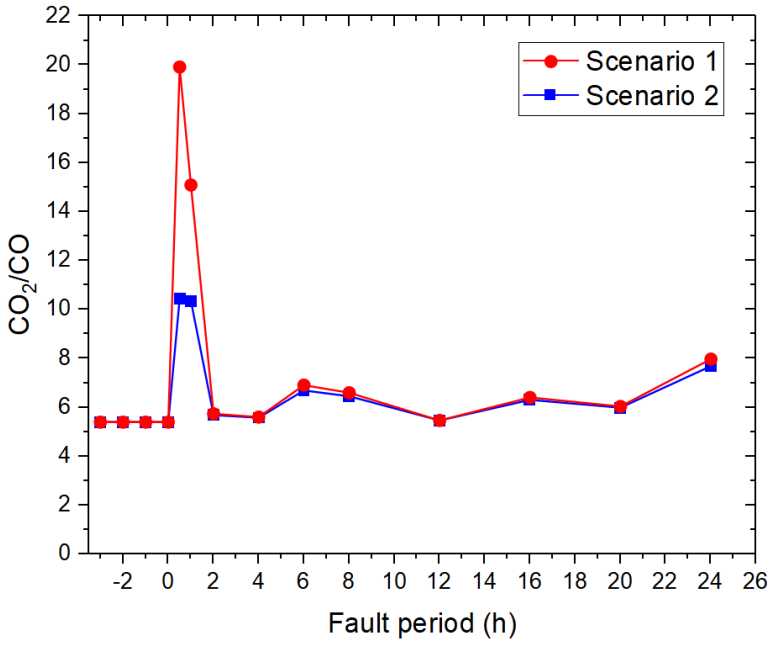

Figure 5-19 A new transformer's CO_2/CO ratio under thermal faults in scenarios 1 and 2

5.8 Summary

This chapter has presented a series of mineral oil-cellulose paper experiments under a 250 ºC thermal fault with different heating durations to investigate the fault gas generation characteristics. There is a negligible generation of carbon oxide gases in the mineral oil only experiments. However, carbon dioxide and carbon monoxide are largely generated in the mineral oil-Kraft paper experiments. According to the DP measurement results of different layers, a temperature gradient up to 8 ºC exists across the paper layers inside the heating tube. Meanwhile, the generation of carbon oxide gases shows an exponential increasing tendency as the DP reduced and a linear increase tendency as the chain scission number increased. These findings indicate that the generation of carbon oxide gases is caused by the decomposition of cellulose. The increase of 2-FAL in oil is another indicator of paper ageing, highlighting a linear relationship with the increasing carbon oxide gases. Compared to accelerated ageing studies, carbon monoxide is generated more under thermal faults, indicating that different carbon monoxide generation mechanisms might exist under different temperatures.

When considering the generation of carbon oxide gases in a practical transformer, the gas-in-oil concentrations of carbon oxide gases increase in large amounts. The gas-in-oil concentrations of carbon oxide gases exponentially increase with the increasing fault duration, whilst the increasing rates of gas-in-oil generation of carbon oxide gases exponentially decrease with the increasing fault duration. The CO_2/CO ratio has a sharp increase when the fault starts to happen, before reducing quickly and fluctuating between 5 and 7. When more solid insulations degrade in a large fault area, the variation of the CO_2/CO ratio is more violent. However, there is no sign of the CO_2/CO ratio going below 3 even when the paper has been seriously degraded. Therefore, a revision of standards may be needed, with further work focused on conducting experiments under other temperatures being necessary to both investigate and compare the results.

Chapter 6 Generation of Carbon Oxide Gases in Synthetic Ester Liquid and Kraft Paper Insulation System under Simulated Thermal Faults

6.1 Introduction

Synthetic ester liquid became an alternative to mineral oil in traction transformers in the late 1970s due to its superior performance in terms of fire safety and biodegradability. In the past decades, synthetic ester has been increasingly used in power transformers. Synthetic ester liquid filled 400 kV, 240 MVA power transformers have been installed in UK National Grid substations [98]. At the same time, challenges are faced in relation to asset management and condition monitoring as the monitoring features of synthetic ester liquid filled transformers might not be the same as mineral oil filled transformers. Many accelerated ageing studies in synthetic ester liquid-paper insulation system were conducted and compared with mineral oil-paper insulation system under a uniform temperature profile [39, 41, 42, 104]. However, DGA was rarely conducted in these ageing studies. Accordingly, it is of great importance to study gas generation characteristics in a synthetic ester liquid-Kraft paper insulation system under laboratory simulated localised thermal faults and conduct a comparison of gas generation characteristics with the mineral oil-Kraft paper insulation system, as reported in Chapter 5.

In this chapter, a series of thermal faults with various fault durations are simulated using the tube-heating method in a synthetic ester liquid-Kraft paper insulation system to investigate fault gas generation characteristics, and in particular, carbon oxide gases. The experimental conditions are initially introduced and the gas-in-oil generation results are then reported. In addition, the conventional paper ageing indicators, like DP and 2-FAL, are measured. The relationships between different indicators are analysed

and further compared with the results of the mineral oil-Kraft paper insulation system.

6.2 Experiment Condition and Procedure

6.2.1 Sample preparation

The investigated liquid-paper insulation system includes a synthetic ester liquid, MIDEL 7131 from M&I Materials, and non-thermally upgraded Kraft paper from Weidmann. The liquid to paper ratio in the heating tube is 21.5:1 based on 0.6 g of Kraft paper and 12.9 g of synthetic ester liquid. Identical to the conditions in a mineral oil-Kraft paper insulation system, the synthetic ester experienced the thermal fault in the heating tube will be largely diluted in 6.6 L of bulk ester liquid (including 6 L of synthetic ester in the oil tank and the other 0.6 L in the pipework) after the simulated faults. The system's headspace is filled with 2.5 L of nitrogen after a 3-hour degassing process.

Three layers of Kraft paper sample are inserted in the 15 cm thermal fault area of the heating tube (as shown in Figure 5-1 in Chapter 5 section 5.2.1) and followed the method introduced in Chapter 5 section 5.2.1 so that it is in tight contact with the inner surface of the heating tube. The length of each Kraft paper layer is also 15 cm and the width is 3 cm. Meanwhile, the names of the three layers in this chapter have been changed to L1TSE, L2MSE and L3OSE, respectively. In the experiments, these three layers are tightly touching each other with no visible gaps between them. After pre-processing, the synthetic ester liquid has a moisture level of less than 10% relatively humidity and the Kraft paper samples have a moisture level of less than 1% by weight. During the experiment, the thermal fault temperature is set at 250 ºC, with 9 different heating durations selected from 0.5 to 24 hours. To observe the repeatability of the experiments, two experiments are repeated for each heating duration. Table 6-1 summarises the experiment conditions.

Table 6-1 Conditions for the synthetic ester liquid-Kraft paper experiments

Insulating liquid	Synthetic ester liquid (MIDEL 7131)
Solid insulation	Non-thermally upgraded Kraft paper
Fault temperature	250 ºC
Heating period	0.5 h, 1 h, 2 h, 4 h, 8 h, 12 h, 16 h, 20 h, 24 h
Liquid weight in heating tube	12.9 g
Paper weight in heating tube	0.6 g
Liquid volume	6.6 L (6 L in the main tank + 0.6 L in the pipework)
Headspace volume	2.5 L N_2 (1.6 L in the main tank + 0.9 L in the pipework)

6.2.2 Test procedure

The test procedure in this chapter is the same as the procedure described in Chapter 5 section 5.2.2. Similarly, the 24-hour fault period of synthetic ester liquid-Kraft paper experiment is used as an example to briefly introduce the experiment in this chapter. The DGA results of the 24-hour experiment are shown in Figure 6-1. The measurements include three background measurements and eight post fault measurements. The dissolved gas concentrations are measured from the liquid phase and thus the gas-in-oil concentrations are reported. It should be noted that the reported gas-in-oil results in this chapter are already calibrated and converted to 25 ºC based on the equations in Chapter 3 section 3.8. It can be seen that there is no generation of hydrocarbon gases after 24 hours of simulated thermal fault, which is the same as in the mineral oil-Kraft paper insulation system experiments. Only carbon dioxide and carbon monoxide are detected by the online DGA monitor and plotted in Figure 6-1. The generation of hydrocarbon gases can be neglected in all fault periods since the 24-hour fault duration is the longest fault period investigated in this chapter.

From the DGA measurement results, an increase in carbon dioxide and carbon monoxide is evident. This is due to carbon oxide gases, including carbon dioxide and carbon monoxide, being by-products of cellulose degradation under a simulated

thermal fault. Both the carbon dioxide and carbon monoxide concentrations reach the steady-state quickly. The gas-in-oil generations of carbon dioxide and carbon monoxide are calculated as the differences between the average values of the last three post fault measurements when reaching the steady status and the average values of three background measurements. There is an approximate 591 ppm increase in carbon dioxide and 85.2 ppm increase in carbon monoxide after experiencing a 250 ºC thermal fault for 24 hours.

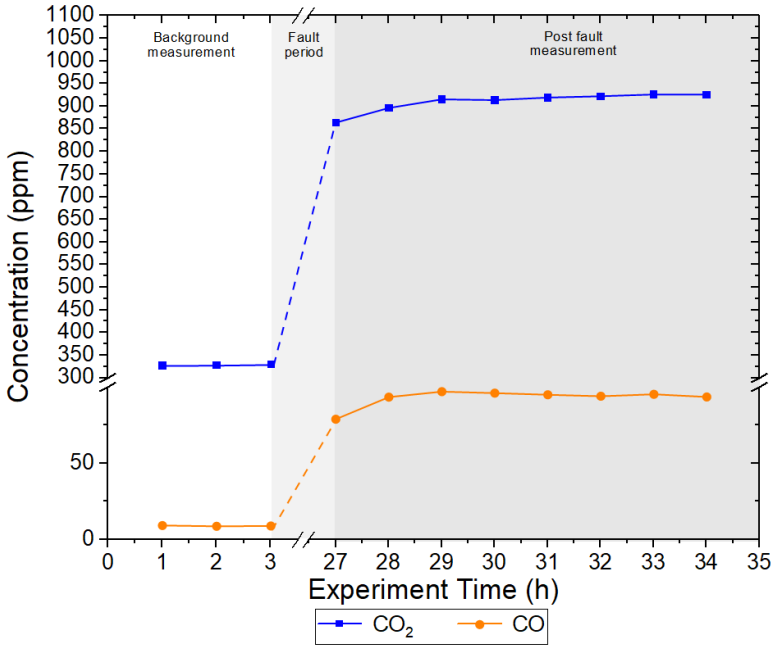

Figure 6-1 DGA measurement results for a 24-hour heating duration in the synthetic ester liquid-Kraft paper insulation system

6.3 Generation of Fault Gases

6.3.1 Synthetic ester liquid only experiments

The insulating liquid used in this chapter is synthetic ester liquid, which has organic compounds and unsaturated hydrocarbons compounds, with the scission of these compounds potentially resulting in the generation of carbon oxide gases [22]. To investigate the generation of carbon oxide gases during the degradation of cellulose paper at a 250 ºC thermal fault, it is important to understand the amount of such gases generated in synthetic ester liquid under the same thermal stress. Additionally, the

results in Chapter 4 section 4.5 already show the carbon oxide gases are more easily generated in synthetic ester liquid. Hence, the synthetic ester liquid only experiments are conducted for each heating duration.

The experiment procedure is the same as the mineral oil only experiment already described in Chapter 5 section 5.3.1. The 24-hour heating duration experiment is used as an example. There are no hydrocarbon oxide gases generated. The DGA results of carbon oxide gases are plotted in Figure 6-2. The same as the 24-hour mineral oil only experiment, the concentrations of carbon dioxide and carbon monoxide quickly reach a steady-state after the simulated thermal fault. There is an approximate 74.6 ppm increase in carbon dioxide and 12.7 ppm increase in carbon monoxide from the synthetic ester liquid only experiment. The carbon oxide gas generation results in the synthetic ester liquid only experiments for each heating duration are listed in Table 6-2. There is a small generation of carbon oxide gases in synthetic ester liquid. When the heating duration is no more than 2 h, the generation of carbon oxide gases is not observed.

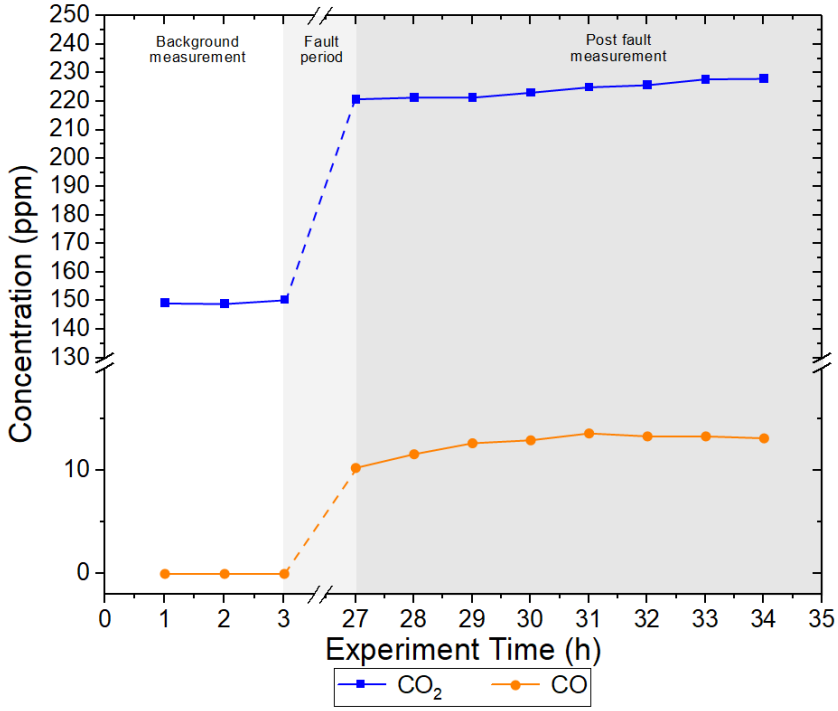

Figure 6-2 DGA measurement results for a 24-hour duration in the synthetic ester liquid only experiment

Table 6-2 Gas-in-oil generation results of carbon oxide gases for synthetic ester liquid only experiments under different heating durations at 250 ºC thermal fault

	0.5 h	1 h	2 h	4 h	8 h	12 h	16 h	20 h	24 h
CO_2	0.0	0.0	0.0	35.7	34.3	55.1	35.2	36.8	77.6
CO	0.0	0.0	0.0	7.3	0.0	2.6	7.2	1.3	13.3

6.3.2 Synthetic ester liquid-Kraft paper experiments

For synthetic ester liquid-Kraft paper experiments, a series of 18 experiments, including repeating experiments, were conducted to investigate fault gas generation characteristics at a 250 ºC thermal fault with different heating durations. In addition, when analysing the results of the synthetic ester liquid-Kraft paper experiments, the gas generation results from the synthetic ester liquid only experiments were subtracted. Hence, the reported values reflect the generation of carbon oxide gases from the decomposition of cellulose paper. As the generation of hydrocarbon gases are negligible, only the gas-in-oil generation results of carbon dioxide and carbon monoxide are summarised in Table 6-3. The results of the two repeating experiments for each heating duration show a reasonable repeatability with the relative difference being within 20%, except for the carbon dioxide results for the 0.5 h and 1 h heating durations.

According to the data listed in Table 6-3, the gas-in-oil generation results against different heating durations are plotted in Figure 6-3. The fitting curve for each gas is based on the average value under each heating duration. It can be seen that the amount of carbon dioxide generated is much higher than carbon monoxide. The amount of carbon dioxide and carbon monoxide generated rapidly increases at the beginning and tends level off until reaching the steady status. There is an exponential increasing trend for both carbon dioxide and carbon monoxide. Pyrolysis is the dominated degradation mechanism of cellulose due to the high temperature thermal fault resulting in a significant formation of carbon oxide gases [37].

Table 6-3 Gas-in-oil generation results of carbon oxide gases for synthetic ester liquid-Kraft paper experiments under different heating durations at 250 ºC thermal fault

Heating duration	CO_2, ppm			CO, ppm		
	Test 1	Test 2	Average	Test 1	Test 2	Average
0.5 h	138.5	100.8	119.6	16.6	17.1	16.9
1 h	133.7	95.0	114.4	13.3	14.7	14.0
2 h	277.5	208.1	242.8	19.8	20.0	19.9
4 h	299.8	369.6	334.7	38.7	51.7	45.2
8 h	320.7	291.4	306.1	34.4	44.0	39.2
12 h	401.1	442.7	421.9	79.5	80.1	79.8
16 h	466.5	427.1	446.8	81.2	89.6	85.4
20 h	498.2	538.0	518.1	88.0	107.5	97.8
24 h	515.2	515.1	515.2	72.5	101.6	87.1

The carbon oxide gas generation results in the mineral oil-Kraft paper experiments are also plotted in Figure 6-3 for comparison. It can be seen that the generation amounts for both carbon oxide gases in the synthetic ester liquid-Kraft paper experiments are much higher than those in the mineral oil-Kraft paper experiments. Similarly, carbon dioxide and carbon monoxide in both oil-paper insulation experiments increase with the increasing fault duration following an exponential trend. Although the same amount of Kraft paper is inserted in the heating tube, the results suggest that more carbon oxide gases are generated from the cellulose in a synthetic ester liquid-Kraft paper insulation system under the same experimental condition when compared with a mineral oil-Kraft paper insulation system. To make a further analysis, the DP of the Kraft paper samples after each thermal fault duration is worth measuring to correlate the carbon oxide generation with the degradation of Kraft paper.

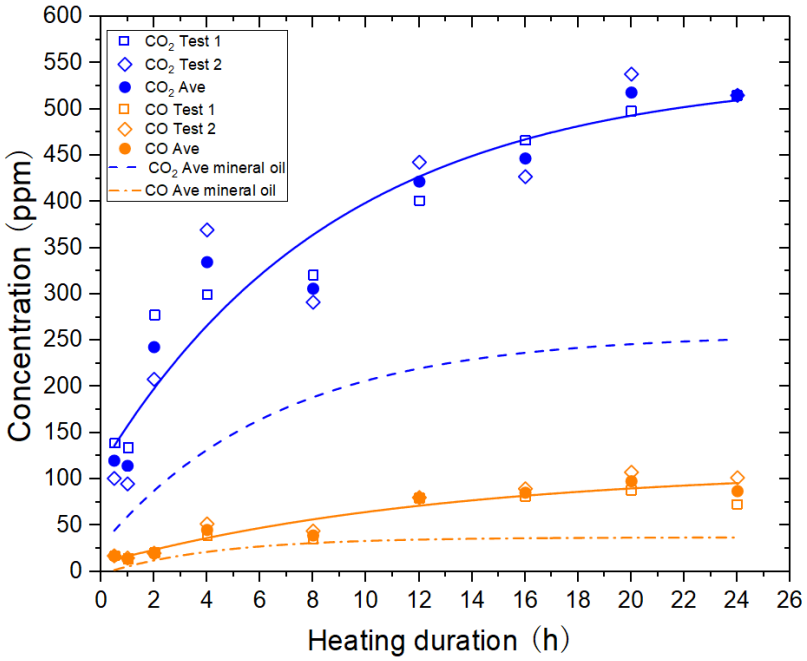

Figure 6-3 Gas-in-oil generation results of carbon oxide gases as a function of different heating durations for synthetic ester liquid-Kraft paper experiments and compared with mineral oil-Kraft paper experiments under different heating duration at 250 ºC thermal fault

6.4 Correlation of Carbon Oxide Gas Generation with Paper Degradation

6.4.1 Paper degradation characterised by DP measurements

Each paper sample layer has separate DP measurements, following the procedure described in ASTM D4243 standard [108]. The DP values for each paper layer sample as a function of heating duration are shown in Figure 6-4. The DP values used to plot the figure are based on the average of two DP measurements. The DP value for new paper is directly measured from the same Kraft paper samples but without degradation, with the measured value of approximately 980. The figure shows that the DP value for all three layers rapidly decrease when the heating duration is shorter than 4 hours. The reduction of the DP then tends to slowly decrease with the increase in heating duration under the trend of reaching a steady-state. When the paper has started to degrade, amorphous regions are easily cleaved at first, resulting in a rapid reduction in the DP value during the early stage. On the other hand, during the later paper degradation stage, crystalline regions degrade much more slowly, resulting in a slower reduction of

DP. There is no doubt that the reduction of DP of the Kraft paper samples indicates a severe decomposition of Kraft paper when the thermal fault is at 250 ºC.

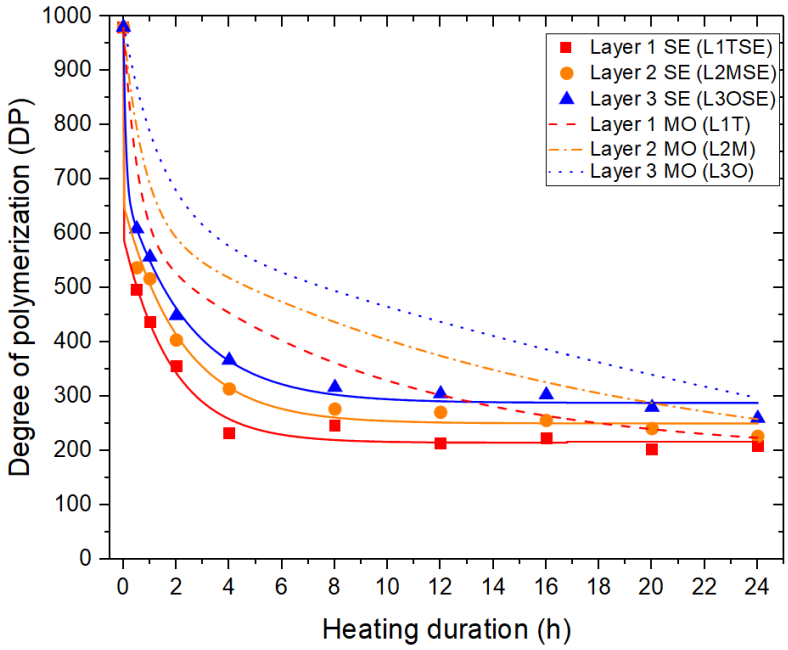

Figure 6-4 DP values of Kraft paper samples of each layer for synthetic ester liquid-Kraft paper experiments and compared with results for mineral oil-Kraft paper experiments under different heating durations at 250 ºC thermal fault

The DP results for each layer in the mineral oil-Kraft paper experiments are also shown in Figure 6-4 for comparison. The DP values for each paper layer sample in the synthetic ester liquid-Kraft paper experiments are smaller than in the mineral oil-Kraft paper experiments at the same heating duration, suggesting that the degradation of Kraft paper samples in synthetic ester liquid-Kraft paper experiments is severer. This is caused by the temperature inside the heating tube when filled with synthetic ester liquid being around 20 ºC higher than that filled with mineral oil. Detailed results for the temperature profile comparison inside the heating tube were investigated and reported in Chapter 3 section 3.5. Synthetic ester liquid has higher viscosity than mineral oil, slowing down the liquid flow and increasing the temperature in naturally cooled transformers [97]. A similar phenomenon should exist in the present experiment setup.

The same as the mineral oil-Kraft paper experiments, the DP values of the different layers are different. Layer 1, which is in direct contact with the inner surface of the

heating tube, is the lowest for all heating durations, whilst those of layer 3 in contact with the oil are the highest. The temperature gradient across the paper layers inside the heating tube also exists in the synthetic ester liquid-Kraft paper experiments. Each Kraft paper layer sample must have experienced different thermal fault temperatures to some extent and the Kraft paper ageing rates for each layer should be different.

In order to obtain the paper ageing rates for each layer, the kinetic studies using SFCU to characterise the degradation of cellulose described in Chapter 5 section 5.4.2 are also used in this chapter. The SFCU as a function of heating duration is firstly plotted in Figure 6-5. The same as in the mineral oil-Kraft paper experiments, points with a DP higher than 300 are used to fit the curve by the straight line. It is clear that with a heating duration increase, the SFCU initially shows a linear increasing tendency and then tends to increase slowly, meaning that the paper ageing rate decreases. The amorphous regions in cellulose are more easily cleaved than in the crystalline regions leading to the paper ageing rate being higher at the beginning. At the later stage of paper ageing, the breaking of the crystalline regions is slow and thus the paper ageing rate is lower than at the beginning [38, 110].

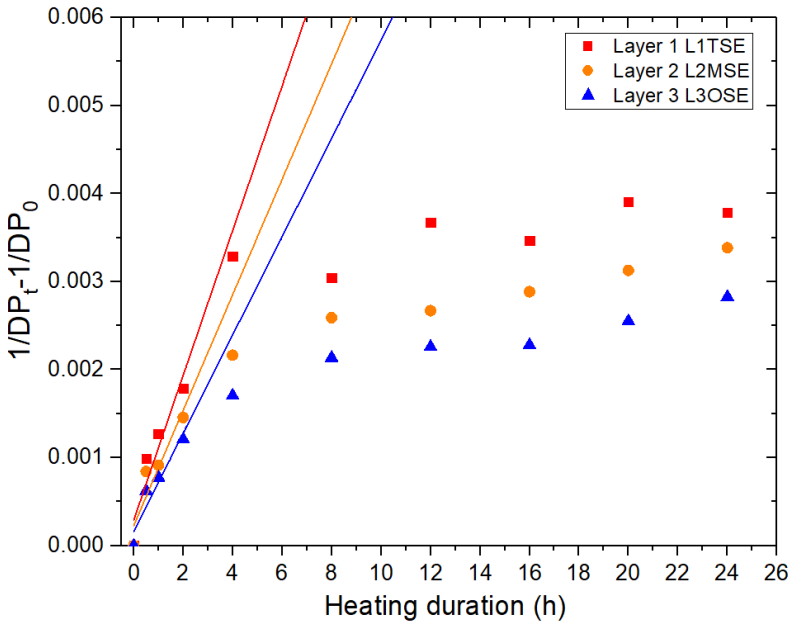

Figure 6-5 SFCU of different Kraft paper layers as a function of heating duration for synthetic ester liquid-Kraft paper experiments at 250 ºC thermal fault

The paper ageing rate is 8.22×10^{-4} for layer 1, 6.56×10^{-4} for layer 2 and for 5.58×10^{-4} for layer 3. It can be seen that layer 1, which is in direct contact with the inner surface of the heating tube, has the highest paper ageing rate, corresponding to the lowest DP values of the three layers (as shown in Figure 6-4). This indicates that layer 1 experiences the highest temperature, leading to the fastest degradation rate. It is clear that the different ageing rates of paper degradation also provide the evidence of the temperature gradient.

6.4.2 Determination of temperature gradient across paper layers

In order to estimate the temperature difference between layers, the method using the kinetic model and Arrhenius expression with activation energy and the pre-exponential factor is used. The procedure and the equations have already been introduced in Chapter 5 section 5.4.2. However, the method using the lifetime estimation of cellulose insulation in Chapter 5 section 5.4.2 is not used since there is no suitable lifetime equation for ester liquid-Kraft paper insulation system.

As the insulating liquid is changed to synthetic ester liquid, the activation energy is changed to 102 kJ mol^{-1} and the pre-exponential factor is changed to 4.96×10^{12} mg $kg^{-1}h^{-1}$. The activation energy and the pre-exponential factor are referred to a previous synthetic ester liquid-Kraft paper ageing study [41]. All the other parameters are the same as those listed in Chapter 5 section 5.4.2. The temperature difference between layer 1 and layer 2 (TF_{L12}) is 2.1 ºC, which is higher than that between layer 2 and layer 3 (TF_{L23}), 1.4 ºC. Therefore, the maximum temperature difference between layer 1 and layer 3 (TF_{L13}) is 3.5 ºC. The temperature differences in the synthetic ester liquid-Kraft paper experiments are smaller than in the mineral oil-Kraft paper experiments reported in Chapter 5, section 5.4.2. The smaller temperature differences between each layer in the synthetic ester liquid-Kraft paper experiments also verify the temperature profile experiments in Chapter 3 section 3.5 that the temperature difference between different positions inside the heating tube in a synthetic ester liquid insulation system is smaller than that in a mineral oil insulation system.

6.4.3 Correlation between carbon oxide generation and DP reduction

To correlate the generation of carbon oxide gases with paper degradation, the average DP values of the three Kraft paper sample layers from two repeated experiments are used to represent the degradation of the Kraft paper samples. Meanwhile, the related chain scission numbers, as a function of the increasing heating duration, are shown in Figure 6-6. The measured DP of the paper without degradation is around 980, which is plotted as the first point. The DP value of the Kraft paper samples falls quickly from 980 to 304 after 4 hours of heating. Then, the DP slowly decreases until it reaches 232 at 24 hours of heating. The overall tendency shows that the DP decreases exponentially with the heating duration increase. Concerning the relationship between chain scission number and heating duration, it can be seen that the chain scission number exponentially increases with the heating duration increase, along with the reduction of the DP. More chain scissions are required to decrease the DP value further when the DP value is already low.

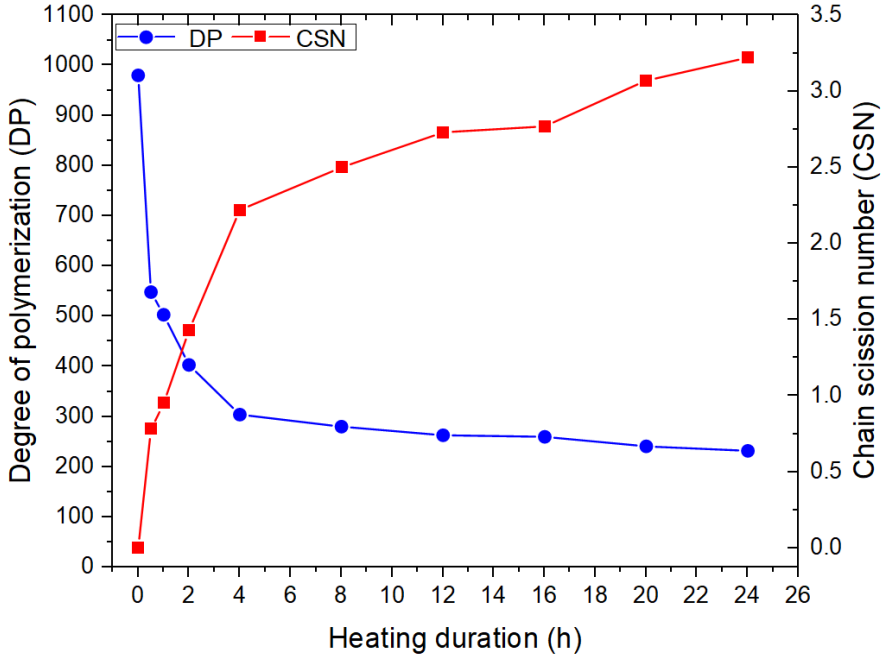

Figure 6-6 Average DP value and chain scission number of 3-layer Kraft paper samples versus heating duration in a synthetic ester liquid-Kraft paper insulation system at 250 ºC thermal fault

Figure 6-7 presents the generation of carbon oxide gases against the reduction of DP in synthetic ester liquid-Kraft paper experiments and the results are compared with mineral oil-Kraft paper experiments. It can be seen that the generation of carbon dioxide and carbon monoxide in synthetic ester liquid-Kraft paper experiments exponentially increases with the reduction of DP. More carbon oxide gases are generated in the synthetic ester liquid-Kraft paper insulation system than the mineral oil-Kraft paper insulation system in the low DP region.

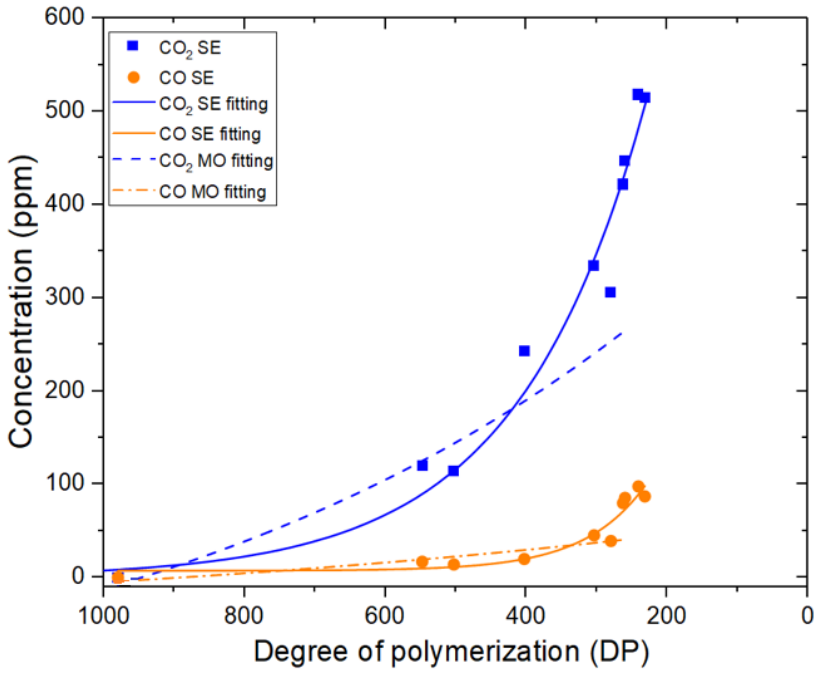

Figure 6-7 Generation of carbon oxide gases as a reduction of DP for synthetic ester liquid-Kraft paper experiments and compared with results for mineral oil-Kraft paper experiments at 250 ºC thermal fault

Figure 6-8 shows the generation of carbon oxide gases as a function of the chain scission number of the cellulose paper samples in both oil-paper insulation systems. It highlights a linear relationship between the generation of carbon oxide gases and the chain scission number in the synthetic ester liquid-Kraft paper experiments, the same as in the mineral oil-Kraft paper experiments. In addition, the amount of carbon oxide gases generated is higher in the synthetic ester liquid-Kraft paper experiment when at the same chain scission number. The relationships between the generation of carbon dioxide/carbon monoxide and the chain scission number can be represented as

equation (6-1) and equation (6-2):

$$C_{CO_2} = 155.02 \times CSN \quad \textbf{(6-1)}$$

$$C_{CO} = 26 \times CSN \quad \textbf{(6-2)}$$

Where C_{CO_2}, C_{CO} represent the concentration of carbon dioxide and carbon monoxide generated, respectively.

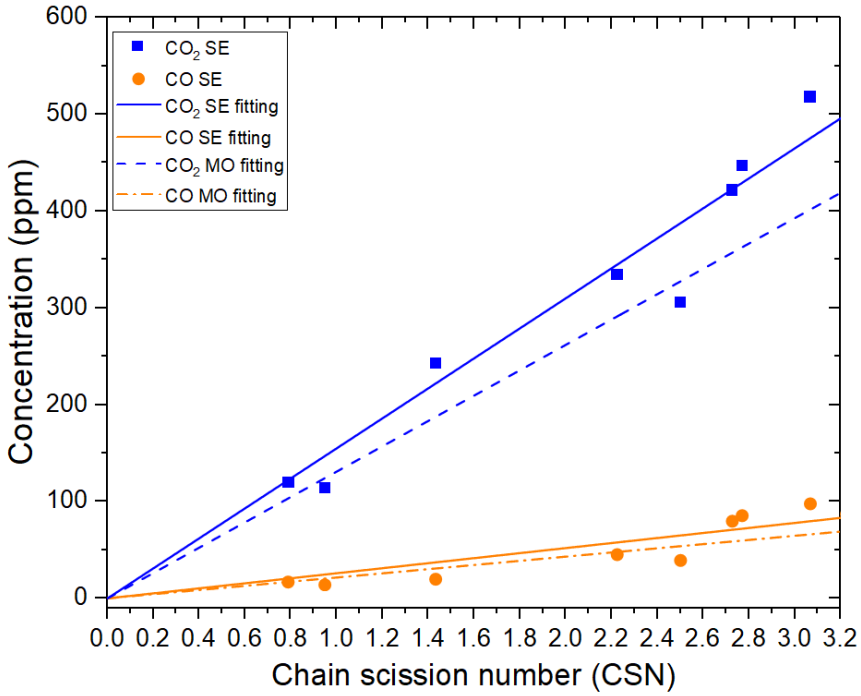

Figure 6-8 Generation of carbon oxide gases as a function of chain scission number for synthetic ester liquid-Kraft paper experiments and compared with results for mineral oil-Kraft paper experiments at 250 ºC thermal fault

From Figure 6-7 and Figure 6-8, after correlating the generation of carbon oxide gases with the DP or chain scission number, the difference in the amount of carbon oxide gases generated between the synthetic ester liquid-Kraft paper insulation and mineral oil-Kraft paper insulation are much smaller than those results shown in Figure 6-3. There is no doubt that the generated amounts of carbon oxide gases in the synthetic ester liquid-Kraft paper insulation are a little higher than in the mineral oil-Kraft paper insulation at the same DP or chain scission number. The generation of carbon oxide gases should be no different if the carbon oxide gases are purely generated from the decomposition of cellulose. Although the results in the synthetic ester liquid only experiments are subtracted, the Kraft paper samples are impregnated by synthetic

ester liquid before each experiment, with approximately 30% of the of Kraft paper samples' pores filled with synthetic ester liquid [126]. The synthetic ester liquid filled in the pores can hardly move and degrades during the fault duration, resulting in the generation of carbon oxide gases. Therefore, a small difference in the generation of carbon oxide gases is observed between the two liquid-paper insulation systems.

6.5 Comparison between Carbon Oxide Gases and 2-FAL

6.5.1 Generation of 2-FAL from paper degradation

Besides the DP values of Kraft paper being an ageing indicator, 2-FAL is an indirect indicator of paper ageing and generated from cellulose and pentosan [120]. During the experiment, 2-FAL is measured before and after the thermal fault, with the difference used to represent the concentration of 2-FAL in liquid for each hearing duration. The concentration of 2-FAL in liquid corresponding to different thermal fault durations are shown in Table 6-4. As the stressed synthetic ester liquid in the heating tube will be mixed with the bulk liquid in the main tank after the simulated thermal faults, the concentration of 2-FAL in liquid is largely diluted leading to the detected amounts of 2-FAL in the liquid being quite small.

Figure 6-9 shows the 2-FAL concentration results as a function of heating duration. The average value of the two repeated experiments is used to plot the curve. It is clear that the 2-FAL concentration linearly increases with the heating duration increase. The correlations between 2-FAL and DP are plotted in Figure 6-10. The DP of the Kraft paper samples directly drops from 980 for the brand-new Kraft paper to 548 in 0.5 h of heating in the synthetic ester liquid-Kraft paper experiment. When the DP is lower than 500, a small DP decrease can lead to a large 2-FAL increase. The overall tendency shows that 2-FAL exponentially increases with the reduction of DP. The similar exponential increasing tendency is also observed in ageing studies [41, 104], highlighting that 2-FAL is best able to be an indicator for the later paper ageing stage [40, 105, 122].

Table 6-4 2-FAL concentration for synthetic ester liquid-Kraft paper experiments under different heating durations at 250 ºC thermal fault

Heating duration	2-FAL concentration, ppb		
	Test 1	Test 2	Ave
1 h	55	9	32
2 h	53	--	53
4 h	146	149	147
8 h	99	91	95
12 h	--	151	151
16 h	158	186	172
20 h	187	176	182
24 h	268	242	255

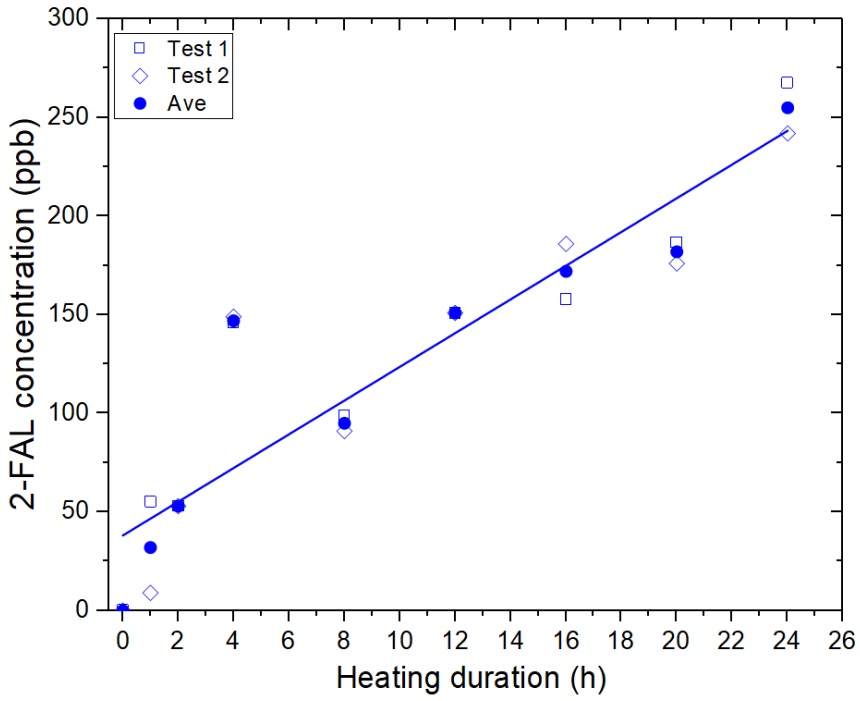

Figure 6-9 2-FAL concentration as a function of heating duration in a synthetic ester liquid-Kraft paper insulation system at 250 ºC thermal fault

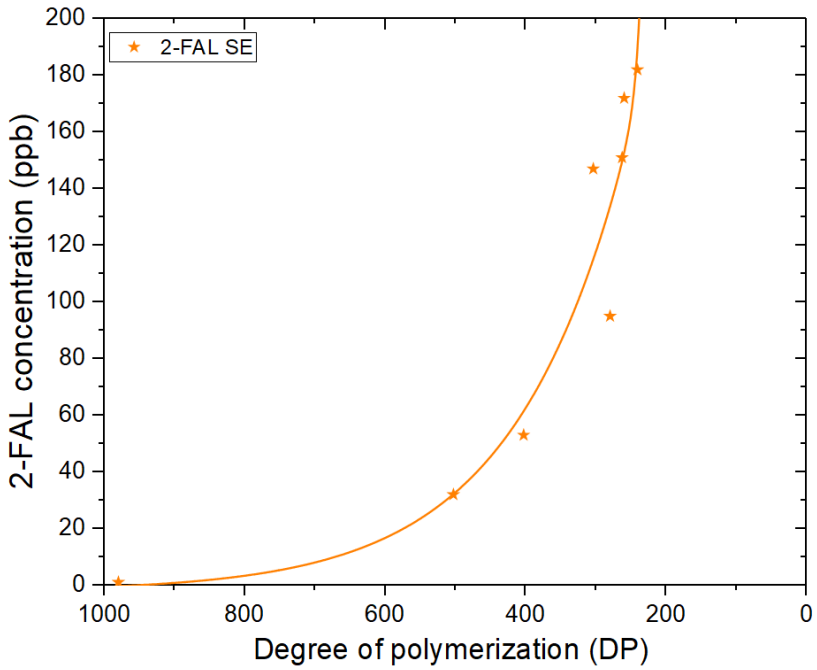

Figure 6-10 2-FAL concentration as a reduction of DP in a synthetic ester liquid-Kraft paper insulation system at 250 ºC thermal fault

6.5.2 Correlation between carbon oxide gases and 2-FAL

Figure 6-11 shows the correlation between the generation of carbon oxide gases and 2-FAL in both oil-paper insulations. There is a linear relationship between the generation of carbon oxide gases and the 2-FAL in the synthetic ester liquid-Kraft paper experiments. The generations of carbon dioxide and carbon monoxide increase with the increase of 2-FAL in liquid. Compared with the results in mineral oil-Kraft paper experiments almost the same relationship between the generation of carbon monoxide and 2-FAL in liquid is obtained in synthetic ester liquid-Kraft paper experiments. However, concerning the relationship between the generation of carbon dioxide and 2-FAL in liquid, more carbon dioxide is generated in synthetic ester liquid-Kraft paper insulation when 2-FAL concentration is lower than 100 ppb, whilst more carbon dioxide is generated in mineral oil-Kraft paper insulation when the 2-FAL concentration is higher than 100 ppb.

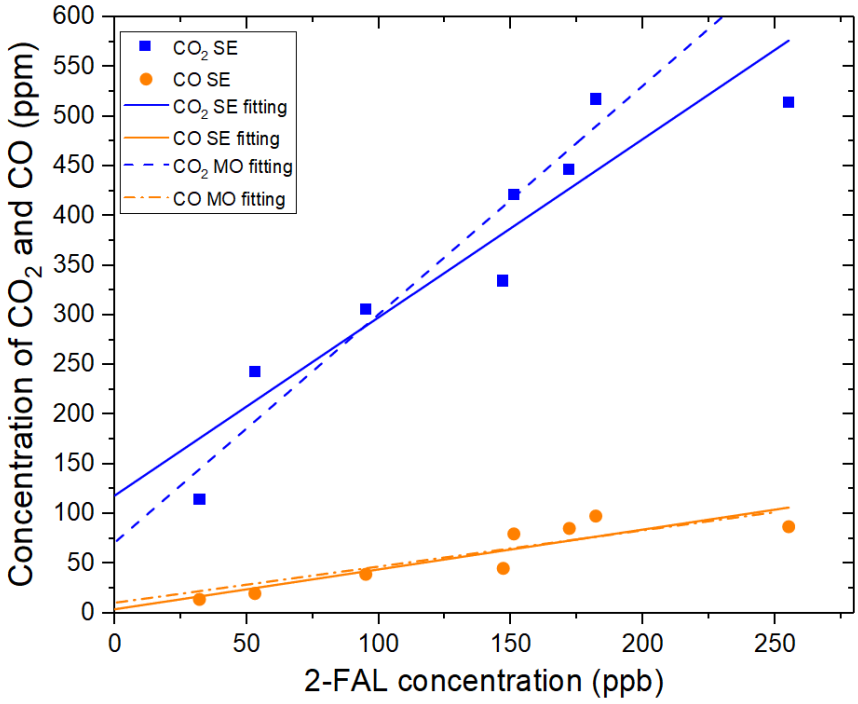

Figure 6-11 Correlation between generations of carbon oxide gases against the concentration of 2-FAL for synthetic ester liquid-Kraft paper experiments and compared with results for mineral oil-Kraft paper experiments at 250 ºC thermal fault

6.6 Comparison of Carbon Oxide Gases Generation with the Literature

The ageing experiments conducted in [39] also investigated a synthetic ester liquid-Kraft paper insulation system. The experiment conditions for synthetic ester liquid-Kraft paper ageing experiments were the same as the mineral oil-Kraft paper ageing experiments described in Chapter 5 section 5.6. Glass ampoules were used to hold 150 ml of synthetic ester liquid and 0.5 g of Kraft paper samples, or only 150 ml of synthetic ester liquid. The glass ampoules' headspace was filled with nitrogen. A number of glass ampoules were put in an air circulating oven. The ageing temperature was firstly set at 70 ºC for one week, with the temperature then raised to 110 ºC for another week. The same procedure continued at 130 ºC, 150 ºC and 190 ºC. At each temperature, several samples were taken out to measure the generation of carbon oxide gases, DP of the Kraft paper samples and the concentration of 2-FAL in liquid.

The results showed that the carbon oxide gases were not only generated in synthetic ester liquid-Kraft paper ageing experiments but also in the synthetic ester liquid only experiment. When Kraft paper was presented in an experiment, much higher amounts of carbon oxide gases were generated, especially when the ageing temperature was above 110 ºC. Meanwhile, hydrocarbon gases especially methane and ethane were generated in small amounts. In addition, the DP showed a decreasing trend with the increase of the ageing temperature. Concerning the 2-FAL in liquid results, there were negligible amounts of 2-FAL detected for all the ageing temperatures.

The same equations (5-12) and (5-13) in Chapter 5 section 5.6 used to calculate the generation of carbon dioxide/carbon monoxide per gram of Kraft paper are used to obtain the generation of carbon oxide gases per gram of Kraft paper in synthetic ester liquid-Kraft paper experiments. This method can eliminate the influence of the oil to paper ratio. Also, the fault gas generation is correlated with chain scission number to eliminate the influence of temperature. Figure 6-12 and Figure 6-13 show the comparison of the generation of carbon oxide gases per gram of Kraft paper as a function of increasing the chain scission number between the present study and [39] in both synthetic ester liquid-Kraft paper insulation system and mineral oil-Kraft paper insulation system. It needs to be noted that when analysing the results from [39], the generations of carbon oxide gases in the synthetic ester liquid only experiments have also been subtracted from the results for the synthetic ester liquid-Kraft paper ageing experiments to ascertain the amounts of carbon oxide gases have been generated by the decomposing cellulose. In addition, there are no hydrocarbon gases detected in present study when compared with literature. The reason may due to the generation of hydrocarbon gases in fault area is quite small, and the online DGA monitor TM8 cannot detect out the fault gases as the fault area oil is largely diluted in bulk oil leading to the concentrations of fault gases are lower than detection limit of TM8.

Figure 6-12 presents the comparison results of the generation of carbon dioxide as the chain scission number increases. The results show that the generation of carbon

dioxide per gram of paper in the synthetic ester liquid-Kraft paper insulation system for both studies increases with the increase of the chain scission number, with the generated amounts comparable under the same chain scission number between the two studies. Although the methods simulating thermal stress between the two studies differ, there is no influence on the relationship between the generation of carbon dioxide per gram of Kraft paper and the chain scission number. Accordingly, the carbon dioxide generation mechanism from the decomposition of cellulose for both studies is the same at the investigated temperature range.

On the other hand, Figure 6-13 shows that the generation of carbon monoxide per gram of paper in the synthetic ester liquid-Kraft paper insulation system in this study is clearly higher than that in prior ageing studies [39]. The results indicate that carbon monoxide can be largely generated under higher temperature thermal faults when compared with ageing experiments. The comparisons imply that there are different mechanisms involved in generating carbon monoxide under different temperatures, a finding deserved further research. As the discussion in Chapter 5 section 5.6, the moisture content of the Kraft paper can also affect the generation of carbon oxide gases in mineral oil-Kraft paper insulation systems. It is worth to verify such a conclusion in the ester liquid- Kraft paper insulation system.

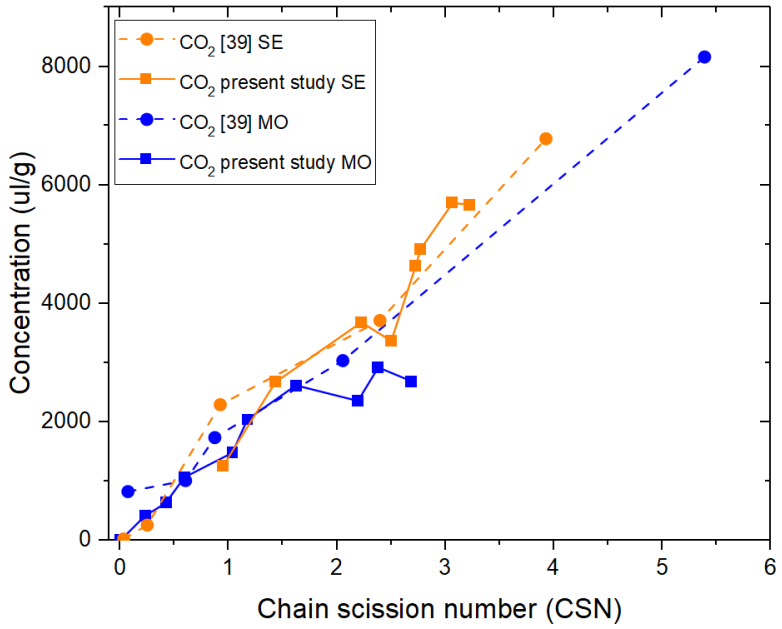

Figure 6-12 Comparison of the generation of carbon dioxide between this study and [39]

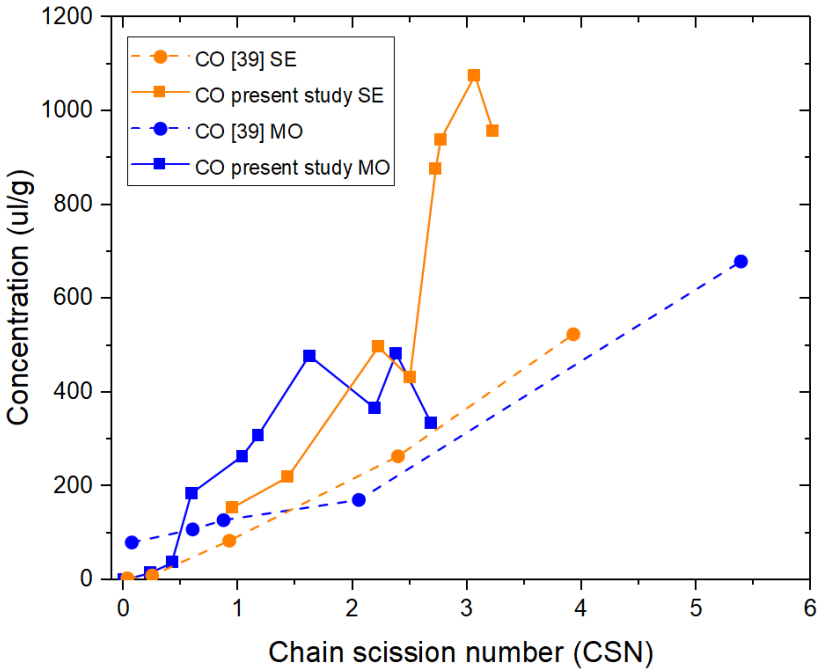

Figure 6-13 Comparison of the generation of carbon monoxide between this study and [39]

In addition, when analysing results in ageing studies [39] using larger chain scission numbers, the generation of carbon dioxide and carbon monoxide in synthetic ester liquid-Kraft paper insulation is also higher than in mineral oil-Kraft paper insulation, verifying the findings of the present study. Therefore, the findings in [39] also confirm that small amounts of synthetic ester liquid filled in the Kraft paper samples' pores during the impregnation process are degraded during the fault and contributed to the

generation of more carbon oxide gases in synthetic ester liquid-Kraft paper insulation.

The laboratory ageing experiments that simulate a uniform temperature profile in an oven show that ester liquids can retard paper ageing when compared to the use of mineral oils [38, 41]. The reasons include higher water saturation in ester liquids leading to more moisture being absorbed from cellulose insulation, hydrolysis of ester liquids reducing moisture in the oil-cellulose insulation system and esterification of the reactive hydroxyl groups in the cellulose insulation with fatty acids through a transesterification process [127, 128]. Hence, a higher DP value of Kraft paper samples is obtained in a synthetic ester liquid-Kraft paper insulation system under the same temperature ageing period when compared to a mineral oil-Kraft paper insulation system.

However, in thermal fault experiments that simulate a hotspot temperature on the inner surface of the heating tube surface, lower DP values of Kraft paper samples are obtained in synthetic ester liquid-Kraft paper experiments under the same thermal fault temperature and duration, corresponding to a higher generation of carbon oxide gases and 2-FAL. The reason is that the cooling efficiency of synthetic ester liquid is lower than mineral oil caused by higher viscosity of synthetic ester liquid. Since the thermal faults temperatures are much higher than uniform ageing temperatures, together with the thermal fault periods being much shorter, pyrolysis is considered as the dominant degradation mechanism.

6.7 Discussion of the CO_2/CO Ratio as a Paper Degradation Indicator

In general, the generation of carbon oxide gases together with further evidence of other paper ageing indicators can be an indicator of the decomposition of cellulose. IEEE C57.155-2014 [68], which is used for the interpretation of gases generated in ester liquid immersed transformers, also indicates that the CO_2/CO ratio can be used to

identify paper related thermal faults in a synthetic ester liquid-Kraft paper insulation system. The CO_2/CO ratio for a normally operating transformer filled with ester liquids is higher than 7. When using the CO_2/CO ratio, the respective values should be higher than 5000 ppm of carbon dioxide and 500 ppm of carbon monoxide. An increase in carbon monoxide will result in a decrease in the CO_2/CO ratio and indicate possible degradation of cellulosic insulation.

Different from high benchmark concentrations of carbon oxide gases defined in IEEE standards to distinguish paper related faults, the benchmark concentrations of carbon oxide gases before and after thermal faults in this current study are much lower due to the small fault size controlled in the heating tube. As carbon oxide gases can also be generated from the decomposition of synthetic ester liquid itself, not only the CO_2/CO ratio based on the generation results of carbon oxide gases from the decomposition of Kraft paper samples, the CO_2/CO ratio based on total generation from synthetic ester liquid-Kraft paper insulation is also compared.

Table 6-5 lists the gas-in-oil generation CO_2/CO ratio for each heating duration. The ratios for each heating duration are calculated based on the average gas-in-oil generation results at each heating duration. Similar CO_2/CO ratios are obtained when only considering the decomposition of Kraft paper samples and when considering both the decomposition of Kraft paper samples and synthetic ester liquid.

Table 6-5 Gas-in-oil generation CO_2/CO ratio for synthetic ester liquid-Kraft paper experiments under different heating duration at 250 ºC thermal fault

	CO_2/CO ratio	
Fault period	**Paper**	**Liquid + paper**
0.5 h	7.10	7.10
1 h	8.17	8.20
2 h	12.20	11.30
4 h	7.40	7.10

8 h	7.81	8.70
12 h	5.29	5.80
16 h	5.23	5.20
20 h	5.30	5.60
24 h	5.92	6.00

Figure 6-14 shows the results of the gas-in-oil generation CO_2/CO ratio as a reduction of the DP value of Kraft paper samples when only considering the decomposition of Kraft paper samples and when considering both the decomposition of Kraft paper samples and synthetic ester liquid. For both conditions, the CO_2/CO ratio is higher than 7 when the DP is higher than 300 but remains stable around 5.5 when the DP is lower than 300. When in a low DP range, the CO_2/CO ratio is comparable with the value in the IEEE standard C57.155-2014 [68], suggesting that a CO_2/CO ratio lower than 7 can indicate a paper related thermal fault. A further reduction of the DP values in the Kraft paper samples means severer decomposition of the Kraft paper samples, resulting in higher amounts of carbon monoxide being generated and leading to a smaller CO_2/CO ratio.

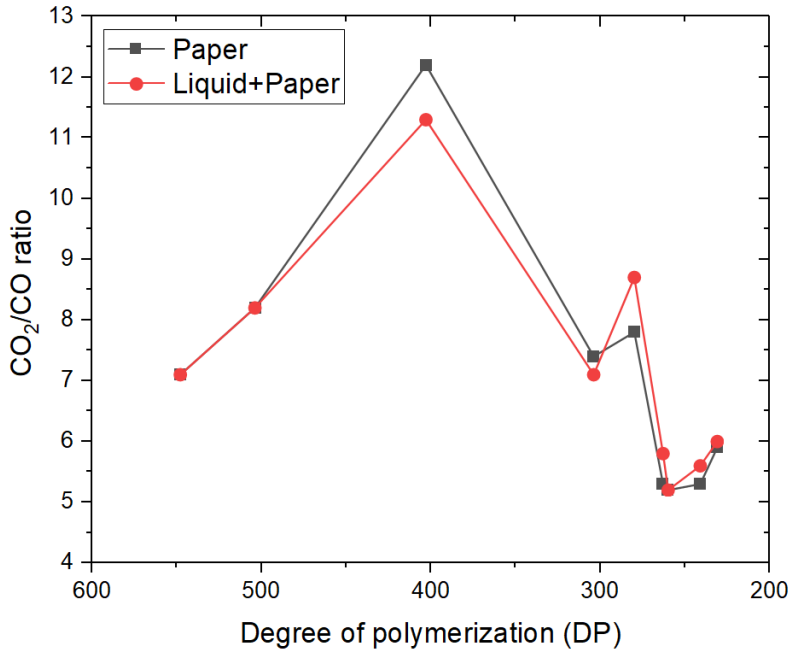

Figure 6-14 Gas-in-oil generation CO_2/CO ratio as a function of DP value for synthetic ester liquid-Kraft paper experiments

6.8 Summary

This chapter has presented a series of synthetic ester liquid-Kraft paper experiments at 250 ºC thermal fault with different heating durations to investigate fault gas generation characteristics. Carbon dioxide and carbon monoxide are largely generated in synthetic ester liquid-Kraft paper experiments. However, different from the negligible generation of carbon oxide gases in mineral oil only experiments, carbon oxide gases are generated from synthetic ester liquid only experiments. These values have been subtracted from the liquid-paper experiments to obtain the amount of carbon oxide gases generated by the decomposition of Kraft paper samples.

Compared to the carbon oxide gas generation results for mineral oil-Kraft paper insulation, the degradation of Kraft paper samples in synthetic ester liquid-Kraft paper insulation is severer. The reason is that the cooling efficiency of synthetic ester liquid is not as good as mineral oil, resulting in the generation of more carbon oxide gases under the same fault conditions. According to the DP measurement results of the different layers, a temperature gradient around 3.5 ºC exists in the synthetic ester liquid-Kraft paper experiments across the paper layers inside the heating tube. The temperature gradient in synthetic ester liquid-Kraft paper insulation system is lower than that in the mineral oil-Kraft paper insulation system.

Meanwhile, the generation of carbon oxide gases shows an exponential increasing tendency as the DP reduces, a linear increasing tendency as the chain scission number increases and a linear relationship with the increasing 2-FAL in liquid. Compared with the results for the mineral oil-Kraft paper insulation under the same fault condition, carbon oxide gas generation is slightly higher in synthetic ester liquid-Kraft paper insulation when correlated with the DP or chain scission number. This is due to the small amounts of synthetic ester liquid filling the Kraft paper samples' pores being degraded and contributing to the generation of carbon oxide gases. Compared to the accelerated ageing studies, carbon monoxide is generated more under thermal faults,

indicating that different generation mechanisms for carbon monoxide might exist under different temperatures.

Chapter 7 Conclusions and Future Work

7.1 Conclusions

7.1.1 General

This thesis has focused on the experimental study of the gas generation characteristics of transformer liquid and solid insulations under laboratory simulated thermal faults using the online DGA technique. A tube-heating experimental setup was developed to simulate a localised thermal fault for both liquid only and liquid-solid insulation systems. Mineral oil has already been widely used as transformer liquid for over a century, with synthetic ester liquid increasingly used during recent decades as an alternative to mineral oil due to its environmentally friendly and fire safety properties. Therefore, to compare fault gas generation characteristics between different transformer insulations, a series of DGA experiments were performed in mineral oil and synthetic ester liquid under various levels of thermal fault. In addition, a series of DGA experiments were conducted in a mineral oil-Kraft paper insulation system and a synthetic ester liquid-Kraft paper insulation system at the 250 ºC thermal fault but with various heating durations. Paper ageing indicators, including DP and 2-FAL, were also measured to correlate with the generation of fault gases.

The following research topics have been covered in this PhD thesis:

- ❖ Development of a tube-heating setup suitable for both liquid only and liquid-solid insulation system experiments
    - Method to install solid insulation in the designated fault area
    - Temperature profile inside the heating tube under various levels of thermal fault
    - Effect of liquid type on temperature profile inside the heating tube

- ❖ Gas generation in mineral oil and synthetic ester liquid under various thermal fault temperatures
    - Gas-in-oil fault gas generation characteristics of mineral oil under 350 ºC, 450 ºC, 550 ºC, 650 ºC and 750 ºC thermal faults
    - Gas-in-oil fault gas generation characteristics of synthetic ester liquid under 350 ºC, 450 ºC, 550 ºC, 650 ºC and 750 ºC thermal faults
- ❖ Gas-in-oil fault gas generation in a mineral oil-Kraft paper insulation under a 250 ºC thermal fault with various heating durations
    - Gas-in-oil fault gas generation characteristics, especially carbon oxide gases
    - Characterisation of paper degradation under the thermal fault
    - Correlation of carbon oxide gas generation with conventional paper ageing indicators
- ❖ Gas-in-oil fault gas generation in a synthetic ester liquid-Kraft paper insulation under a 250 ºC thermal fault with various heating durations
    - Gas-in-oil fault gas generation characteristics in particular of carbon oxide gases
    - Characterisation of paper degradation under the thermal fault
    - Correlation of carbon oxide gas generation with conventional paper ageing indicators
    - Comparison of mineral oil-Kraft paper and synthetic ester liquid-Kraft paper insulation systems.

7.1.2 Summary of results and main findings

- Development of a tube-heating setup suitable for both liquid only and liquid-solid insulation system experiments

A tube-heating based experimental setup was developed enabling the thermal fault tests in both liquid only and liquid-solid insulation systems. This tube-heating experimental setup is able to cover a wide range of thermal fault temperatures to investigate gas generation characteristics using the online DGA measurement technique. Due to the natural liquid flow inside the heating tube during the heating process, a temperature gradient exists in the insulating liquids inside the heating tube. **It is found that when the controlled temperature at the top outer surface of the heating tube increases by 50 ºC, the temperature difference between the top outer surface and central position inside the heating tube increases by 25 ºC.** Moreover, the temperature gradient is also influenced by the type of insulating liquids. **The temperature inside the heating tube, when filled with the synthetic ester liquid, is higher than when filled with the mineral oil because the higher viscosity of the synthetic ester liquid reduces its cooling performance under the natural liquid flow.**

- Gas-in-oil fault gas generation characteristics of mineral oil and synthetic ester liquid under various thermal fault temperatures

A series of DGA experiments were conducted in a mineral oil and a synthetic ester liquid, respectively, under a wide range of thermal fault temperatures, including 350 ºC, 450 ºC, 550 ºC, 650 ºC and 750 ºC. **In the mineral oil experiments, methane is the typical gas of the 350 ºC thermal fault, Ethane is the typical gas for the 450 ºC and 550 ºC thermal faults and ethylene is the typical gas for the 650 ºC and 750 ºC thermal faults. In the synthetic ester liquid experiments, carbon dioxide and carbon monoxide are the dominant fault gases from the 350 ºC to 650 ºC thermal faults** since the organic compounds and unsaturated hydrocarbon compounds in the

chemical structure of synthetics ester liquid contribute to the generation of carbon oxide gases. **Excluding carbon oxide gases, ethylene is the typical gas for the 350 ºC thermal fault and ethane is the typical gas for the 450 ºC to 650 ºC thermal faults. When the temperature reaches 750 ºC, ethylene is the typical gas.** In addition, for both insulating liquids, hydrogen starts being generated after the thermal fault rising above 550 ºC. Acetylene is only generated in extremely high temperature thermal faults, including 650 ºC and 750 ºC thermal faults in mineral oil and the 750 ºC thermal fault in synthetic ester liquid. Meanwhile, free gases are generated in the 650 ºC and 750 ºC thermal faults.

- Gas-in-oil fault gas generation characteristics of a mineral oil-Kraft paper insulation system under a 250 ºC thermal fault with various heating durations

A series of experiments were conducted in a mineral oil-Kraft paper insulation system to investigate gas-in-oil gas generation characteristics under a 250 ºC thermal fault with different heating durations from 0.5 to 24 hours. According to the results of the mineral oil only experiments and mineral oil-Kraft paper experiments, carbon oxide gases are confirmed to be generated from the decomposition of cellulose. **It is found that the generated carbon dioxide and carbon monoxide exponentially increase with the reduction of DP and increase linearly with an increasing chain scission number. In addition, there is a linear relationship found between carbon oxide gases and a common paper ageing indicator 2-FAL in oil.**

Compared with an accelerated ageing study carried out at lower temperatures up to 190 ºC in [39], the same correlation between carbon dioxide and DP reduction is found in both studies. However, more carbon monoxide is generated in this study under higher temperature thermal faults than in the ageing study [39] under lower ageing temperatures when considering the same level of DP reduction. This indicates that different carbon monoxide generation mechanisms exist under different temperatures.

In addition, the generated carbon oxide gases were scaled up according to the

insulation material ratios for power transformers specified in IEC standard 62332-1-2011 [124]. Baseline carbon oxide gases were added and two scenarios with different fault size were considered. The results show that the CO_2/CO ratio is around 5.4 before the occurrence of the thermal fault, with the CO_2/CO ratio seeing a sharp increase when the thermal fault starts. When the solid insulation is continuously degraded with a prolonged fault duration, the CO_2/CO ratio reduces quickly and then fluctuates between 5 and 7. Moreover, the variation of the CO_2/CO ratio is more significant when a large fault area is considered. Therefore, **a static CO_2/CO ratio might be hardly useful to indicate paper degradation, whereas the dynamic change of the CO_2/CO ratio should be explored in the future to indicate the occurrence of a thermal fault involving the paper insulation.**

- Gas-in-oil fault gas generation characteristics of a synthetic ester liquid-Kraft paper insulation system under a 250 ºC thermal fault with various heating durations

A series of experiments were conducted to investigate the gas-in-oil fault gas generation characteristics of a synthetic ester liquid-Kraft paper insulation system under a 250 ºC thermal fault with different heating durations from 0.5 to 24 hours. As carbon oxide gases are also generated from the decomposition of the synthetic ester liquid itself, the results of the generated carbon oxide gases in synthetic ester liquid only experiments are subtracted in the synthetic ester liquid-Kraft paper experiments. **The same as in the mineral oil-Kraft paper experiments, the generated carbon dioxide and carbon monoxide gases have an exponential increasing trend with the reduction of the DP and a linear increasing trend with an increase in the chain scission number. A linear relationship between the generated carbon oxide gases and the paper ageing indicator 2-FAL in liquid is also found.** In addition, carbon monoxide is generated more under higher temperature thermal faults when compared with an accelerated ageing study in [39], which echoes the finding in the mineral oil-Kraft paper experiment that different carbon monoxide generation

mechanisms exist under different temperatures.

Different from the results in the mineral oil-Kraft paper experiments, the generation of carbon oxide gases in the synthetic ester liquid-Kraft paper experiments are much higher, although under the same controlled fault temperature at the outer tube surface and the same heating duration. The reason is that the degradation of Kraft paper samples in the synthetic ester liquid-Kraft paper insulation is severer due to the higher overall liquid temperature inside the heating tube. When correlating the generated carbon dioxide and carbon monoxide with the DP or chain scission number, the carbon oxide gas generation in synthetic ester liquid-Kraft paper insulation becomes slightly higher than in the mineral oil-Kraft paper insulation. This might be due to the small amounts of synthetic ester liquid filled in the pores of the Kraft paper samples that are degraded and contribute to the generation of carbon oxide gas.

7.2 Future Research

In this thesis, some useful conclusions can be presented concerning the gas-in-oil fault gas generation characteristics of different transformer insulations under laboratory simulated thermal faults using the tube-heating method. Meanwhile, there are also new questions raised and more research that can be conducted in the future.

For the fault gas generation characteristics in the insulating liquid only study:

i. Based on the findings of this study, the main advantage of the tube-heating experiment setup is that it has the ability to cover a wide range of thermal faults. According to the results, only the fault gases dissolved in the oil phase were analysed after the simulated thermal faults in the mineral oil and the synthetic ester liquid. The free gases are generated under extremely higher thermal fault temperatures of 650 ºC and 750 ºC. Meanwhile, there must be some of the generated fault gases that are diffused to the gas phase for lower temperature thermal faults. Therefore, future research should measure fault

gas concentrations in the gas phase and combine them with fault gas concentrations in the oil phase to ascertain the total generation of fault gases.

ii. When considering the concentrations of generated fault gases in the gas phase, Ostwald coefficients need to be taken into account since the diffusion of fault gases from the oil phase to the gas phase is affected by Ostwald coefficients. Several factors, such as the environment temperature and pressure, can influence the Ostwald coefficient values. Meanwhile, the published Ostwald coefficients for mineral oil and synthetic ester liquid among different research institutions are less consistent. Therefore, accurate Ostwald coefficients for different insulating liquids need to be measured.

iii. In this study, the thermal fault was only simulated on a hotspot area in the heating tube, with the insulating liquid largely diluted in bulk oil after experiencing a thermal fault and then measuring the dissolved fault gases using an online DGA monitor. In real transformers, insulation materials not only include insulating liquid but also solid insulation such as Kraft paper and pressboard. In addition, the generated fault gases from the fault area might be absorbed by Kraft paper or pressboard outside the fault area. Therefore, it is recommended that future research puts Kraft paper or pressboard in the oil tank to further mimic real transformer conditions and investigate fault gas generation and diffusion characteristics.

For the fault gas generation characteristics in the insulating liquid-Kraft paper insulation study:

i. In the insulating liquid-Kraft paper insulation experiments, the investigations under a 250 ºC thermal fault with various heating durations were performed in this study. To further confirm the findings obtained for both the mineral oil-Kraft paper insulation system and synthetic ester liquid-Kraft paper insulation system, the same experiments under other thermal fault

temperatures are worthily performed. Meanwhile, it has been found that the CO_2/CO ratio for a normally operating transformer filled with mineral oil is below 7, with there being a sharp increase of the CO_2/CO ratio after experiencing a thermal fault, which could be potentially used as an indicator of paper related thermal faults in mineral oil filled transformers. Therefore, future research should be performed under different temperatures to explore this idea.

ii. From literature, the partitioning of carbon dioxide and carbon monoxide between insulating liquid and solid insulation is found. Meanwhile, it has been found that the carbon dioxide and carbon monoxide concentrations in oil are temperature dependent due to the partitioning behaviours. Hence, it is difficult to predict the status of real transformers using carbon dioxide and carbon monoxide measurements as they might be absorbed by solid insulation even after a thermal fault has happened. Therefore, future research should investigate the partitioning characteristics of carbon dioxide and carbon monoxide between different solid insulation materials and insulating liquids.

References

[1] M. Heathcote, "J & P transformer book″, Printed in Great Britain, 2011.

[2] A. Nynas Naphthenics, "Transformer oil handbook," Printed in Sweden, 2004.

[3] J. D. Glover, M. S. Sarma, and T. Overbye, "Power system analysis & design," Printed in the United States of America, 2012.

[4] O. Seevers, "Power systems handbook: Design, Operation and Maintenance," Printed in the United States of America, 1991.

[5] A. Abu-Siada, "Power transformer condition monitoring and diagnosis," Printed in Great Britain, 2018.

[6] S. Tapan Kumar and P. Prithwiraj, *Transformer insulation materials and ageing*, pp. 1-33, 2017.

[7] E. A. Goodman, "Today's transformer insulation systems," *IEEE Transactions on Industry Applications,* vol. IA-8, no. 4, pp. 404-411, 1972.

[8] A. Lokhanin, G. Shneider, V. Sokolov, V. Chornogotsky, and T. Morozova, "Internal insulation failure mechanisms of HV equipment under service conditions," *Cigre Report 15,* vol. 201, pp. 1-6, 2002.

[9] M. Wang, A. J. Vandermaar, and K. D. Srivastava, "Review of condition assessment of power transformers in service," *IEEE Electrical Insulation Magazine,* vol. 18, no. 6, pp. 12-25, 2002.

[10] K. T. Muthanna, A. Sarkar, K. Das, and K. Waldner, "Transformer insulation life assessment," *IEEE Transactions on Power Delivery,* vol. 21, no. 1, pp. 150-156, 2006.

[11] B. Gorgan *et al.*, "Calculation of the remaining lifetime of power transformers paper insulation," *13th International Conference on Optimization of Electrical and Electronic Equipment*, Brasov, Romania, 2012.

[12] A. Van Schijndel, P. Wouters, E. Steennis, and J. Wetzer, "Approach for an integral power transformer reliability model," *European Transactions on Electrical Power,* vol. 22, no. 4, pp. 491-503, 2012.

[13] X. Zhang and E. Gockenbach, "Asset-management of transformers based on condition monitoring and standard diagnosis," *IEEE Electrical Insulation Magazine,* vol. 24, no. 4, pp. 26-40, 2008.

[14] D. Feng, Z.D. Wang, and P. Jarman, "Getting the most out of historic reliability data," *IEEE Prognostics and System Health Management Conference*, Beijing, China, 2012.

[15] D. Zhou, Z.D. Wang, P. Jarman, and C. Li, "Data requisites for transformer statistical lifetime modelling—Part II: combination of random and aging-related failures," *IEEE Transactions on Power Delivery,* vol. 29, no. 1, pp. 154-160, 2014.

[16] CIGRE Brochure 642, "Transformer reliability survey," 2015.

[17] Z. Moravej and S. Bagheri, "Condition monitoring techniques of power

transformers: A review," *Journal of Operation and Automation in Power Engineering,* vol. 3, no. 1, pp. 71-82, 2015.

[18] Y. Han and Y. H. Song, "Condition monitoring techniques for electrical equipment-a literature survey," *IEEE Transactions on Power Delivery,* vol. 18, no. 1, pp. 4-13, 2003.

[19] A. E. B. Abu-Elanien and M. M. A. Salama, "Survey on the transformer condition monitoring," *Large Engineering Systems Conference on Power Engineering*, Montreal, QC, Canada, pp. 187-191, 2007.

[20] M. Duval, "Dissolved gas analysis: It can save your transformer," *IEEE Electrical Insulation Magazine,* vol. 5, no. 6, pp. 22-27, 1989.

[21] U. K. Imad, Z.D. Wang, I. Cotton, and S. Northcote, "Dissolved gas analysis of alternative fluids for power transformers," *IEEE Electrical Insulation Magazine,* vol. 23, no. 5, pp. 5-14, 2007.

[22] IEEE Standard C57.104, "Guide for the interpretation of gases generated in mineral oil-immersed transformers," 2019.

[23] IEC Standard 60567, "Oil-filled electrical equipment-Sampling of gases and analysis of free and dissolved gases-Guidance," 2012.

[24] IEC Standard 60599, " Mineral oil-filled electrical equipment in service-Guidance on the interpretation of dissolved and free gases analysis," 2016.

[25] N. A. Muhamad, B. T. Phung, and T. R. Blackburn, "Dissolved gas analysis for common transformer faults in soy seed-based oil," *IET Electric Power Applications,* vol. 5, no. 1, pp. 133-142, 2011.

[26] H. Borsi, K. Durnke, and E. Gockenbach, "Relation between faults and generated gases in transformer liquids," *IEEE 13th International Conference on Dielectric Liquids*, Nara, Japan, 1999.

[27] M. Jovalekic, D. Vukovic, and S. Tenbohlen, "Dissolved gas analysis of natural ester fluids under electrical and thermal stress," *16th International Symposium on High Voltage Engineering*, Cape Town, South Africa, 2009.

[28] M. Jovalekic, D. Vukovic, and S. Tenbohlen, "Dissolved gas analysis of alternative dielectric fluids under thermal and electrical stress," *2011 IEEE International Conference on Dielectric Liquids*, Trondheim, Norway, pp. 1-4, 2011.

[29] M. Jovalekic, D. Vukovic, and S. Tenbohlen, "Gassing behavior of various alternative insulating liquids under thermal and electrical stress," *IEEE International Symposium on Electrical Insulation*, San Juan, PR, USA, pp. 490-493, 2012.

[30] Z.D. Wang, X. Yi, J. Huang, J. V. Hinshaw, and J. Noakhes, "Fault gas generation in natural-ester fluid under localized thermal faults," *IEEE Electrical Insulation Magazine,* vol. 28, no. 6, pp. 45-56, 2012.

[31] X. F. Wang, Z.D. Wang, Q. Liu, and P. Dyer, "Dissolved gas analysis of thermal faults in transformer liquids simulated using immersed heating method," *IEEE Transactions on Dielectrics and Electrical Insulation,* vol. 25, no. 5, pp. 1749-1757, 2018.

[32] P. Przybylek and J. Gielniak, "Analysis of gas generated in mineral oil, synthetic ester, and natural ester as a consequence of thermal faults," *IEEE Access,* vol. 7, pp. 65040-65051, 2019.

[33] J. L. Dave Hanson, Kevin Li, Art Lemm, Jorge Plascencia, "Understanding dissolved gas analysis - Part 2: Thermal decomposition of ester fluids," *TJH2B EuroTechCon*, Warwick, UK, 2012.

[34] Y. Liu, J. Li, and Z. Zhang, "Gases dissolved in natural ester fluids under thermal faults in transformers," *IEEE International Symposium on Electrical Insulation*, San Juan, PR, USA, pp. 223-226, 2012.

[35] D. Hanson *et al.*, "Understanding dissolved gas analysis of ester liquids: An updated review of gas generated in ester liquid by stray gassing, thermal decomposition and electrical discharge," *IEEE Electrical Insulation Conference*, Montreal, QC, Canada, pp. 138-144, 2016.

[36] C. Xiang, Q. Zhou, J. Li, Q. Huang, H. Song, and Z. Zhang, "Comparison of dissolved gases in mineral and vegetable insulating oils under typical electrical and thermal faults," *Energies,* vol. 9, no. 5, pp. 1-22, 2016.

[37] L. E. Lundgaard, W. Hansen, D. Linhjell, and T. J. Painter, "Aging of oil-impregnated paper in power transformers," *IEEE Transactions on Power Delivery,* vol. 19, no. 1, pp. 230-239, 2004.

[38] R. Liao, S. Liang, C. Sun, L. Yang, and H. Sun, "A comparative study of thermal aging of transformer insulation paper impregnated in natural ester and in mineral oil," *European Transactions on Electrical Power,* vol. 20, no. 4, pp. 518-533, 2010.

[39] M. A. G. Martins and A. R. Gomes, "Comparative study of the thermal degradation of synthetic and natural esters and mineral oil: Effect of oil type in the thermal degradation of insulating kraft paper," *IEEE Electrical Insulation Magazine,* vol. 28, no. 2, pp. 22-28, 2012.

[40] S. Y. Matharage, Q. Liu, and Z.D. Wang, "Aging assessment of Kraft paper insulation through methanol in oil measurement," *IEEE Transactions on Dielectrics and Electrical Insulation,* vol. 23, no. 3, pp. 1589-1596, 2016.

[41] S. Y. Matharage, Q. Liu, Z.D. Wang, G. Wilson, and C. Krause, "Aging assessment of synthetic ester impregnated thermally non-upgraded Kraft paper through chemical markers in oil," *IEEE Transactions on Dielectrics and Electrical Insulation,* vol. 25, no. 2, pp. 507-515, 2018.

[42] U. M. Rao, Y. N. Kumar, and R. K. Jarial, "Understanding the ageing behaviour of transformer oil–paper insulation with ester and mixed dielectric fluids," *IET Science, Measurement & Technology,* vol. 12, no. 7, pp. 851-857, 2018.

[43] J. Haema and R. Phadungthin, "Condition assessment of the health index for power transformer," *Power Engineering and Automation Conference*, Wuhan, China, pp. 1-4, 2012.

[44] IEC Standard 60599, "Guide for the interpretation of the analysis of gases in transformers and other oil-filled electrical equipment in service," 1979.

[45] IEC Standard 60599, "Mineral oil-impregnated electrical equipment in

service-Guide to the interpretation of dissolved and free gases analysis," 1999.

[46] J. Bidlack, "Molecular structure and component integration of secondary cell walls in plants," *Oklahoma Academy of Science*, 1992.

[47] IEEE Standard C57.104, "Guide for the interpretation of gases generated in oil-immersed transformers," 2009.

[48] C. Krause, "Power transformer insulation–history, technology and design," *IEEE Transactions on Dielectrics and Electrical Insulation,* vol. 19, no. 6, pp. 1941-1947, 2012.

[49] S. Jeszenszky, "History of transformers," *IEEE Power Engineering Review,* vol. 16, no. 12, p. 9, 1996.

[50] J. J. Kelly, "Transformer fault diagnosis by dissolved-gas analysis," *IEEE Transactions on Industry Applications,* vol. IA-16, no. 6, pp. 777-782, 1980.

[51] O. Eschholz, "Characteristics of transformer oils," *The Electric Journal,* p. 74, 1919.

[52] M. Buchholz, "The Buchholz protection system and its application in practice," *ETZ,* vol. 49, no. 34, pp. 1257-1262, 1928.

[53] R. R. Rogers, "IEEE and IEC codes to interpret incipient faults in transformers, using gas in oil analysis," *IEEE Transactions on Electrical Insulation,* vol. EI-13, no. 5, pp. 349-354, 1978.

[54] J. J. Kelly, "Predicting transformer incipient faults by dissolved gas in oil analysis," *EIC 14th Electrical/Electronics Insulation Conference*, Chicago, IL, USA, pp. 15-21, 1979.

[55] H. Ding, R. Heywood, J. Lapworth, and S. Ryder, "Learning from success and failure in transformer fault gas analysis and interpretation," *IET Conference on Reliability of Transmission and Distribution Networks,* London, UK, 2011.

[56] W. Halstead, "A thermodynamic assessment of the formation of gaseous hydrocarbons in faulty transformers," *Journal of the Institute of Petroleum,* vol. 59, no. 569, pp. 239-41, 1973.

[57] E. Dornenburg and W. Strittmatter, "Monitoring oil-cooled transformers by gas-analysis," *Brown Boveri Review,* vol. 61, no. 5, pp. 238-247, 1974.

[58] IEC Standard 60567, "Guide for the sampling of gases and of oil from oil-filled electrical equipment and for the analysis of free and dissolved gases," 1978.

[59] IEEE Standard C57.104, "Guide for the detection and determination of generated gases in oil-immersed transformers and their relation to the serviceability of the equipment," 1978.

[60] IEEE Standard 60567, "Guide for the sampling of gases and of oil from oil-filled electrical equipment and for the analysis of free and dissolved gases," 1993.

[61] IEC Standard 60567, "Oil-filled electrical equipment-Sampling of gases and of oil for analysis of free and dissolved gases-Guidance," 2005.

[62] IEEE Standard C57.104, "Guide for the interpretation of gases generated in

oil-immersed transformers," 1992.
[63] ASTM D3612-02, "Standard test method for analysis of gases dissolved in electrical insulating oil by gas chromatography," 2017.
[64] H. C. Sun, Y. C. Huang, and C. M. Huang, "A review of dissolved gas analysis in power transformers," *Energy Procedia,* vol. 14, pp. 1220-1225, 2012/01/01/ 2012.
[65] F. Jakob, "Dissolved gas analysis: Past, Present, and Future," *Weidmann–ACTI Inc,* 2003.
[66] S. Bustamante, M. Manana, A. Arroyo, P. Castro, A. Laso, and R. Martinez, "Dissolved gas analysis equipment for online monitoring of transformer oil: A review," *Sensors,* vol. 19, no. 19, p. 4057, 2019.
[67] IEEE Standard C57.147, "Guide for acceptance and maintenance of natural ester fluids in transformers," 2008.
[68] IEEE standard C57.155, "Guide for interpretation of gases generated in natural ester and synthetic ester-immersed transformers," 2014.
[69] IEEE Standard C57.147, "Guide for acceptance and maintenance of natural ester insulating liquid in transformers," 2018.
[70] CIGRE Brochure 296, "Recent developments on the interpretation of dissoved gas analysis in transformers," 2006.
[71] CIGRE Brochure 779, "Field experience with transformer solid insulation ageing markers," 2019.
[72] ASTM D7150, "Standard test method for the determination of gassing characteristics of insulating liquids under thermal stress at low temperature," 2013.
[73] D. Martin, N. Lelekakis, J. Wijaya, M. Duval, and T. Saha, "Investigations into the stray gassing of oils in the fault diagnosis of transformers," *IEEE Transactions on Power Delivery,* vol. 29, no. 5, pp. 2369-2374, 2014.
[74] IEC Standard 60296, "Fluids for electrotechnical applications-Unused mineral insulating oils for transformers and switchgear," 2012.
[75] I. Hohlein, "Unusual cases of gassing in transformers in service," *IEEE Electrical Insulation Magazine,* vol. 22, no. 1, pp. 24-27, 2006.
[76] T. Oommen, R. Ronnau, and R. Girgis, "New mechanism of moderate hydrogen gas generation in oil filled transformers," *CIGRE paper,* pp. 12-206, 1998.
[77] S. Besner, J. Jalbert, and B. Noirhomme, "Unusual ethylene production of in-service transformer oil at low temperature," *IEEE Transactions on Dielectrics and Electrical Insulation,* vol. 19, no. 6, pp. 1901-1907, 2012.
[78] J. Weesmaa, M. Sterner, B. Pahlavanpour, L. Bergeld, J. Nunes, and K. Sundkvist, "Study of stray gassing measurements by different methods," *Annual Report Conference on Electrical Insulation and Dielectric Phenomena*, Shenzhen, China, pp. 184-189, 2013.
[79] I. A. Hohlein, "Stray gassing cases of insulating liquids in HV equipment," *IEEE Transactions on Dielectrics and Electrical Insulation,* vol. 22, no. 5, pp. 2718-2722, 2015.

[80] S. Eeckhoudt, S. Autru, and L. Lerat, "Stray gassing of transformer insulating oils: impact of materials, oxygen content, additives, incubation time and temperature, and its relationship to oxidation stability," *IEEE Electrical Insulation Magazine,* vol. 33, no. 6, pp. 27-32, 2017.

[81] CIGRE Brochure 443, "DGA in non-mineral oils and load tap changers and improved DGA diagnosis criteria," 2010.

[82] C. Ciulavu, "Techniques for incipient fault diagnosis," *Journal of Sustainable Energy,* vol. 4, no. 2, pp. 1-4, 2013.

[83] M. Duval, "Fault gases formed in oil-filled breathing EHV power transformers-Interpretation of gas-analysis data," *IEEE Transactions on Power Apparatus and Systems,* no. 6, pp. 1745-1746, 1974.

[84] M. Duval and L. Lamarre, "The duval pentagon-a new complementary tool for the interpretation of dissolved gas analysis in transformers," *IEEE Electrical Insulation Magazine,* vol. 30, no. 6, pp. 9-12, 2014.

[85] M. Duval, "The Duval Triangle for load tap changers, non-mineral oils and low temperature faults in transformers," *IEEE Electrical Insulation Magazine,* vol. 24, no. 6, pp. 22-29, 2008.

[86] M. Duval and L. Lamarre, "The new Duval Pentagons available for DGA diagnosis in transformers filled with mineral and ester oils," *IEEE Electrical Insulation Conference*, Baltimore, Maryland, pp. 279-281, 2017.

[87] Susilo *et al.*, "Study on dissolved gas due tue thermally degraded insulating paper in transformer oil," *Procedia Technology,* vol. 11, pp. 257-262, 2013.

[88] M. Tsuchie, M. Kozako, M. Hikita, and E. Sasaki, "Modeling of early stage partial discharge and overheating degradation of paper-oil insulation," *IEEE Transactions on Dielectrics and Electrical Insulation,* vol. 21, no. 3, pp. 1342-1349, 2014.

[89] X. F. Wang, "Dissolved Gas Analysis (DGA) of Transformer Insulating Liquids under Laboratory Simulated Thermal Faults," PhD thesis, The University of Manchester, 2016.

[90] T. Rouse, "Mineral insulating oil in transformers," *IEEE Electrical Insulation Magazine,* vol. 14, no. 3, pp. 6-16, 1998.

[91] M. Eklund, "Mineral insulating oils; functional requirements, specifications and production," *IEEE International Symposium on Electrical Insulation*, Toronto, Canada, pp. 68-72, 2006.

[92] N. Lelekakis, D. Martin, W. Guo, and J. Wijaya, "Comparison of dissolved gas-in-oil analysis methods using a dissolved gas-in-oil standard," *IEEE Electrical Insulation Magazine,* vol. 27, no. 5, 2011.

[93] M. Eklund, "Mineral insulating oils; functional requirements, specifications and production," *IEEE International Symposium on Electrical Insulation*, Toronto, Canada, pp. 68-72, 2006.

[94] V. Haramija, D. Vrsaljko, and V. Đurina, "Thermal properties of synthetic ester-based transformer oil during ageing in laboratory conditions," *IEEE 18th International Conference on Dielectric Liquids*, Bled, Slovenia, pp. 1-4, 2014.

[95] P. Boss and T. V. Oommen, "New insulating fluids for transformers based on biodegradable high oleic vegetable oil and ester fluid," *IEE Colloquium on Insulating Liquids*, pp. 7/1-710, 1999.

[96] S. Tenbohlen and M. Koch, "Aging performance and moisture solubility of vegetable oils for power transformers," *IEEE Transactions on Power Delivery,* vol. 25, no. 2, pp. 825-830, 2010.

[97] M. Lashbrook, A. Gyore, R. Martin, R. Cselko, and B. Nemeth, "Design considerations for the use of ester-based dielectric liquids in transmission equipment," *IEEE 19th International Conference on Dielectric Liquids*, Manchester, UK, pp. 1-6, 2017.

[98] P. Jarman, K. Hampton, M. Lashbrooke, and G. J. Pukel, "Reliable, optimised power transformers with heat recovery for urban areas," *Transformers Magazine,* vol. 4, no. 2, pp. 84-90, 2017.

[99] L. Lewand, "Laboratory evaluation of several synthetic and agricultural-based dielectric liquids," Doble Engineering Company, USA, 2001.

[100] K. Giese, "The effects of cellulose insulation quality on electrical intrinsic strength," *IEEE Electrical Insulation Magazine,* vol. 10, no. 5, pp. 38-42, 1994.

[101] R. J. Heywood, A. M. Emsley, and M. Ali, "Degradation of cellulosic insulation in power transformers. I. Factors affecting the measurement of the average viscometric degree of polymerisation of new and aged electrical papers," *IEE Proceedings - Science, Measurement and Technology,* vol. 147, no. 2, pp. 86-90, 2000.

[102] N. A. Bakar, A. Abu-Siada, and S. Islam, "A review of dissolved gas analysis measurement and interpretation techniques," *IEEE Electrical Insulation Magazine,* vol. 30, no. 3, pp. 39-49, 2014.

[103] A. Bejan and A. D. Kraus, "Heat transfer handbook," Printed in the United States of America, 2003.

[104] M. Coulibaly, C. Perrier, M. Marugan, and A. Beroual, "Aging behavior of cellulosic materials in presence of mineral oil and ester liquids under various conditions," *IEEE Transactions on Dielectrics and Electrical Insulation,* vol. 20, no. 6, pp. 1971-1976, 2013.

[105] J. Jalbert, R. Gilbert, P. Tétreault, B. Morin, and D. Lessard-Déziel, "Identification of a chemical indicator of the rupture of 1,4-β-glycosidic bonds of cellulose in an oil-impregnated insulating paper system," *Cellulose,* vol. 14, no. 4, pp. 295-309, 2007.

[106] H. Z. Ding and Z.D. Wang, "On the degradation evolution equations of cellulose," *Cellulose,* vol. 15, no. 2, pp. 205-224, 2008.

[107] C. Krause, L. Dreier, A. Fehlmann, and J. Cross, "The degree of polymerization of cellulosic insulation: Review of measuring technologies and its significance on equipment," *IEEE Electrical Insulation Conference*, Philadelphia, Pennsylvania, USA, pp. 267-271, 2014.

[108] ASTM D4232, "Standard test method for measurement of average

viscometric degree of polymerization of new and aged electrical papers and boards," 2009.

[109] P. Kolseth, A. De Ruvo, and J. Bristow, "The cell wall components of wood pulp fibers," ed: New York: Marcel Dekker, 1986, pp. 3-25.

[110] R. Liao, C. Tang, L. Yang, and S. Grzybowski, "Thermal aging micro-scale analysis of power transformer pressboard," *IEEE Transactions on Dielectrics and Electrical Insulation,* vol. 15, no. 5, pp. 1281-1287, 2008.

[111] V. P.M and S. Thomas, "Preparation of bionanomaterials and their polymer nanocomposites from waste and biomass," *Waste and Biomass Valorization,* vol. 1, pp. 121-134, 2010.

[112] P. Calvini and A. Gorassini, "On the rate of paper degradation: Lessons from the past," *Restaurator-international Journal for The Preservation of Library and Archival Material - RESTAURATOR,* vol. 27, pp. 275-290, 2006.

[113] IEC Standard 60076-7, "Loading guide for oil-immersed power transformers," 2005.

[114] H. M. Wilhelm *et al.*, "Thermal faults involving thermally upgraded Kraft paper," *2018 IEEE PES Transmission & Distribution Conference and Exhibition - Latin America (T&D-LA)*, Lima, Peru, pp. 1-4, 2018.

[115] M. Daghrah, X. Zhang, Z.D. Wang, Q. Liu, P. Jarman, and D. Walker, "Flow and temperature distributions in a disc type winding-part I: Forced and directed cooling modes," *Applied Thermal Engineering,* vol. 165, p. 114653, 2020.

[116] X. Zhang, M. Daghrah, Z.D. Wang, and Q. Liu, "Flow and temperature distributions in a disc type winding-Part II: Natural cooling modes," *Applied Thermal Engineering,* vol. 165, p. 114616, 2020.

[117] T. Widyanugraha, R. Rachmad, Wendhy, and Suwarno, "DGA and tensile strength test on accelerated thermal aging of ester oil and kraft paper," *International Conference on Electrical Engineering and Informatics*,Bali, Indonesia, pp. 177-180, 2015.

[118] N. Lelekakis, W. Guo, D. Martin, J. Wijaya, and D. Susa, "A field study of aging in paper-oil insulation systems," *IEEE Electrical Insulation Magazine,* vol. 28, no. 1, pp. 12-19, 2012.

[119] R. Stebbins, D. Myers, and A. Shkolnik, "Furanic compounds in dielectric liquid samples: review and update of diagnostic interpretation and estimation of insulation ageing," *7th International Conference on Properties and Applications of Dielectric Materials*, Nagoya, Japan, pp. 921-926, 2003.

[120] J. Scheirs, G. Camino, M. Avidano, and W. Tumiatti, "Origin of furanic compounds in thermal degradation of cellulosic insulating paper," *Journal of applied polymer science,* vol. 69, no. 13, pp. 2541-2547, 1998.

[121] S. Y. Matharage, Q. Liu, Z.D. Wang, P. Mavrommatis, G. Wilson, and P. Jarman, "Ageing assessment of transformer paper insulation through detection of methanol in oil," *IEEE 11th International Conference on the Properties and Applications of Dielectric Materials*, Sydney, Australia, pp. 392-395, 2015.

[122] S. Tee *et al.*, "Practice of IEC 60422 in ageing assessment of in-service transformers," *The 19th International Symposium on High Voltage Engineering*, Pilsen, Czech Republic, 2015.

[123] R. Tamura, H. Anetai, T. Ishii, and Y. Makino, "A Diagnosis on the Overheating Deterioration of Insulating Paper in Transformers by Gas Analysis," *The transactions of the Institute of Electrical Engineers of Japan. A,* vol. 100, no. 7, pp. 409-414, 1980.

[124] IEC Standard 62332-1, "Electrical insulation system (EIS) thermal evaluation of combined liquid and solid components-Part 1," 2005.

[125] H. M. M. G. G. T. Herath, "Data analytics for transformer asset management," Second Year PhD Transfer Report, The University of Manchester, 2020.

[126] J. Dai and Z.D. Wang, "A comparison of the impregnation of cellulose insulation by ester and mineral oil," *IEEE Transactions on Dielectrics and Electrical Insulation,* vol. 15, no. 2, pp. 374-381, 2008.

[127] H. P. Gasser, C. Krause, M. Lashbrook, and R. Martin, "Aging of pressboard in different insulating liquids," *2011 IEEE International Conference on Dielectric Liquids*, Trondheim, Norway, pp. 1-5, 2011.

[128] K. J. Rapp, C. P. McShane, and J. Luksich, "Interaction mechanisms of natural ester dielectric fluid and Kraft paper," *IEEE International Conference on Dielectric Liquids,* Coimbra, Portugal, pp. 393-396, 2005.